Doctoral Dissertations

Graduate School

Spring 2015

Creep and shrinkage behavior of fly ash based geopolymer concrete

Md Rashedul Islam
Louisiana Tech University

CREEP AND SHRINKAGE BEHAVIOR OF FLY ASH

BASED GEOPOLYMER CONCRETE

by

Md Rashedul Islam, B.S., M.S.

A Dissertation Presented in Partial Fulfillment
of the Requirements of the Degree
Doctor of Philosophy

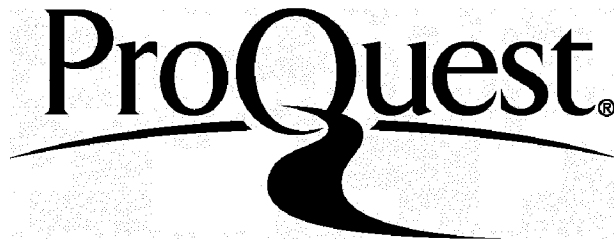COLLEGE OF ENGINEERING AND SCIENCE
LOUISINA TECH UNIVERSITY

March 2015

ProQuest Number: 3664376

ProQuest 3664376

ProQuest LLC
789 East Eisenhower Parkway
P.O. Box 1346
Ann Arbor, MI 48106-1346

LOUISIANA TECH UNIVERSITY

THE GRADUATE SCHOOL
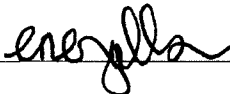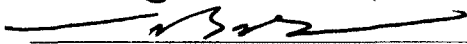
12/17/2014
_____
Date
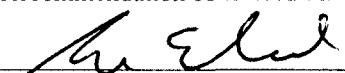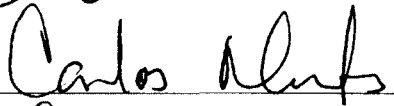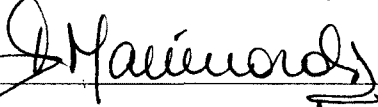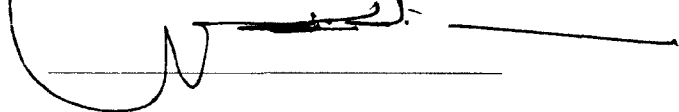
We hereby recommend that the dissertation prepared under our supervision

by__Md Rashedul Islam_____

entitled_____

CREEP AND SHRINKAGE BEHAVIOR OF FLY ASH BASED GEOPOLYMER

CONCRETE

_____

_____

be accepted in partial fulfillment of the requirements for the Degree of

Doctor of Philosophy in Engineering

_____
Supervisor of Dissertation Research

_____
Head of Department

Engineering
_____
Department

Recommendation concurred in:

Advisory Committee

Approved:

_____
Director of Graduate Studies

_____
Dean of the College

Approved:

_____
Dean of the Graduate School

ABSTRACT

The manuscript presented herein is based on the investigation of the short and long term properties of fly ash based geopolymer concrete (GPC) and their link to fly ash characteristics. Fly ash (FA) exhibits a significantly different particle morphology, which impacts the mechanical properties of the resulting GPC and typically contains impurities that fluctuate from one FA source to another. A key contribution of this research work is the capturing of the variability posed by the FA stockpile with a wide range of physical, chemical, and crystallographic characteristics as a source material to select the GPC mix design. In the case of prestressed GPC application, there are concerns on prestress loss caused by elastic shortening, shrinkage, and creep. Thus, the values of mechanical strength, ultimate shrinkage strain, and creep coefficient of the GPC have to be estimated reasonably and accurately at the design stage to avoid any loss of structural capacity the premature structural failure.

The test study was conducted to evaluate the mechanical strength of fly ash based geopolymer concrete. Fly ash samples from different sources were tested to see the impact of the chemical and physical properties of the FA element on the fresh and hardened properties of the GPC. Samples from 50 different power plants were collected and analyzed to develop the regression equation. The empirical model was developed to predict the flexural strength from the compressive strength, the unit weight from the density of the FA, the elastic modulus from the unit weight, and compressive strength of

the GPC and the compressive strength from the chemical and physical properties of the FA. A second set of 10 FA samples was selected randomly to validate the test results. It was observed that the prediction equation is accurate within 5 to 7 percent of the experimental values. The restrained shrinkage and free shrinkage test was conducted to observe the shrinkage of the GPC. Free shrinkage of the GPC plot was compared with the available empirical model for compatibility. In this study, an apparatus was designed to determine the creep of the GPC and an effective creep testing procedure was developed and documented. Experimental results obtained from this study were compared with the available empirical models.

The results obtained from this study show that the compressive strength of the GPC can be presented with reasonable accuracy by analyzing the physical and chemical property of the FA. Also, it was found that the mechanical behavior of the GPC can be predicted with the equations given in the American Concrete Institute's Building Code (ACI 318, 2008) with minor modifications. Experimental results obtained from this study were compared with the available empirical models. It has been observed that the free shrinkage strain and creep compliance prediction equations for the GPC are akin to those given in the SAKATA model and GL 2000 model.

APPROVAL FOR SCHOLARLY DISSEMINATION

The author grants to the Prescott Memorial Library of Louisiana Tech University the right to reproduce, by appropriate methods, upon request, any or all portions of this Dissertation. It is understood that "proper request" consists of the agreement, on the part of the requesting party, that said reproduction is for his personal use and that subsequent reproduction will not occur without written approval of the author of this Dissertation. Further, any portions of the Dissertation used in books, papers, and other works must be appropriately referenced to this Dissertation.

Finally, the author of this Dissertation reserves the right to publish freely, in the literature, at any time, any or all portions of this Dissertation.

Author _____

Date   12/17/2014 _____

DEDICATION

To my Mom and Dad, Mrs. Mazedunnesa and Md. Huzur Ali, for everything they have done and are doing for their child, my beautiful wife, Dr. Mahabuba Akhter Mila, and my loving sisters and brothers for their great support and encouragement.

TABLE OF CONTENTS

LIST OF TABLES

xv

LIST OF FIGURES

xviii

ACKNOWLEDGEMENTS

It is my immense pleasure in thanking the persons and organizations that helped me over the years to bring my PhD dissertation to the final form.

I would like to express my deep gratitude and sincere appreciation to Professor Dr. Erez Allouche for his technical guidance, continuous support, and constructive suggestions throughout the course of this research.

I express great appreciation to members of my supervisory committee Dr. Sven Eklund, Dr. Daniela Mainardi, and Dr. Wasiuddin Nazimuddin for your enlightment and keen research assistance. My sincere gratitude also goes to Dr. Carlos Montes for his advice and helping me edit this manuscript.

I would like to thank all my colleagues in cementitious binder lab at the alternative cementitious material lab of Louisiana Tech University. Neil Keen, Chris Morgan, Chris Burtlett, Morgan Marks, Ben Cury, and Tyler Baus are acknowledged for their help with the setup of instrumentation to conduct the tests.

At last my sincere thanks goes to my parents for their persistent encouragement and unconditional love which motivated me to complete my study. I believe the fulfillment of my study will bring you joy which is the only thing you need from your child.

CHAPTER 1

INTRODUCTION

1.1 Background and Research Needs

Coal ash constitutes one of the largest waste streams in the United States. The American Coal Ash Association, an industry group, estimates that every year the nation's coal plants produce 140 million tons of coal ash pollution, the toxic by-product that is left over after the coal is burned. In the past, fly ash (FA) was generally released into the atmosphere, but pollution control equipment mandated in recent decades now require that it be captured prior to release. In the US fly ash is generally placed in landfills or stored in precarious surface waste ponds. About 43% is recycled, often used as a pozzolan to produce hydraulic cement or a partial replacement for Portland cement in concrete production. The US Environmental Protection Agency (EPA) is currently developing new regulations that many of the current beneficial applications of FA, such as soil stabilization and mine reclamation which are considered as "un-encapsulated," may be banned allowing only the recycling of FA in encapsulated applications such as making concrete. Though FA has been used in ordinary concrete as a supplementary cementitious material for many years to improve the rheology and fresh property, it typically occupies up to 20% of the total mix. However, when activated under highly alkaline conditions, FA alone is capable of producing a strong cementitious binder, which is often called the geopolymer. The main challenges for a widespread use of FA based geopolymer concrete

1

(GPC) is the significant variability of FA in terms of chemical properties, type, particle size and composition of its precursor coal. The reactive molecules contained in the FA are the main components of the geopolymer network; thus, the amount and ratio of these elements influence the resulting mechanical properties of GPC. This study attempts to provide a series of linear regression models derived from a database of 50 FA stockpiles. Each FA sample was examined in terms of chemical composition, crystallographic characteristics and particle size distribution. A key contribution of the first part of the proposed research work is the capturing of the variability posed by FA stockpiles as source materials to manufacture geopolymer concrete.

The second part of this research work deals with the long term properties of the GPC, such as creep and shrinkage. Time dependent deformations have great influence on the structural behavior of reinforced and prestressed concrete elements. Those are directly related to long-term deflection, losses to prestressing and cracking. As concrete ages, it undergoes volume changes responding to its environment, member size and stress. While most engineers understand immediate deformation, many do not fully understand concrete time dependent deformation. In general, the concrete time dependent volume changes are several times greater than the time independent volume changes. Compressive creep and shrinkage are two major mechanisms to consider in assessment of damage and performance of concrete structures. Shrinkage of restrained concrete components causes stress in the material, whereas compressive creep adds to this situation. The creep behavior of concrete has been the focus of attention for engineers and may still be an area of focus for decades to come because of the complexity of the creep properties of concrete.

Over the years many attempts have been made to develop general constitutive equations for the description of time dependent behavior of concrete. Most of them are empirical in nature and are limited to the scopes of the experiment. The creep property of concrete is very important for pre-stressed girders for long span bridge, pre-stressed shell concrete structure for the storage of water or gas, nuclear reactor vessels and offshore oil drilling platforms, and so on are widely used in the U.S. as well as other countries in around world. This is attributed mainly to the advantages of pre-stressed concrete structure which is similar to reinforced concrete and more pleasing aesthetically. It is very important to consider the elastic shortening, shrinkage and creep of concrete in the design calculation and the application of pre-stressed concrete. Failure to do this may cause the reduction of pre-stressed concrete capacity and premature failure of the structure.

1.2 Hypotheses

The following are the hypotheses to be tested:

- Silica and alumina are the main precursors for the geopolymeric reaction, and calcium oxide has also a positive impact on the mechanical behavior of geopolymer.

- Amorphous compounds in the fly ash are easier to dissolve than crystalline compounds in the geopolymerization. They yield higher amounts of reactive SiO_2 and Al_2O_3 to combine in the coagulation phase, resulting in a higher degree of geopolymerization and consequently higher mechanical strength.

- The finer the particle of fly ash, the greater the surface area and the more reactive is the FA. Also, high content of unburned carbon can adversely impact the mechanical strength of GPC.

- Shrinkage of concrete is related to its water content and other mechanical properties, especially the strength and elastic modulus. Thus, it is possible to estimate shrinkage behavior of concrete from its water content and hardened properties.

- Creep in the GPC is related to the other mechanical properties. There is a strict relationship exists among the strength, elastic modulus and creep of the concrete. Hence, it is possible to predict the creep behavior based on the knowledge of the other mechanical properties.

- Creep coefficient of the GPC with a different mix design may vary according to its chemical content and concrete chemistry. Thus, an empirical model can be developed to predict creep coefficient at different ages of concrete from experimental data.

1.3 Objective of Study

The major objectives of this research are as follows:

- To provide an approximation to the functional relationship between the mechanical properties of the GPC and FA characteristics. To determine the relationship among compressive strength, flexural strength and the modulus of elasticity of the GPC with crystallographic and physical characteristics of fly ash.

- To develop an effective and convenient laboratory setup and procedure for evaluating GPC restrained shrinkage strain.

- To design and recommend an effective and reliable laboratory testing setup and procedure for performing creep tests of the GPC.

- To evaluate the long term behavior of the GPC and to calculate the coefficients to be used in the design equation.

- To compare experimental data with the prediction equation or models and observe the similarity of the GPC's long term behavior with the existing models.

1.4 Scope of Study

The scope of the research covered the following major tasks:

- Experiments were conducted to evaluate the effect of concrete drying on compressive creep.

- Along with the restrained shrinkage ring test, the relative humidity and temperature of the concrete and their gradients across the test specimen was measured in order to model their effect on the creep shrinkage interaction.

- Test setup designed to cover certain ranges of activator solution to fly ash ratio and a limited range of GPC compressive strength. The best models that suit early age behavior were selected. Analytical techniques to model different components of tensile creep and its interaction with shrinkage were developed accordingly.

- Several fly ashes were used to develop the prediction equation to predict the early age mechanical strength, but only one fly ash was chosen to test the long term properties.

- Creep apparatus designed in this test method can test the maximum of three six-twelve cylinders with a maximum compressive strength of ten thousand pounds per square inch (psi).

1.5 Research Approach

Following are the research approaches:

- Characterization of raw material's chemical properties and selection to produce GPC with selected design characteristics.

- Conducting ASTM standard test to determine the fresh and hardened properties of the concrete.

- Performing statistical analysis to create a set of prediction equations to infer the hardened properties of the test specimens.

- Designing the apparatus and the test schedule to run the test and preparing the adequate number of specimen to run the tests either destructive or nondestructive at different ages of the specimen.

- Data collection from the test and regression analysis to fit the experimental result with the proper model for evaluation of shrinkage and creep behavior of the concrete.

CHAPTER 2

LITERATURE REVIEW

2.1 Introduction

Fly ash based geopolymer concrete is the construction material with some unique structural advantages. With the advancement of curing technology, it can reach a high early strength which can be used in places where quick setting is necessary. Though GPC technology is well known among material researchers for decades now, long term properties of this material is still not available to design engineers.

Concrete undergoes certain volumetric changes because of aging and induced load exerted upon it, which is named as the shrinkage and creep of the concrete. Shrinkage is the volumetric contraction on a load free specimen of concrete. It is one of the most fundamental characteristics of concrete which results from the loss of water from the surface of the concrete.

Contraction of the concrete takes place when water moves out of the porous body which is not fully rigid. This movement of water occurs in concrete from its fresh state to its later stage. Cement paste in the plastic stage means that the concrete will not come back to its initial condition after deformation takes place. The magnitude of this volumetric contraction is of the order of one percent of the absolute volume of the dry cement [1]. Shrinkage can be influenced by factors such as temperature, surrounding relative humidity, water/cement ratio, aggregate quantity, shape of the structure, and the

amount of water loss from the surface of the concrete. A vital parameter is to determine the initiation of stress which can cause subsequent cracking in the concrete. Shrinkage does not include change in length due to temperature difference. Shrinkage values are presented as dimensionless strains (length change over a given length) expressed as percent mm/mm, or in/in. It is common to express shrinkage in micro strain or millionths as the value of strain 1×10^6. Thus, 1000 micro strain is equivalent to 1×10^{-3} mm/mm.

Geopolymer concrete gains strength as a result of a chemical reaction known as the polymerization reaction between the oxides of the fly ash and the activator solution. For a given concrete mixture, the strength at any age in normal conditions is related to the degree of polymerization. The rate of polymerization and strength development of a given concrete is related to its temperature and humidity history. Shrinkage which takes place while the concrete is still in the plastic state is known as plastic shrinkage. It undergoes a volumetric contraction whose magnitude is the order of one percent of the absolute volume of raw fly ash. Withdrawal of water from the hardened matrix in a dry atmosphere can cause the drying shrinkage. A large part of this contraction is irreversible and should be distinguished from the reversible moisture movement caused by alternating storage under wet and dry conditions.

Although creep is observed for all materials, the fundamental basis for creep of the concrete must be quite different from those of metals, because it causes a significant change in volume at ambient temperature and the presence of moisture in the material plays an important role. It is commonly assumed that creep and shrinkage are interrelated phenomena because there are a number of similarities in these two characteristics of concrete. The strain-time curves are similar; constituent materials and environmental

factors affect creep in much the same way as shrinkage; the magnitudes of strains are similar and include a considerable amount of irreversibility. Thus providing a sufficient temperature and humidity controlled environment tensile cracking in the concrete can be determined. The relationship between various measured and derived strain values are shown in Figure 2.1.
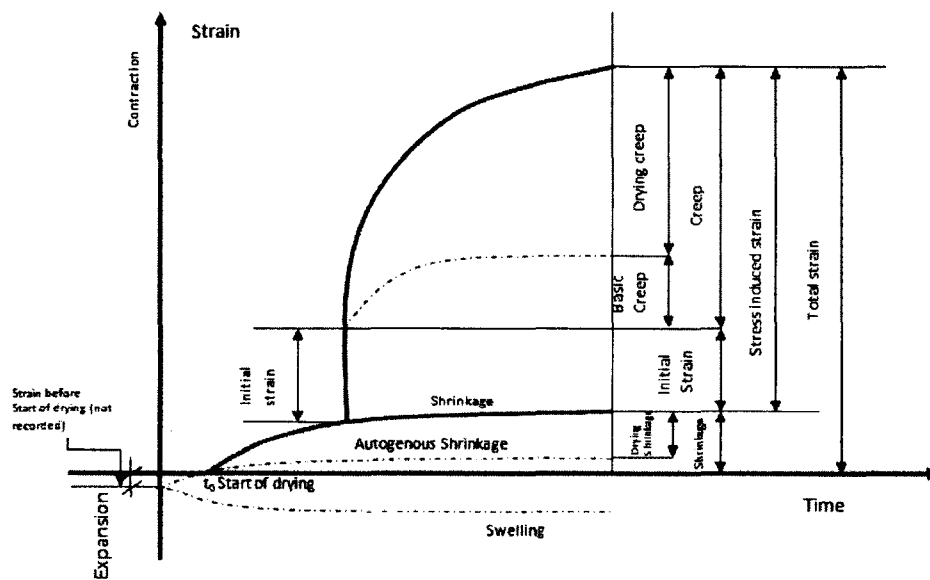
Figure 2.1 Shrinkage in concrete.

The experimental determination of creep and shrinkage of concrete is simple in concept. Deformation is measured over time for the loaded and unloaded specimen in the same environment. Shrinkage is measured only on unloaded specimens, while creep is determined by subtracting the shrinkage deformation and the elastic deformation from the total deformation measured on the loaded specimen. Although simple in concept, there are many experimental details that must be considered and carefully controlled to obtain meaningful test results. These include maintaining a constant load on the test specimen for the entire testing period and uniform distribution and load transfer when several

specimens are loaded with a single load frame. It is also important to maintain a controlled test environment with standard temperature and humidity.

A test program consistent with the knowledge on creep and shrinkage and the use of the test results in structural design and analysis in the development of prediction model is based on the following assumptions:

- Creep and shrinkage are separate and they do not interact.

- Separation exists between the strain components exclusively from the environmental and load conditions.

- The gradient of strain is linear and uniform.

- Instantaneous strain in creep causes the elastic deformation in the concrete.

The more comprehensive the test programs are, the better the possibility of estimating the prediction parameters or understanding the phenomena of creep and shrinkage. The scope of the test program depends upon how critical is the effect of creep and shrinkage on the structural behavior, on the model of prediction, on the method of analysis, on the time and facilities available for testing, and on the budget allocated for the test program. Typically, the test is designed from months to several years. The simplest test program consists of determining the static modulus of elasticity E_c at 3, 7, 14, 28, 56, and 90 days following ASTM C469. Sometimes the prediction equations are used to find the elastic modulus. Geopolymer concrete is different from ordinary Portland cement concrete in terms of the curing process. It may require heat curing for complete strength gain. Specimen curing condition plays a significant role on its shrinkage and creep behavior.

2.2 Types of Shrinkage

Shrinkage in concrete can occur in different ways. Shrinkage can be classified as it takes place at different phases and different loading conditions. The water content of concrete affects shrinkage as long as it reduces the volume of restraining the aggregate. Thus, the water content of a mix would indicate the order of shrinkage to be expected, but it is not the primary factor. As a result, mixes having the same water content but widely varying composition may exhibit different values of shrinkage.

2.2.1 Plastic Shrinkage

Plastic shrinkage is generally a physical action and is occurred by surface tension forces [2]. Water can be evaporated from the plastic concrete surface, which results in contraction known as plastic shrinkage [3]. Complete prevention of evaporation can prevent plastic shrinkage cracking. When the surface dries, menisci are formed between the solid particles and consequently capillary tension forces act. The magnitude of the shrinkage is affected by the quantity of water lost from the surface which is governed by the temperature, ambient relative humidity, and wind velocity. The rate of loss of water does not necessarily predict the occurrence of plastic shrinkage, rather the stability of the mix. When the amount of water lost due to evaporation is greater than the rate of bleed, there is a net reduction in volume. The surface layer of the concrete starts to shrink but is restrained by layers beneath that are not subjected to the same reduction in volume [4].

Reinforcement also provides partial restraint and friction at the surface of the framework or sub-base. The effect of the restraint is that tensile stresses develop in the surface layer. During the time the concrete is in a plastic state and has very little strength, cracks develop at the surface. The phenomenon is similar to the drying shrinkage of

clays, which is discussed in a later part of this literature review. Admixtures significantly alter the chemical forces between the cementitious and the fine particles inside the concrete. The rheological behavior as well as setting time can be profoundly altered. It is vital to assess the mix design, the bleeding capacity and set time, and plan accordingly. The use of water reducers in the concrete mix may be a solution which can cause the concrete to bleed less and therefore be more prone to plastic shrinkage.

2.2.2 Drying Shrinkage

The drying shrinkage of concrete is usually caused by movement of the cement paste [5]. Concrete stored in unsaturated air undergoes drying shrinkage by withdrawal of water from it. Most of the natural aggregates do not undergo any appreciable drying shrinkage. Indeed, most aggregate restrain concrete shrinkage because they are less elastic than the cement paste to which they are bonded. Concretes with higher aggregate contents shrink substantially less than cement-rich mixes all else being equal. However, some aggregates undergo unusually large volume changes on wetting and drying. These aggregates are typically weathered, and contain clay or mica minerals, and sometimes have high absorption. The absorption of the rock is sometimes high. These aggregates produce concrete with poor volume stability and a tendency to deflect and crack. The change in the volume of drying concrete is not equal to the volume of water removed from the concrete by evaporation. The loss of free water, which takes place first, causes very little shrinkage. As drying continues, the water layer is removed and the change in the volume of unrestrained hydrated cement paste at this stage is approximately one molecule thick from the surface of the gel particle. Drying shrinkage is also related to the

removal of intracrystalline water. Calcium silicate hydrate has been shown to undergo a change in lattice spacing from 1.4 to 0.9 nm in drying [6].

2.2.3 Thermal Shrinkage

Like any other material concrete can be subjected to volumetric changes of thermal origin [7]. However, because concrete behaves differently from other construction materials, during hardening, temperature increases, and therefore the mechanical links that are developed within the concrete during this period are formed at a service life [8]. Moreover, these links are created at a temperature that evolves after maximum temperature is reached. The physical laws that govern this heat exchange within concrete are well known. It is quite easy to develop models in order to predict the variation of the temperature of a concrete cast in a specific structural element exposed to specific ambient conditions when it cools down.

ASTM C531-85 for the determination of linear shrinkage and the coefficient of thermal expansion of mortars, grouts, and monolithic surfacing. This test was slightly modified to determine the coefficient of the thermal expansion of the concrete [9]. The test involves measuring the length of a small concrete beam after being placed in a room at 22° C, after being heated in an oven to 100° C for 24 hours, and again after being placed in the 22° C room for 24 hours. The samples are oven dried at 100° C for 1 day before testing in order to reduce the effect of drying shrinkage, particularly for the water-cured samples. The coefficient of thermal expansion is determined by dividing the change in length by the change in temperature.

2.2.4 Autogenous Shrinkage

Autogenous shrinkage can be described as the macroscopic volume reduction of cementitious materials when cement hydrates after initial setting [10]. Autogenous shrinkage does not embrace volume change due to loss or ingress of substance, temperature variation, application of an external force, and restraint. Autogenous shrinkage can be expressed as the percentage of volume reduction, "autogenous shrinkage ratio," or one dimensional length change, "autogenous shrinkage strain". Volume change in the concrete can occur in the form of shrinkage or swelling after the setting takes place. A continuous supply of water after the hydration reaction can lead to the expansion of the concrete. When there is any restriction of movement of water to or from the cement paste, then shrinkage occurs. This is because of the consumption of capillary water for hydration reaction of un-hydrated cement. This process is known as self-desicassion.

The shrinkage that occurred in this process is called autogenous shrinkage. Autogenous shrinkage is restrained by already hardened cement paste and aggregate present in the concrete. Its magnitude is smaller than the net cement paste [11]. Autogenous shrinkage is three dimensional, but to consider it alongside with drying shrinkage, it is expressed as a linear strain. Typical values of autogenous shrinkage are about 40×10^{-6} at the age of one month and 100×10^{-6} after five years [12]. Autogenous shrinkage increases with temperature, high cement content and with the presence of finer cement, and with cement having high calcium content [13]. At very low water cement ratio, autogenous shrinkage is expected to increase. This is not always true as at low

water cement ratio the cement paste becomes very rigid. At very low water cement ratio as 0.17 an autogenous shrinkage value 700 x 10^{-6} was reported [14].

2.2.5 Carbonation Shrinkage

Carbonation shrinkage is caused by the reaction between carbon dioxide (CO_2) present in the atmosphere and calcium hydroxide (Ca (OH) 2) present in the cement paste [15]. The carbon dioxide molecules enter into the concrete and reacts with the solid calcium hydroxide gel. This carbon dioxide reacts with the calcium ions and the pore solutions and decreases the alkalinity. At this stage the pH fall from 14.0 to 8.0 and the corrosion is initiated by destruction of protective oxide layer (Fe_2O_3 or Fe_3O_4). The reactions that take place during carbonation are as follows:

$$CO_2 + H_2O \rightarrow H_2CO_3 \ (Carbonic \ acid) \qquad [2.1]$$

$$H_2CO_3 = H^+ + HCO_3^- \ (Decrease \ in \ pH) \qquad [2.2]$$

$$H_2CO_3 + Ca(OH)_2 \rightarrow CaCO_3.2H_2O. \qquad [2.3]$$
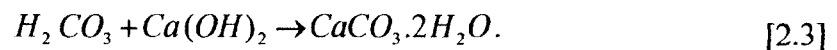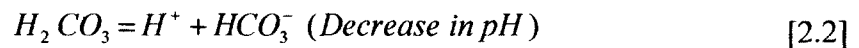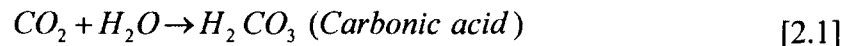
The pH drops as soon as the calcium hydroxide is removed. The amount of combined shrinkage varies according to the sequence of occurrence of carbonation and the drying process. If both phenomena take place simultaneously, less shrinkage develops. The process of carbonation however is dramatically reduced at relative humidity below 50%. Pearson suggested that the carbonation rate of high performance concrete was related to the age and water cement ratio [16]. The condition for carbonation shrinkage of high performance concrete (HPC) was settled related to water cement ratio (w/c) and the content of the silica fume. At low w/c and high content of the silica fume all the calcium hydroxide was consumed in high performance concrete (HPC), which more or less eliminated the carbonation, and thus also the carbonation shrinkage.

2.2.6 Factors Influencing Shrinkage

As far as shrinkage of the hydrated cement paste itself is concerned, shrinkage is larger the higher the water/cement ratio. The water/cement ratio determines the amount of evaporated water and the rate at which water can move towards the surface of the specimen. Shrinkage of hydrated cement paste is directly proportional to the water to cement ratio between the values of about 0.2 and 0.6 [17]. At higher water/cement ratio, the additional water dries up without resulting in any shrinkage in the concrete. Another parameter that influences the shrinkage is the type and amount of aggregate present in the concrete. Table 2.1 gives the typical values of drying shrinkage of mortar and concrete specimen. The most important role is exerted by aggregate which restrains the amount of shrinkage that can actually be realized. The ratio of shrinkage of concrete S_c to the shrinkage of neat cement paste S_p depends upon the aggregate content of the concrete, a, and is [18]:

$$S_c = S_p(1-a)^n. \qquad [2.4]$$

Table 2.1 Typical values of shrinkage of mortar and concrete specimens, 5 in. (127 mm) square in cross section, stored at a relative humidity of 50% and 21° C (70° F).

Aggregate/cement ratio	Shrinkage after six months (10^{-6}) for water cement /ratio of :			
	0.4	0.5	0.6	0.7
3	800	1200	.....	.....
4	550	850	1050	.....
5	400	600	750	850
6	300	400	550	650
7	200	300	400	500

The experimental value of n varies between 1.2 and 1.7. Increasing aggregate content of concrete from 71 to 74 percent at the same water/cement ratio will reduce

shrinkage by about 20 percent [19]. In practical condition, the constant water/cement ratio shrinkage increases with an increase in the cement content because this results in a larger volume of hydrated cement paste which is susceptible to shrinkage. Concrete made with shrinking aggregate may lead to service ability problems in the structure due to excessive deflection or warping. High shrinkage leads to cracking, and durability of the structure may be impaired. Light weight aggregate leads to higher shrinkage, largely because the aggregate has a lower modulus of elasticity. The properties of cement have little influence on the shrinkage of concrete. The chemical composition of cement is now believed not to affect shrinkage except that cement deficient in gypsum exhibit a greatly increased shrinkage. Shrinkage of concrete made with high alumina content cement is of the same magnitude as the concrete made with ordinary Portland cement, but it takes place much more rapidly. The addition of fly ash and blast furnace slag in the mix increases shrinkage. At a constant water/cement ratio, an increased proportion of fly ash or slag in the blended cement leads to higher shrinkage some 20 percent with the fly ash and with up to 60 percent with very high contents of slag [20]. Effect of water reducing admixtures on the shrinkage of concrete is indirect. Those result in the change in the water content or the cement content of the concrete mix. Super plasticizers increase the shrinkage by some 10 to 20 percent [21]. Entrainment of air has been found to have no effect on shrinkage. Added calcium chloride increases shrinkage, generally between 10 to 50 percent, because a finer gel is produced and because of carbonation [22].

2.3 Measurement of Shrinkage

A few test procedures have been used to determine the early-age behavior of concrete under restrained shrinkage. Historically, ring tests (Figure 2.2) have been

performed to determine the time for a material to crack under restrained shrinkage [23].

When the concrete ring deforms due to shrinkage, the steel ring restrains the concrete and

tensile stresses are induced.
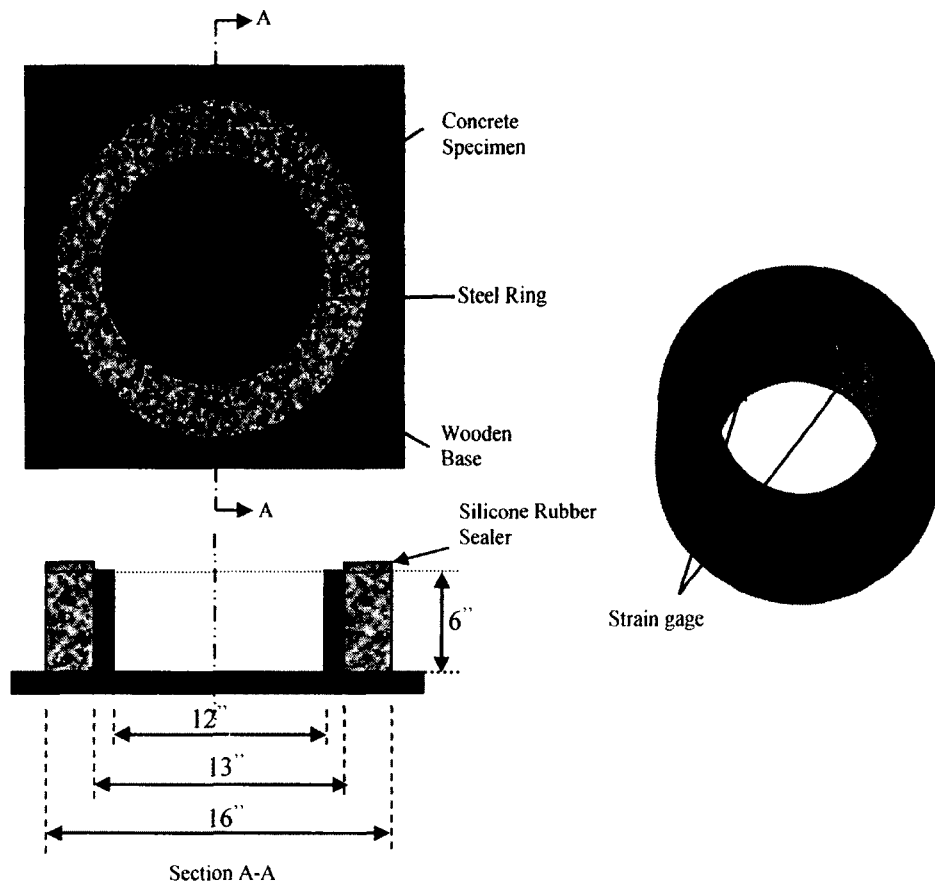
Figure 2.2 Schematic diagram of shrinkage test.

Elapsed time, t, for the test specimen is calculated. For each strain gage on the test

specimen, the net strain is calculated at each recorded time. This strain value is recorded

as the difference in strain between the strain in the steel at each recorded time and the

initial strain. Strain rate factor α is obtained by plotting the net strain against the square

root of elapsed time.

Linear regression analysis is used to fit the graphical straight line through the data. The strain rate factor is the slope of the line:

$$\varepsilon_{net} = \alpha\sqrt{t} + k,$$
[2.5]

where ε_{net} = net strain, in/in (m/m)

A = strain rate factor for each strain gage on the test specimen (in/in)/day$^{1/2}$

t = elapsed time, days and

k = regression constant.

Stress rate q is calculated for each specimen at cracking or at the time the test is terminated, q is calculated as:

$$q = \frac{G|\alpha_{avg}|}{2\sqrt{t_r}},$$
[2.6]

where q = the stress rate in each test specimen, psi/day

G = 10.47 x 10^6 psi

α_{avg} = absolute value of the average strain rate factor for each test specimen, (in/in)/day$^{1/2}$.

t_r = elapsed time at cracking or elapsed time when the test is terminated for each test specimen, days.

Stress development cannot be monitored for test setup in which the degree of restraint is such that no measurable deformation occurs in the steel as the concrete shrinks. Such test setups have provided qualitative evaluations and have not enabled a simple procedure to be established to routinely quantify the restrained shrinkage characteristics of concrete. The ring setup provides a high degree of restraint while still allowing sufficient strain in the steel as the concrete shrinks. Strain gages are utilized to

measure the steel strain to provide an accurate assessment of the time to crack. The method, however, does not provide quantitative information on the concrete tensile stress and creep to evaluate the condition for cracking. A uni-axial restrained test (Figure 2.2) has been used in a number of studies to determine the time of cracking and tensile creep characteristics of concrete under restrained shrinkage at early ages [24]. This test method covers the determination of the creep of concrete cylinders subjected to the longitudinal compressive load. The purpose of this test is to compare the creep potential of different concretes initially loaded for 28 days. When complete creep behavior of a given concrete is desired, specimen for testing 2, 7, 28, and 90 days and 1 year is required.

The test setup includes two identical specimens, where one specimen is free to shrink while the other is fully restrained. When the deformation due to shrinkage in the restrained specimen reaches a predetermined value, a tensile force is applied to bring the specimen back to its original position. The induced load is recorded and the total elastic strain is calculated as the sum of the elastic strain increments in each loading cycle. The creep strain is calculated as the difference between the free shrinkage strain and the cumulative elastic strain. While this test setup is very valuable, it does not lend itself to routine use by most laboratories.

The cure reference method (CRM) is one of the methods that use the Moiré interferometer [25]. In the CRM method, the gratings on the concrete records in-place deformation of the concrete on a full-field scale. The CRM method avoids destruction of the specimen and does not reinforce the specimen. In this method the grating does not degrade with time so time dependent deformation can be measured. The Moiré interferometer is an optical method where full-field in plane displacement can be

measured with high sensitivity. Data obtained by this method are the fringe patterns which represent the intensity distribution from the interference between two rays of light. An automated strain analysis system based on the phase shifting theory measure the strain in the specimen.

2.4 Creep in Concrete

Creep is the tendency of a solid material to move slowly or deform permanently under the influence of stress [26]. Creep occurs as a result of long term exposure to high levels of stress that are below the yield strength of the material. This phenomenon is more severe to the materials that are subjected to heat for long periods. One of the most important external factors influencing creep is the relative humidity of the air surrounding the concrete.

2.5 Factors Influencing Creep

Creep depends upon the magnitude of the stress and the rate of its application, the duration of the stress, the age of the concrete at commencement of loading, the type of cement, water cement ratio and method of mixing, fineness of the cement, characteristics of the aggregate, the size of the specimen, and the atmospheric condition, i.e. temperature and humidity. Within the range of working stress, creep is proportional to stress [27]. For higher stresses it increases rapidly and not in proportion to the increase in stress. Also, the creep increases with magnitude of the stress. The amount of creep depends upon the rate of application of the load. Creep increases if the load is applied slowly. Creep increases with time though the rate of creep decreases. Glanville found that creep may continue even up to seven years. It has been found that the creep for about the first month after applying the load depends on the age of the concrete on loading [28]. The creep

value decreases with increasing age. However, the later rates of creep depend on the actual age of the concrete at the time of observation of creep and not on the age when loaded. Creep also depends upon the type of cements. For Portland cement, the creep increases very rapidly over the first year and then only very slow. In high alumina cement, the creep increases almost in proportion with time for ages between 1 to 5 years, almost doubled at 5 years. Creep is a function of the volumetric content of cement paste in concrete, but the relation is not linear. Creep of concrete, c, the volumetric content of aggregate, g, and the volumetric content of hydrated cement, u, are related by:

$$\log \frac{c_p}{c} = \alpha \log \frac{1}{1-g-u},$$ [2.7]

where c_p is creep of neat cement paste of the same quality as used in concrete and:

$$\alpha = \frac{3(1-\mu)}{1+\mu+2(1-2\mu_a)\frac{E}{E_a}}.$$ [2.8]

Here, μ = Poisson's ratio of concrete, μ_s = Poisson's ratio of aggregate, E = Modulus of elasticity of concrete, and E_a = Modulus of elasticity of aggregate. There are certain physical properties of aggregate which influence the creep of concrete. The modulus of elasticity is the most important factor. Porosity of aggregate influences the creep of concrete. However it is not an independent factor as aggregate with a higher porosity has a lower modulus of elasticity. There is no fundamental difference between normal and lightweight aggregates as far as the creep properties are concerned. Elastic deformation of light weight aggregate concrete is usually larger than in ordinary concrete. Therefore, the ratio of creep to elastic deformation is smaller for lightweight aggregate concrete.

2.5.1 Influence of Stress and Strength

Regarding the intensity of the applied stress, Troxell *et al.* found a direct proportionality between the magnitude of sustained stress and the creep of concrete made with 0.69 water-cement ratio (20 MPa nominal compressive strength) [29]. Specimens cured for 90 days and then loaded for 21 years showed 680, 1000, and 1450 x 10^{-6} creep strain, corresponding to sustained stress levels of 4, 6, and 8 MPa, respectively.

2.5.2 Influence of Ambient Relative Humidity

Increased atmospheric humidity is expected to slow down the relative rate of moisture flow from the inner to the outer surface of the concrete. With a defined condition of exposure, the effect of relative humidity (RH) of air on the drying shrinkage strain and creep coefficient are illustrated in the charts published by the Comite Euro-International du Beton (CEB). At 100 percent RH, the drying shrinkage is assumed to be zero, rising to about 200 micro strain at 80 percent RH, and 400 micro strain at 45 percent RH. Similarly, the relation observed for creep coefficient, which is one of the five partial coefficients contributing to the total creep, is assumed to be 1 at 100 percent RH. It rises to about 2 at 80 percent RH, and 3 at 45 percent RH.

2.5.3 Relationship between Creep and Time

Creep with time is measured with constant stress while the specimen is stored under an appropriate condition. The ASTM C512-87 method is used to measure the load-induced time-dependent compressive strain at selected ages for concrete under an arbitrary set of controlled environment conditions. Fabricated specimens are loaded at an age of 28 days when the purpose of the test is to compare the creep potential of different concrete. To determine the complete creep behavior of a given concrete, the specimens

are loaded at the ages of 2, 7, 28, and 90 days, and 1 year. Transmission of the adsorbed water and the water held by capillary tension in small pores (under 50 nm) of the hydrated cement paste into large capillary voids within the concrete system or to the atmosphere is a time dependent process that takes place over long periods. Observing long term creep and drying shrinkage tests on concrete more than 20 years, Troxell *et al.* found that with a wide range of concrete mixture proportions, aggregate types, and environmental and loading conditions, only 20 to 25 percent of the 10 year drying shrinkage was realized in 2 weeks, 50 to 60 percent in 3 months, and 75 to 80 percent in 1 year. Ross and Lorman suggested a mathematical expression to determine creep c after time t under load as [30]:

$$c = \frac{t}{a + bt}.$$
[2.9]

When t = ∞, then c = 1/b, which is the limiting value of creep. Here 'a' and 'b' are constants determined from the experimental results. These values are obtained by putting a graph t/c vs. t. The slope of the graph is b and the straight line where it intercepts the line t/c gives the value of a. The U.S. Bureau of Reclamation made an extensive study of creep of concrete in dams and represented the following expression:

$$c = F(k)\log_e(t+1),$$
[2.10]

where K = age at which the load is applied.

F (k) = a function representing the rate of creep deformation with time, and

t = time under load in days.

F (k) is found from a plot on semi-logarithmic paper.

A reliable prediction of creep at any condition is not possible; short term tests are necessary for all loaded condition. Extrapolation is then possible. For the majority of the

concrete regardless of the water/cement ratio or the type of aggregate, specific creep at the age of t days (t > 28), creep with time (c_t) can be related to a specific creep after 28 days under load c_{28} by the following expressions:

Basic creep $$c_t = c_{28} \times 0.50 t^{0.21}$$ [2.11]

Total creep $$c_t = c_{28} \times (-6.19 + 2.15 \log_e t)^{0.38},$$ [2.12]

where c_t = long term specific creep in 10^{-6} per MPa.

2.5.4 Creep at Elevated Temperature

The temperature to which concrete is exposed can have two counteracting effects on the creep. If a concrete member is exposed to higher than the normal temperature as a part of the curing process before it is loaded, the strength will increase and the creep strain will be less than that of a corresponding concrete stored at a lower temperature. On the other hand, exposure to high temperature during the period under load can increase the creep. Nasser and Neville found that, in the temperature range of 21° C to 71° C, the 365-day creep increased approximately 3.5 times with temperature.

2.6 Effects of Creep

Creep in concrete affect strains and deflection and often also stress distribution. These effects vary with the type of structure. Creep of plain concrete does not affect the strength. Under very high stress creep hastens the approach of the limiting strain at which failure takes place. This happens when the sustained load is 85 to 90 percent of the rapidly applied static ultimate load. Under a low sustained load, the volume of the concrete decreases, and this would be expected to increase the strength of concrete. In reinforced concrete columns creep results in a gradual transfer of load from the concrete to the reinforcement. When the steel yields, any increase in load is taken by the concrete.

Before failure, full strength of concrete and steel is developed. In statically indeterminate structures, creep may relieve stress concentrations induced by shrinkage, temperature change, or movement of support. In all concrete structure, creep reduces internal stresses due to non-uniform shrinkage so that there is a reduction in cracking. Creep itself may be a cause of cracking when a restrained concrete mass undergoes a cycle of temperature change due to the development of the heat of hydration and subsequent cooling.

Compressive stress is induced by the rapid rise in temperature in the interior of the concrete mass. This stress development is not very high because the modulus of elasticity of concrete at the early stage is low. As the temperature of the concrete mass reduces, the compressive stress disappears. On further cooling of the concrete, tensile stress develops, and because the rate of creep is reduced with age, cracking may occur even before the temperature has dropped to the initial (placing) value. Because of these reasons, the rise in temperature in the interior of a large concrete mass must be controlled. The effect of the creep may thus be harmful, but on the whole, creep unlike shrinkage is beneficial in relieving stress concentrations.

2.7 Carbonation in Concrete

Alkalinity of concrete serves as an excellent protection to the reinforcement embedded [30]. The alkaline environment forms a protective oxide film which passivates the steel and protects it from corrosion. Concrete initially has a pH value of about 12 to 13. Due to leaching, carbonation and defective construction practices, the pH value drops rapidly. Once the pH value in the concrete at the cover zone drops below 10, corrosion of steel reinforcement is inevitable, and therefore concrete durability is at stake. This is however dependent upon the quality of the concrete and its porosity mainly in the cover

area. A dense good quality concrete offers good protection to steel embedded in it. It is also essential to produce concrete using low water cement ratio so that it has minimum unblocked capillary pores. Since the concretes of higher strength have low water cement ratio, those are preferred in construction.

2.7.1 Mechanism of Carbonation in Concrete

The carbon dioxide present in the atmosphere reacts in the presence of water with the concrete surface and concrete gets carbonated or in other words turns acidic [31]. This chemical reaction starts at the surface and gradually proceeds inside the concrete mass and is generally measured as depth of carbonation. As hydrated calcium silicates and aluminates are less stable than calcium carbonate, carbonation in the concrete cannot be avoided.

2.7.2 Effect of Carbonation

Carbonation of concrete improves several characteristics of ordinary concrete but can also affect the durability of reinforced concrete significantly [32]. If the concrete is dense and well compacted, carbonation reduces the total porosity specific surfaces of the cement paste as well as water permeability which in turn increases resistance to sulfate and aggressive chloride ion penetration. In reinforced concrete, these beneficial effects are accompanied by a large decrease in alkalinity or a drop in pH value. On carbonation, concrete loses its pH value from around 13.5 to 8.3 [33]. Therefore, steel is no longer passivated by the alkaline concrete around it. Oxidation of reinforcement steel therefore takes place when the presence of moisture and oxygen and corrosion (rusting) occurs. The corrosion increases the volume and ultimately results in cracking and spalling of concrete.

2.7.3 Rates and Factors Influencing Carbonation

Carbonation shrinkage occurs as a result of chemical interaction between atmospheric carbon dioxide (CO_2) and hydration products of cement. Carbonation shrinkage is probably caused by dissolving crystals of $Ca(OH)_2$ while under compressive stress imposed by drying shrinkage and the subsequent deposition of $CaCO_3$ in spaces free from stress. Hydration products near the pore dissolve continuously to furnish C^{++} ions to the liquid phase from which the ions migrate to the $CaCO_3$ nucleating site, where the crystal growth takes place. Since it takes place concurrently with drying shrinkage, most reported data do not distinguish between the two and designate both carbonation and drying shrinkage. As the cement hydrate is carbonated, the mass of the sample increases. Drying shrinkage accompanied by a loss of water results in mass loss. This inverse relationship can prove misleading when the specimen mass is used to determine the equilibrium point of drying. The rate of carbonation is dependent on several factors such as porosity of the concrete, the size of the member, relative humidity, temperature, CO_2 concentration, time of exposure method of curing, and the sequence of drying and carbonation.

Carbonation proceeds slowly and usually produces little shrinkage at relative humidity below 25% or near saturation. At low humidity, there is sufficient water in the pores for the CO_2 to form carbonic acid and react with the alkaline cement hydrates. As the pore humidity approaches saturation, the diffusion rate of CO_2 decreases. With permeable concrete the magnitude of carbonation shrinkage may approach the magnitude of drying shrinkage in a CO_2 rich environment at 50-65% relative humidity. Concrete that has been subjected earlier to carbonation shrinkage will still shrink or swell with changes

in relative humidity; however, the magnitude of those volume changes will be smaller than before carbonation.

2.7.4 Measurement of Carbonation in Concrete

The apparent pH profiling is an inexpensive, simple and reliable method to establish the effect of carbonation on concrete [34]. It varies depending on the type of binder and exposure period. The rate of carbonation derived from pH profiles can be utilized to estimate the service life structure when the deterioration is caused by carbonation induced corrosion of steel in concrete. The extent of carbonation as shown by the pH profiles has been shown to be reliable by favorable comparison with the result from thermo gravimetric analysis. Substantially, more information can be obtained from pH profiling, relating to the rate of advancement of carbonation and critical pH levels than from traditional methods such as the phenolphthalein test.

2.8 The Mechanism of Free and Restrained Shrinkage

When a volumetric change caused by shrinkage or temperature, and the concrete is restrained by adjacent structural element, tensile stresses occur and cause cracking. The tensile stresses can also be induced from differential drying throughout the thickness of a slab. This kind of cracking occurs when the concrete is thick and the thermal reaction takes place for a long period. When these stresses exceed the tensile strength of concrete, cracking is likely to occur. Concrete is very strong in compression but is weak in tension, and it is very much susceptible to restrained shrinkage cracking. Once cracking occurs, the concrete element is subjected to a decrease in service life due to the negative effects that are developed from water transport through the crack. These harmful effects can be minimized by reducing the crack size or crack width propagation. When stress is applied

to a concrete body, it experiences an elastic deformation which is independent of time. If however, this stress is maintained for a considerable amount of time, the specimen suffers a further time dependent deformation. This additional deformation can be considered as creep. If the length of the stressed specimen is kept constant, the creep leads to a gradual reduction of the stress initially present. This process is called relaxation. The early age of concrete creep is considered as beneficial relaxation mechanism because it reduces tensile stress development that leads to cracking. In some cases, a reduced capacity of creep could have a negative impact on a restrained structure in terms of cracking and durability.

2.8.1 Restrained Shrinkage Test or Ring Test of Concrete

Quantifying restrained shrinkage cracking in concrete has been a challenge for many years. Free shrinkage test do not provide enough information to characterize the behavior of restrained concrete. Sufficient information to characterize the behavior of restrained concrete several tests have been developed over the years. Studies have been performed using three main specimen geometries: rings, bars and plates. Ring specimens are more commonly used because of the benefits that they can easily be cast and end effects are removed providing axi-symmetric specimen geometry. If the concrete deforms because of shrinkage, the steel ring restrains the material and tensile stresses are induced. If the thickness of the steel is too large no measurable deformation occurs in the steel. Such test setups have provided qualitative evaluation, but have not established a simple procedure to quantify the restrained shrinkage of the material. In the ASTM C1581 test, the ring setup provides a high degree of restraint while still allowing sufficient strain in the steel as the concrete shrinks. The steel strain is measured by strain gages attached to

the surface of the steel ring, which provides an accurate assessment of the time to cracking.

The geometry of the ASTM C1581 is given in the Figure 2.2 with the inner radius of the steel ring given as R_{is}, the outer radius of the steel and the inner radius of the concrete given as $R_{os} = R_{ic}$ and the outer radius of the concrete given as R_{oc}. ASTM C1581 is applicable for concrete mixtures with aggregates of a maximum size of half an inch and is not suitable for mortar that exhibit expansion during the initial curing period. Cracking of the test specimen is indicated by a sudden decrease of compressive strain in the steel ring. The measured strain provides the basis for quantifying the restrained shrinkage behavior of the test specimens.

2.8.2 Measuring the Stress Within the Restrained Shrinkage Specimen

The instrumentation of strain gages are used to quantify the stress development inside the concrete, providing an accurate assessment of the time of cracking. Strain gages are placed at mid height of the steel annulus, where the average strain measured. Research study from Swamy and Stavrides converted the stress in steel to stresses in the concrete by applying equilibrium concepts, where the compressive force in the steel ring was set to equal to the tensile force in the concrete ring [35]. With this concept, determination of average tensile stresses in the concrete ring is defined as the strain measured in the steel ring:

$$\sigma_{avg} = -E_s * \varepsilon_{st} * \frac{(R_{ic} - R_{is})}{2(R_{oc} - R_{ic})} \left(1 + \frac{R_{ic}^2 - R_{oc}^2}{2R_{oc}}\right). \qquad [2.13]$$

It is assumed that the concrete rings are dried from the outer surface.

The maximum stress for these thin walled specimens can be computed using Equation 2.14:

$$\sigma_{max} = -\varepsilon_{st} * E_s \frac{R_{ic}(R_{ic} - R_{is})}{R_{is}(R_{oc} - R_{ic})}.$$ [2.14]

For calculating the circumferential $\sigma_\theta(r)$ and radial $\sigma_r(r)$ stresses in the concrete ring at any radius, Weiss, Ferguson and Hossain developed the equations [36]:

$$\sigma_\theta(r) = -\varepsilon_{st} * E_s \frac{R_{ic}^2 - R_{is}^2}{2(R_{oc}^2 - R_{ic}^2)}\left(1 + \frac{R_{oc}^2}{r^2}\right)$$ [2.15]

$$\sigma_r(r) = -\varepsilon_{st} * E_s \frac{R_{ic}^2 - R_{is}^2}{2(R_{oc}^2 - R_{ic}^2)}\left(1 + \frac{R_{oc}^2}{r^2}\right).$$ [2.16]

Hossain and Weiss also developed an equation to determine the elastic stress at any point along the radial direction $\sigma_{elastic}(r)$ in the concrete ring and expressed using Equation 2.17:

$$\sigma_{elastic}(r) = \Delta p_{elas} \frac{R_{os}^2}{R_{oc}^2 - R_{os}^2}\left(1 + \frac{R_{oc}^2}{r^2}\right).$$ [2.17]

The interface pressure Δp_{elas} is equal to:

$$\sigma_{elastic}(r) = \Delta p_{elas} \frac{R_{os}^2}{R_{oc}^2 - R_{os}^2}\left(1 + \frac{R_{oc}^2}{r^2}\right)$$ [2.18]

$$\Delta p_{elas} = -\frac{\Delta\varepsilon_{sh}E_c}{\frac{E_c}{E_s}C_{1r} + C_{2r}},$$ [2.19]

where ε_{sh} is the free shrinkage of the concrete. C_{1r} and C_{2r} are constants for a given geometry.

Assuming Poisson's ratio for the concrete does not vary with time:

$$C_{1r} = \frac{\left[(1+v_s)R_{is}^2 + (1-v_s)R_{os}^2\right]}{(R_{os}^2 - R_{is}^2)}$$ [2.20]

$$C_{2r} = \frac{\left[(1-v_c)R_{os}^2 + (1+v_c)R_{oc}^2\right]}{(R_{oc}^2 - R_{os}^2)},$$ [2.21]

where v_s is the Poisson's ratio of the steel ring. For the computation of maximum elastic stress, another term C_{3r} is used. It was observed that the thicker steel ring demonstrated a higher level of computed elastic stress. This was believed to be caused by the higher level of restraint provided by the thicker steel ring [37]:

$$\Delta\sigma_{elastic-max} = -\frac{\Delta\varepsilon_{sh} E_c C_{3R}}{\frac{E_c}{E_s}C_{1R} + C_{2R}},$$ [2.22]

$$\text{where } C_{3R} = \frac{R_{os}^2 + R_{oc}^2}{R_{oc}^2 - R_{os}^2}.$$ [2.23]

2.8.3 Influence of Direction of Drying

The effect of drying the ring specimen is related to the stress development in the ring specimen. If the outer surface of the ring is covered, then drying occurs only from the top and bottom of the concrete. On the other hand, if the specimen is demoulded from the outer ring, then the drying occurs uniformly throughout the height of the specimen, but not through the radial direction. Since the specimen loses most of the water at the outer circumference, the stresses are highest at the outside surface.

A study was conducted to compare the free shrinkage of an unrestrained ring to the shrinkage of a linear specimen. The same mix design of concrete was used to cast each specimen. The ring specimen was permitted to dry from the circumferential and top and bottom direction, where the linear specimens were permitted to dry from the top and

bottom. It was observed that the free shrinkage of the unrestrained ring specimen drying from the top and bottom was higher than that of the ring specimens drying from the outer circumference. This was thought to be due to a higher exposed surface to volume ratio for the specimens dried from the top and bottom. The linear specimens that were dried from the top and bottom showed a similar performance in free shrinkage to the unrestrained ring that were permitted to dry from the top and bottom, unlike the ring specimens permitted to dry from the circumferential direction. This is due to a similar surface to volume ratio between the two specimens permitted to dry from the top and bottom direction [37].

2.8.4 Influence of Degree of Restraint and Age of Cracking

The degree of restraint is very important for interpreting the result for the restrained ring test. A thicker steel ring will provide a higher degree of restraint. Higher degree of restraint will cause higher stress in concrete. An increase in thickness of steel ring decreases the magnitude of strain that can be measured at the inner surface of the steel ring that is needed for calculating stresses inside the concrete [38]. The age of cracking for restrained ring specimen can be influenced by many factors, including, but not limited to, direction of drying, mixture proportioning, and degree of restraint. It was observed that the thicker the steel ring the earlier the specimen cracks. It was also observed that specimens permitted to dry from the circumferential direction tend to crack at an earlier age, which is believed to be driven by the presence of the moisture gradient. Furthermore, it was found that as the concrete wall thickness increased, the specimens tend to crack at a later age.

2.9 Creep or Stress Relaxation Effect

Creep and relaxation are components of viscoelasticity and are typically nonlinear due to micro-cracking. Creep occurs when a constant stress is applied to a composite and over time the amount of strain or deformation increases. Relaxation occurs when deformation is prevented or is held at a constant state and over time the stress is reduced. Due to the stiffness in the steel ring in the restrained ring test, the concrete is prevented from deforming, therefore creating a stress relaxation within the concrete mix. Hossain and Weiss used the theoretical elastic and residual stresses to describe the effect of stress relaxation in restrained concrete.

2.9.1 Sustained Load Method

A number of different methods of maintaining constant load over time are employed to test creep in compression. Methods to maintain a constant load while the specimen shortens involve weights applied through the smooth disc surface made from the companion cylindrical specimen, spring in the compression and hydraulic pressure. Compression spring hydraulic systems are the more commonly used loading system.

When designing the creep frame, it is necessary to size the compression spring so that the load is maintained constant within a few percent over the range of deformation anticipated from the scheduled deformation of the load frame. Stiff rectangular or of any convenient shaped plate of adequate thickness are needed to limit the plate deflection on the stress distribution in the specimens. Load must be uniformly transferred in to the specimens so that they are subjected to uniaxial compression only. In a typical creep frame, this is accomplished by centering the specimens and by having one end of the loading system hinged. The hinged end can be comprised of a ball seated block or a

spherical seated block or a swivel system. No matter which design system is selected, it is important to make sure that at the initial stage of loading the specimen should experience the load distribution evenly through the entire surface.

Common types of creep specimen are either prismatic or cylindrical. In this test program cylindrical specimens were used. All creep specimens were subjected to sustained compressive stress. These stresses were maintained constant by using a set of railroad springs in the compression. A portable hydraulic jack was used to apply the desired load and load cell was used to monitor the load. After loading, the nuts on the tension threaded rods of the load sustaining apparatus were brought up against the end plates to keep the load constant. Upon releasing the load in the jack, the compression in the spring and the specimen were maintained by the high strength tensile rods.

It is assumed that the creep is proportional to the applied stress up to about 40% of the compressive strength and this is stated in the ASTM C512 to apply the load at this extent. However, it is common to load the specimen at the stresses up to 25% to 35% of the ultimate strength of the specimen. Therefore, consideration should also be given to specimen size relative to the capacity of the creep test equipment and the strength of the concrete. Large test specimens have a slower rate of creep and shrinkage and may require a longer time of drying than the small specimen as those have smaller surface to volume ratios [39].

Specimen end surfaces must be flat and plane. If cylinders are used, the end condition should comply with requirement in ASTM C39 for the compression test specimen. This means that the loaded end surface shall be perpendicular to the central axis of the specimen within 0.5 in and be plane within 0.050 mm. Specimens can be

surface grinded or capped with neat cement, high strength gypsum plaster or Sulfur mortar in accordance with ASTM C617. Grinding is the best end performance method for creep testing. The joints between the specimens with ground ends in the creep frame allow radial drying only. Commonly used cylindrical specimen in ASTM C512 require specimen with a diameter of 150±1.6 mm and a length of 292 mm.

Creep and shrinkage are related to the strength of the concrete. It has been shown that the time dependent deformation of the material is inversely proportional to the concrete strength at the time of application of load [40]. An increase in concrete compressive strength will result in a decrease in both creep and shrinkage strains. In the case of geopolymer, it depends upon the formation of monomers, which is the key component for strength.

The creep behavior of the concrete is directly affected by the quantity of aggregate used in the mix design as well as its mechanical properties. Creep of concrete is usually reduced in mixes containing high aggregate volume, and this is related to the fact that the aggregate does not experience any creep, and therefore increasing the aggregate volume in the mixture results in a creep reduction [41].

2.10 Shrinkage and Creep Prediction Models

The creep coefficient, the creep compliance and the specific creep are generally used to describe creep strain by different models. The creep coefficient is defined as the ratio of creep strain (basic plus drying creep) to elastic strain. The specific creep is defined as the creep strain per unit stress. Creep compliance is defined as the creep strain plus elastic strain per unit stress, where the elastic strain is defined as the instantaneous recoverable deformation of a concrete specimen during the initial stage of loading [42].

Mathematical expressions used to predict the time dependent concrete strain due to creep and shrinkage are presented in the following paragraphs. Designers typically use one of the following models to estimate creep and shrinkage strain in the concrete. Dilger model (1995), American Concrete Institute (ACI 209) model (1982), Model by Sakata (1996), Bazant B3 model (1997), Comite European du Beton, CEB-FIP model, Gardner Lockman GL 2000 model are included in this study.

2.10.1 Dilger Model (1995)

This model is based on the results from experimental data obtained from the University of Calgary and data from the literature. The model is applicable to mixtures with a w/c ratio of 0.15 to 0.4. This model is applicable to both normal weight and lightweight concrete. The input parameters for prediction of creep and shrinkage are: 1) Compressive strength at the age of loading, 2) Elastic modulus, 3) Water binder ratio, 4) relative humidity, and 5) member size. This model predicts creep coefficient [43].

Modulus of elasticity:

The modulus of elasticity (EM) of the concrete at time "t" may be expressed in terms of the concrete strength at that time, using a correction factor α_E, to account for different types of aggregates. Values of α_E for different aggregates are given below. If the type of aggregate is not known, then $\alpha_E = 1$. Equation 2.24 shows the EM as:

$$E_c(t) = 10000 \times \alpha_E \times f_c(t)^{0.333},$$ [2.24]

where $E_c(t)$ = Modulus of elasticity (MPa)

$f_c(t)$ = mean actual compressive strength at age t (MPa)

$\alpha_E = 1.2$ for basalt and dense limestone

$= 1.0$ for quartzitic aggregates

= 0.9 for limestone aggregates

= 0.7 for sandstone aggregates.

The compressive strength at time t can be expressed by Equations 2.25 and 2.26:

$$f_c(t) = [\frac{E_c(t)}{10000\alpha_E}]^3$$ [2.25]

$$f_c(t) = \frac{t}{\gamma_f + \alpha_f \times t} \times f_c',$$ [2.26]

where t = the age of concrete in days.

f_c' = mean concrete strength at fully cured condition.

$$\alpha_f = 1.03 - \frac{w}{3c} \qquad 0.15 < \frac{w}{c} < 0.4$$ [2.27]

$$\gamma_f = 28(1 - \alpha_f).$$ [2.28]

Basic Shrinkage:

The basic shrinkage developing between age t_s and t is:

$$\varepsilon_{bs}(t, t_o) = \varepsilon_{bs}(t) - \varepsilon_{bs}(t_o),$$ [2.29]

where t = time of observation in days

t_o = age of concrete from when shrinkage starts (days),

$$\varepsilon_{bs}(t) = \varepsilon_{bs}(t_o) * \beta_{bs}(t)$$ [2.30]

$$\varepsilon_{bs}(t_o) = 700 * e(-3.5 * w/c).$$ [2.31]

The time function for basic creep is expressed by:

$$\beta_{bs}(t) = \frac{t^{0.7}}{\gamma_{bs} + \alpha_{bs} * t^{0.7}},$$ [2.32]

where $$\alpha_{bs} = 1.04 - \frac{w}{3c} \qquad 0.15 < \frac{w}{c} < 0.4$$ [2.33]

$$\gamma_{bs} = 16.7 * (1 - \alpha_{bs}).$$ [2.34]

The drying shrinkage component $\varepsilon_{ds}(t, t_o)$ may be calculated from Equation 2.35:

$$\varepsilon_{ds}(t, t_o) = \varepsilon_{ds}(t_o) * \beta_{ds}(t, t_o), \qquad [2.35]$$

where

$$\varepsilon_{ds}(t_o) = \left[\left(100\frac{w}{c}\right)^2 * f_c^{\prime -0.23} + 200\right] * 10^{-6}. \qquad [2.36]$$

The effect of the relative humidity is given by:

$$\beta_{RH} = 1.22 - 1.75 * \left(\frac{RH}{100}\right)^3. \qquad [2.37]$$

The time function for drying shrinkage is expressed as follows:

$$\beta_{ds}(t, t_s) = \frac{(t - t_s)^{0.6}}{16 * \left(\frac{v}{100s}\right)^2 \gamma_{ds} + (t - t_s)^{0.6}}, \qquad [2.38]$$

where

$$\gamma_{ds} = 6.42 + 1.5\ln(t_s). \qquad [2.39]$$

Total shrinkage:

The total shrinkage is the sum of the basic shrinkage $\gamma_{bs}(t,t_s)$ and the drying shrinkage $\gamma_{ds}(t,t_s)$:

$$\gamma_s(t, t_s) = \gamma_{bs}(t, t_s) + \gamma_{ds}(t, t_s). \qquad [2.40]$$

Creep:

Within the range of stresses under specified loads ($\sigma_c < 0.5 \ f_c(t_o)$), creep is assumed to be linearly related to stress:

$$\varepsilon_\sigma(t, t_s) = \sigma(t_o) * \frac{1 + \phi_c(t, t_o)}{E_c(t_o)}, \qquad [2.41]$$

where $\phi_c(t,t_o)$ is the total creep coefficient and E_c is the modulus of elasticity of the concrete at the time of loading.

Total creep:

The total creep coefficient is the sum of the basic creep coefficient and the drying creep coefficient:

$$\phi_c(t,t_o) = \phi_{bc}(t,t_o) + \phi_{dc}(t,t_o).$$ [2.42]

Basic Creep:
$$\phi_{bs}(t,t_o) = \phi_{bc}(t_o) + \beta_{bc}(t,t_o)$$ [2.43]

$$\phi_{bc}(t_o) = 0.74 * (1 + t_o^{-0.4})$$ [2.44]

$$\beta_{bc}(t,t_o) = \frac{(t-t_o)^{0.5}}{\gamma_{bc} + (t-t_o)^{0.5}}.$$ [2.45]

The time function for basic creep is given by:

$$\gamma_{bc} = 0.29 + 0.5t_o^{0.7}.$$ [2.46]

Drying creep:
$$\phi_{dc}(t,t_o) = \phi_{dc}(t_o) * \beta_{RH} * \beta_{dc}(t,t_o)$$ [2.47]

$$\phi_{dc}(t_o) = 0.62 + 0.1t_o^{-0.8}.$$ [2.48]

The effect of the relative humidity (RH in %) on basic creep is:

$$\beta_{RH} = 1.22 - 1.75 * \left(\frac{RH}{100}\right)^3,$$ [2.49]

and the development of drying creep is as follows:

$$\beta_{dc}(t,t_o) = \frac{(t-t_o)}{0.04 * \gamma_{dc} * \frac{v}{s} + (t-t_o)^{0.5}}.$$ [2.50]

Here, v/s is the volume to surface ratio and γ_{dc} is defined as:

$$\gamma_{dc} = -3.2 + 8.5t_o^{0.3}.$$ [2.51]

2.10.2 American Concrete Institute (ACI 209) Model (1982)

This model was proposed by Branson *et al.* in 1971. The main inputs for creep

and shrinkage prediction are relative humidity, specimen size, curing period and age of

loading. This model predicts the creep coefficient. Correction factors are applied if the

conditions are different from the ideal condition stated in the standard [44]. The model

can be applied to different kinds of concrete and is very simple to apply.

Shrinkage:

The shrinkage strain $\varepsilon_{sh}(t,t_c)$ at age of concrete t (days) measured from the age of

drying t_c day is calculated using Equation 2.52:

$$\varepsilon_{sh}(t,t_c) = \frac{(t-t_c)^\alpha}{f+(t-t_c)^\alpha} * \varepsilon_{shu},$$ [2.52]

where f (in days) and α are constants for a given member shape and size that define the

time ratio part. For the standard condition in the absence of specific shrinkage data for

local aggregate and conditions, the average value suggested for the ultimate shrinkage

strain ε_{shu} is:

$$\varepsilon_{shu} = 780 \times 10^{-6} \text{ mm/mm (in/in.)}$$ [2.53]

$$f = 26.0e^{\{0.36(V/S)\}} \text{ in in.-lb units.}$$ [2.54]

A study of concrete strength versus time for predicting compressive strength at

any time requires an appropriate general equation in the form of:

$$f_c(t_o) = f_c' * \frac{t_o}{b+c*t_o},$$ [2.55]

where $f_c(t_o)$ = compressive strength of concrete at age of concrete loading, t_o, b, and c are

constants related to the type of element and the curing method used. Compressive

strength is determined in accordance with ASTM C39 from 6"x12" standard cylindrical specimens that are made and cured in accordance with ASTM C192.

Modulus of elasticity:

The modulus of elasticity is not the truly instantaneous modulus, but a modulus which corresponds to loads of 1-5 minutes duration. The modulus of elasticity of concrete is directly related to the concrete unit weight and compressive strength:

$$E_c(t_o) = 33 * \gamma^{1.5} * f_c(t_o).$$ [2.56]

The design approach for predicting creep and shrinkage refers to ideal condition and correction factor. It also requires the test data from an unrestrained shrinkage test at any time. These equations apply for all normal weight, light weight and regular light weight concrete under the standard condition. According to this model, creep and shrinkage is predicted as a fraction of its ultimate creep and shrinkage strain v_u and ε_u. At any time the creep strain is:

$$v_t = v_u * \frac{t^{0.6}}{10 + t^{0.6}},$$ [2.57]

and shrinkage at any time t is defined as:

$$\varepsilon_t = \varepsilon_u * \frac{t}{35 + t}.$$ [2.58]

Correction factor γ are applied to the ultimate values. However since creep and shrinkage for any period are linear functions of the ultimate values, the correction factors in this process may be applied to short term creep and shrinkage as well. Correction factor other than those for concrete composition may be used in conjunction with the specific creep and shrinkage data from a concrete tested in accordance with the ASTM C512.

Age of loading:

For greater than 7 days loading age, the correction factor is:

$$\gamma_{la}=1.25*t_{la}^{-0.118},$$ [2.59]

where t_{la} is the loading age in days.

Differential shrinkage:

For shrinkage considered for other than 7 days for moist cured concrete and other than 3 days for steam cured concrete, the difference in shrinkage for any period starting after this time should be determined. That is, the shrinkage strain between 28 days and one year would be equal to the shrinkage 7 days to 1 year shrinkage minus the 7 days to 28 days shrinkage.

Ambient relative humidity:

For ambient relative humidity greater than 40%, the following correction factors should be used for creep and shrinkage. Here λ stands for relative humidity in percent.

Creep $\gamma_\lambda = 1.27-0.0067*\lambda$ for $\lambda > 40$

Shrinkage $\gamma_\lambda = 1.4-0.01*\lambda$ for $40 < \lambda < 8 0$

Shrinkage $\gamma_\lambda = 3-0.03*\lambda$ for $80 > \lambda > 100$.

Average thickness of concrete other than 6 in or volume to surface ratio other than 1.5 in. The effect of the member size on concrete creep and shrinkage is basically influenced in two ways: the first one is the time ratio and the second one is the ultimate creep co efficient υ_u and the ultimate shrinkage strain, ε_{shu}.

Two methods are offered for estimating the effect of the member size on υ_u and ε_{shu}, which are the average thickness method and volume-surface ratio method.

Average-thickness method:

For members greater than 6" and up to about 12" to 15", the following equations are used.

During the first year of loading:

For creep $\gamma_h = 1.14 - 0.023*h$

For ultimate values,

Creep $\gamma_h = 1.1 - 0.017*h$

During the first year of drying:

Shrinkage $\gamma_h = 1.23 - 0.038*h$

For ultimate values:

Shrinkage $\gamma_h = 1.17 - 0.029*h$,

where h is the average thickness in inches of the part of the member under consideration.

Volume surface ratio method:

Equations 2.60 and 2.61 are used:

$$\text{Creep } \gamma_{vs} = \frac{2}{3}\left(1 + 1.13e^{\left(-0.54\frac{v}{s}\right)}\right) \qquad [2.60]$$

$$\text{Shrinkage } \gamma_{vs} = 1.2 * e^{\left(-0.12\frac{v}{s}\right)}, \qquad [2.61]$$

where v/s is the volume to surface ratio of the member in inches.

Correction for the composition of concrete:

The main disadvantage of the concrete composition correction factors is that concrete mix characteristics are unknown at the design stage and have to be determined. Since these correction factors are normally not excessive and tend to offset each other, in most cases these are neglected.

Correction for slump:

$$\text{Creep } \gamma_s = 0.82 + 0.067*S \qquad [2.62]$$

$$\text{Shrinkage } \gamma_s = 0.89 + 0.041*S, \qquad [2.63]$$

where s is the observed slump in inches.

Correction for fine aggregate percentage:

$$\text{Shrinkage } \gamma_\psi = 0.30 + 0.014*\psi \quad \psi < 50\% \qquad [2.64]$$

$$\text{Shrinkage } \gamma_\psi = 0.9 + 0.002*\psi \quad \psi > 50\%. \qquad [2.65]$$

Here, ψ is the ratio of the fine aggregate to total aggregates by weight expressed as percentage.

Cement content:

The cement content has a negligible effect on the creep co-efficient. An increase in cement content causes a reduced creep strain if the water content is kept constant. If the cement content is increased and the water content ratio is kept constant, slump and creep will also increase. Shrinkage is calculated using Equation 2.66:

$$\text{Shrinkage } \gamma_c = 0.75 + 0.00036*c, \qquad [2.66]$$

where c is the cement content in pounds per cubic yard. Equation 2.67 gives the effect of the air content:

$$\text{Creep } \gamma_a = 0.46 + 0.09*\alpha \text{ but not less than 1}, \qquad [2.67]$$

where α is the air content in percent.

The compliance function $J(t,t_o)$ that represents the total stress-dependent strain by unit stress is given by:

$$J(t,t_o) = \frac{1 + \phi(t,t_o)}{E_{cmt_o}}, \qquad [2.68]$$

where E_{cmto} is the modulus of elasticity at the time of loading to (MPa or psi), and $\emptyset$ (t, t_o) is the creep coefficient as the ratio of the creep strain to the elastic strain at the start of loading at the age t_o (days).

The secant modulus of elasticity of concrete E_{cmto} at any time t_o of loading is given by:

$$E_{cmt_o} = 33\gamma_c^{1.5}\sqrt{f_{cmt_o}}\ (\text{psi})\ \text{in in.-lb units,} \qquad [2.69]$$

where γ_c is the unit weight of concrete (kg/m^3 or lb/ft^3), and f_{cmto} is the mean concrete compressive strength at the time of loading (MPa or Psi) and is shown in Equation 2.70:

$$f_{cmto} = \left[\frac{t}{a+bt}\right]f_{cm28}, \qquad [2.70]$$

where f_{cm28} is the concrete mean compressive strength at 28 days in MPa or psi, a and b are constants and t is the age of concrete. Creep coefficient:

$$\phi(t,t_o) = \frac{(t-t_o)^\psi}{d+(t-t_o)^\psi}\phi_u, \qquad [2.71]$$

where $\phi(t,t_o)$ is the creep coefficient at concrete age t, due to a load applied at the age t_o, d (in days) and ψ are constants for a given member shape and size that define the time ratio part. The average value proposed for the ultimate creep coefficient ϕ_u is 2.35.

2.10.3 Model by Sakata (1996)

Sakata proposed this model for creep and shrinkage on concrete by a statistical method on the basis of experimental data. The equation can estimate the concrete creep and shrinkage strain [45]. These prediction equations of creep and shrinkage were adopted as the Japanese standard methods by Japan Society of Civil Engineers (JSCE) in

the revised standard Specification for Design of Construction and Concrete Structure published in 1996.

Equations predicted in this model are as follows:

$$\varepsilon_{cc}(t, t_1, t_o) = \varepsilon_{cr} * (1 - e^{-0.09(t-t_1)^{0.6}})$$ [2.72]

$$\varepsilon_{cr} = \varepsilon_{bc} + \varepsilon_{dc},$$ [2.73]

where ε_{cc} is the predicted specific creep (N/mm^2), ε_{bc} is the basic creep (N/mm^2), ε_{dc} is the drying creep (N/mm^2), t is the age of the concrete (days), t_1 is the age of loading of concrete (days), t_o is the age of the beginning of drying (days). This model can be used to calculate the basic creep with the w/c ratio as:

$$\varepsilon_{bc} = 15 * (c + w)^2 * \left(\frac{w}{c}\right)^{2.4} * \ln(t_1)^{-0.67},$$ [2.74]

where c is cement content (kg/m^3) and w is the water content (kg/m^3).

Considering parameters w/c, w+c , v/s , RH and t_o, drying creep is given in Equation 2.75:

$$\varepsilon_{dc} = 4500 * (c + w)^{1.4} * \left(\frac{w}{c}\right)^{4.2} * \ln\left(\frac{v}{10s}\right)^{2.2} * \left(1 - \frac{RH}{100}\right)^{0.36} * t_o^{-0.3},$$ [2.75]

where v/s is volume surface ratio of concrete member (mm) and RH is the relative humidity (%). Shrinkage is predicted by Equations 2.76 and 2.77:

$$\varepsilon_{cs}(t, t_o) = \varepsilon_{sh} * \left(1 - e^{-0.108*(t-t_o)^{0.6}}\right)$$ [2.76]

$$\varepsilon_{sh} = -50 + 78 * \left(1 - e^{\frac{RH}{100}}\right) + 38 * \ln(w) - 5(\ln(\frac{v}{10s}))^2,$$ [2.77]

where $\varepsilon_{cs}(t, t_o)$ is the predicted shrinkage and ε_{sh} is the ultimate shrinkage.

2.10.4 Bazant B3 Model (1997)

This model is proposed by Bazant and Baweja (1995). It was developed at Northwestern University. The latest B3 model considers more parameters than other prediction models. The following parameters are used: a) relative humidity, b) exposure of concrete specimen to temperature prior to drying, c) size, d) cement type, e) coarse and fine aggregate, f) concrete density, g) concrete age, h) specimen ultimate strength. This model is predicted for w/c ratio of 0.30 to 0.85 and strength 2500 to 10000 psi; it also has limitations for cement and aggregate. The model outputs are shrinkage strain and creep compliance [46].

The prediction model of the material parameters of the present model from strength and composition is restricted to Portland cement concrete with the following parameter ranges:

$$0.35 < \frac{w}{c} < 0.85 \qquad 2.5 < \frac{a}{c} < 13.5$$

$$2500 \text{ psi} < f_c', \text{ f} < 10000 \text{ psi} \qquad 10 \text{lbs/ft}^3 < c < 45 \text{ lbs/ft}^3,$$

where f_c is the ultimate strength of concrete in psi, w/c is the water cement ratio by weight, c is the cement content in lb/ft^3 and a/c is the aggregate to cement ratio by weight. The formulae are valid for concretes cured for at least one day. This model is valid for both normal weight and lightweight concrete [47].

The prediction model is restricted to the service stress range (for up to about 0.45f_c). The mean shrinkage strain ε_{sh} (t,t_c) in the cross section at the age of concrete t (days), measured from the start of drying at t_c is calculated from Equation 2.78:

$$\varepsilon_{sh}(t,t_c) = -\varepsilon_{sh\infty} k_h S(t - t_c), \qquad\qquad [2.78]$$

where $\varepsilon_{sh\infty}$ is the ultimate shrinkage strain, k_h is the humidity dependence factor, and

$S(t-t_c)$ is the time curve. The ultimate shrinkage $\varepsilon_{sh\infty}$ is given by:

$$\varepsilon_{sh\infty} = -\varepsilon_{s\infty}\frac{E_{cm607}}{E_{cm(t_c+\tau_{sh})}},$$ [2.79]

where $\varepsilon_{s\infty}$ is a constant which is defined as:

$$\varepsilon_{s\infty} = -\alpha_1\alpha_2\left[0.02565w^{2.1}f_{cm28}^{-0.28} + 270\right]\times10^{-6} \text{ in in.-lb units}$$ [2.80]

$$E_{cmt} = E_{cm28}\left(\frac{t}{4+0.85t}\right),$$ [2.81]

where w is the water content in lb/yd^3, f_{cm28} is the concrete mean compressive strength at

28 days in psi, and α_1 and α_2 are the constants.

The time function for shrinkage is:

$$S(t-t_c) = \tanh\sqrt{\frac{(t-t_c)}{\tau_{sh}}}.$$ [2.82]

Here, τ_{sh} is the size dependence of shrinkage given by:

$$\tau_{sh} = 190.8t_{cm28}^{-0.25}\left[2k_s(v/s)\right]^2 \text{ in in.-lb units.}$$ [2.83]

The average compliance function $J(t,t_o)$ at concrete age t caused by a unit uniaxial

constant stress applied at age t_o incorporating instantaneous deformation, basic and

drying creep is calculated from:

$$J(t,t_o) = q_1 + c_o(t,t_o) + c_d(t,t_o,t_c),$$ [2.84]

where q_1 is the instantaneous strain due to unit stress.

$$q_1 = \frac{0.6}{E_{cm28}}$$ [2.85]

$$E_{cm28} = 57000\sqrt{f_{cm28}} \text{ in in.-lb units.}$$ [2.86]

According to this model, the basic creep is composed of three terms, a) an aging viscoelastic term, b) a non-aging viscoelastic term, and c) an aging flow term:

$$C_o(t,t_o) = q_2 Q(t,t_o) + q_3 * \ln\left[1 + (t-t_o)^n\right] + q_4 * \ln\left(\frac{t}{t_o}\right),$$ [2.87]

where $q_2 Q(t,t_o)$ is the aging viscoelastic compliance term.

$$q_2 = 86.814 \times 10^{-6} c^{0.5} f_{cm28}^{-0.9} \quad \text{in in.-lb units.}$$ [2.88]

Q (t,to) is an approximate binomial integral that must be multiplied by the parameter q_2 to obtain the aging viscoelastic term.

Here,
$$Q(t,t_o) = Q_f(t_o)\left[1 + \left(\frac{Q_f(t_o)}{Z(t,t_o)}\right)^{r(t_o)}\right]^{-\frac{1}{r(t_o)}}$$ [2.89]

$$Q_f(t_o) = \left[0.086(t_o)^{\frac{2}{9}} + 1.21(t_o)^{\frac{4}{9}}\right]^{-1}$$ [2.90]

$$Z(t,t_o) = (t_o)^{-m} * \ln\left[1 + (t-t_o)^n\right]$$ [2.91]

$$r(t_o) = 1.7(t_o)^{0.12} + 8.$$ [2.92]

q_3 is the non-aging viscoelastic compliance parameter and q_4 is the aging flow compliance parameter; c is the cement content in lb/yd³ and a/c is the aggregate-cement ratio. These coefficients ar defined in Equations 2.93 and 2.94:

$$q_3 = 0.29(\frac{w}{c})^4 * q_2$$ [2.93]

$$q_4 = 0.14 \times 10^{-6}(\frac{a}{c})^{-0.7} \text{in in.} - \text{lb units}.$$ [2.94]

The compliance factor for drying creep is defined as:

$$C_d(t,t_o,t_c) = q_5\left[e^{\{-8H(t)\}} - e^{\{8H(t_o)\}}\right]^{\frac{1}{2}}.$$ [2.95]

q_5 is the drying creep compliance parameter and is given in Equation 2.96:

$$q_5 = 0.757 f_{cm28}^{-1} (\varepsilon_{sh\infty} \times 10^6)^{-0.6}.$$

[2.96]

H(t) and H(t$_o$) are spatial averages of pore relative humidity and are calculated as:

$$H(t) = 1 - (1 - h)S(t - t_c)$$

[2.97]

$$H(t_o) = 1 - (1 - h)S(t_o - t_c),$$

[2.98]

where S(t-t$_c$) and S(t$_o$-t$_c$) are the time function for shrinkage calculated at the age of concrete t and the age of concrete at loading t$_o$ in days, respectively, and τ_{sh} is the shrinkage halftime.

Time function for shrinkage calculation are given in Equations 2.99 and 2.100:

$$S(t - t_c) = \tanh\left[\left(\frac{t - t_c}{\tau_{sh}}\right)^{\frac{1}{2}}\right]$$

[2.99]

$$S(t_o - t_c) = \tanh\left[\left(\frac{t_o - t_c}{\tau_{sh}}\right)^{\frac{1}{2}}\right].$$

[2.100]

2.10.5 Comite European du Beton, CEB-FIP Model:

This model is recommended by CEB-FIP code. The model is based on the work of Muller and Hillsdorf. The main input factors for the prediction of creep and shrinkage are ultimate compressive strength, volume surface ratio, age of curing, age of loading, and relative humidity. This model predicts the creep coefficient [48]. Unless special provisions are given, the model is valid for ordinary structural concrete having a compressive strength of 3000 psi to 15000 psi. The concrete will also be subjected to a compressive stress $\sigma_c < 0.4 f_c$ (t$_o$) at an age of loading and a mean relative humidity of 50%

and at a temperature of $73° \pm 2°$ F. The total shrinkage strains of concrete $\varepsilon_{sh}(t,t_c)$ may be calculated from:

$$\varepsilon_{sh}(t,t_c) = \varepsilon_{cso}\beta_s(t-t_c),$$ [2.101]

where ε_{cso} is the notional shrinkage coefficient, $\beta_s(t-t_c)$ is the coefficient describing the development of shrinkage with time of drying, t is the age of the concrete (in days) at the moment considered, t_c is the age of the concrete at the beginning of drying (days), and $(t-t_c)$ is the duration of drying (days). The notional shrinkage coefficient can be obtained from Equations 2.102 and 2.103:

$$\varepsilon_{cso} = \varepsilon_s(f_{cm28})\beta_{RH}(h)$$ [2.102]

$$\varepsilon_s(f_{cm28}) = \left[160 + 10\beta_{sc}\left(9 - \frac{f_{cm28}}{f_{cm0}}\right)\right] \times 10^{-6}$$ [2.103]

$$\beta_{RH}(h) = -1.55\left[1 - \left(\frac{h}{h_o}\right)^3\right] \text{ for } 0.4 \le h \le 0.99.$$ [2.104]

The development of shrinkage with time is given by:

$$\beta_s(t-t_c) = \left[\frac{(t-t_c)}{350\left[\frac{v}{2s}\right]^2 + \frac{(t-t_c)}{t_1}}\right]^{0.5}.$$ [2.105]

The total load dependent strain at time t, $\varepsilon_{c\sigma}(t,t_0)$ of a concrete member uniaxially loaded at time t_0 with a constant stress $\sigma_c(t_0)$ is subdivided as follows:

$$\varepsilon_{c\sigma}(t,t_0) = \varepsilon_{ci}(t_0) + \varepsilon_{cc}(t,t_0),$$ [2.106]

where $\varepsilon_{ci}(t_0)$ is the initial elastic strain at loading and $\varepsilon_{cc}(t,t_0)$ represents the creep strain at time $t > t_0$. Both strain components may also be expressed by means of the tangent modulus of elasticity $E_c(t_0)$.

The creep coefficient $\varepsilon\,(t,t_o)$ is given in Equations 2.107 and 2.108:

$$\varepsilon_{ci}\left(t_o\right) = \frac{\sigma_c\left(t_o\right)}{E_c\left(t_o\right)}$$

[2.107]

$$\varepsilon_{cc}\left(t,t_o\right) = \frac{\sigma_c\left(t_o\right)}{E_c} * \phi\left(t,t_o\right).$$

[2.108]

Here, $E_c(t_o)$ is the tangent modulus of elasticity at a concrete age of t_0 and E_c is the elastic modulus at 28 days. By combining Equations 2.107 and 2.108 we get:

$$\varepsilon_{c\sigma}\left(t,t_o\right) = \sigma_c\left(t_o\right) * \left(\frac{1}{E_c\left(t_o\right)} + \frac{\phi\left(t,t_o\right)}{E_c}\right)$$

[2.109]

$$\varepsilon_{c\sigma}\left(t,t_o\right) = \sigma_c\left(t_o\right) * J\left(t,t_o\right).$$

[2.110]

The compliance function J (t,t_o) that represents the total stress-dependent strain by unit stress is given in Equation 2.111:

$$J\left(t,t_o\right) = \frac{1}{E_{cmto}} + \frac{\phi_{28}\left(t - t_o\right)}{E_{cm28}}.$$

[2.111]

The modulus of elasticity of the concrete at a concrete age t different than 28 days may be estimated from Equation 2.112:

$$E_{cmt} = E_{cm28}e^{\left[\frac{s}{2}\left(1 - \sqrt{\frac{28t_1}{t}}\right)\right]}.$$

[2.112]

S = the coefficient which depends on the type of concrete

t = age of concrete in days

t_1 = 1 day.

The effect of elevated and reduced temperature on the modulus of elasticity of concrete at an age of 28 days may be estimated from Equation 2.113:

$$E_{cm28} = 3118310 \left[\frac{f_{cm28}}{f_{cmo}} \right]^{\frac{1}{3}} \text{ in in.-lb units,} \qquad [2.113]$$

where f_{cm28} is the mean compressive cylinder strength of the concrete at 28 days (psi) and $f_{cmo} = 1450$ psi.

The mean compressive cylinder strength of the concrete is:

$$f_{cm28} = f_c' + 1160 \text{ in in.-lb units,} \qquad [2.114]$$

where f_c' is the specified compressive cylinder strength (psi) defined as that strength below which 5% of all possible strength measurements for the specified concrete may be expected to fall.

Within the range of service stresses, the 28-day creep coefficient $\phi_{28}(t - t_o)$ may be calculated from Equation 2.115:

$$\phi_{28}(t - t_o) = \phi_o \beta_c (t - t_o), \qquad [2.115]$$

where ϕ_o is the notional creep coefficient, $\beta_c(t - t_o)$ is the coefficient that describes the development creep with time after loading, t is the age of the concrete (days) at the moment considered, and t_o is the age of the concrete at loading (days). The notional creep coefficient ϕ_o may be determined from Equations 2.116 to 2.121:

$$\phi_o = \phi_{RH}(h)\beta(f_{cm28})\beta(t_o) \text{ with,} \qquad [2.116]$$

$$\phi_{RH}(h) = \left[1 + \frac{1 - \dfrac{h}{h_o}}{\left(\dfrac{0.1v}{2s} \right)} \alpha_1 \right] \alpha_2 \qquad [2.117]$$

$$\beta\left(f_{cm28}\right) = \frac{5.3}{\sqrt{\dfrac{f_{cm28}}{f_{cmo}}}}$$

[2.118]

$$\beta\left(t_o\right) = \frac{1}{0.1 + \left(\dfrac{t_o}{t_1}\right)^{0.2}}$$

[2.119]

$$\alpha_1 = \left[\frac{3.5 f_{cmo}}{f_{cm28}}\right]^{0.7}$$

[2.120]

$$\alpha_2 = \left[\frac{3.5 f_{cmo}}{f_{cm28}}\right]^{0.2},$$

[2.121]

where f_{cm28} is the mean compressive strength of concrete at the age of 28 days (psi), f_{cmo} = 1450 psi, h is the relative humidity of the ambient environment in decimals, h_o = 1, v/s is the volume to surface ratio (in).The coefficient $\beta_c\left(t - t_o\right)$ that describes the development of creep with time after loading may be determined from Equations 2.122 to 2.124:

$$\beta_c\left(t - t_o\right) = \left[\frac{\dfrac{\left(t - t_o\right)}{t_1}}{\beta_H + \dfrac{\left(t - t_o\right)}{t_1}}\right]^{0.3} \quad \text{with,}$$

[2.122]

$$\beta_H = 150\left[1 + (1.2\frac{h}{h_o})^{18}\right]\frac{v}{2s} + 250\alpha_3 \leq 1500\alpha_3$$

[2.123]

$$\alpha_3 = \left[\frac{3.5 f_{cmo}}{f_{cm28}}\right]^{0.5}.$$

[2.124]

The prediction model for shrinkage given in CEB-FIP model code predicts the time dependent strain of a nonleaded, plain structural concrete member which is exposed to a dry or moist environment after curing. The model is valid for ordinary normal weight structural concrete, moist cured at normal temperature for no more than 14 days, and

exposed to mean relative humidity in the range of 40 to 100 percent at mean temperature ranges from 10° F to 73° F. Strain due to shrinkage or swelling at normal temperature may be calculated from Equation 2.125:

$$\varepsilon_{cs}(t,t_s) = \varepsilon_{cso} + \beta_s(t-t_s),$$ [2.125]

where ε_{cso} = shrinkage coefficient

β_s = coefficient to describe the development of shrinkage with time

t = age of concrete in days

t_s = age of concrete in days at the beginning of shrinkage or swelling.

$$\varepsilon_{cso} = \varepsilon_s(f_{sm}) * \beta_{RH}$$ [2.126]

$$\varepsilon_s(f_{sm}) = \left[160 + 10 * \beta_{sc} * \left(9 - \frac{f_{cm}}{f_{cmo}}\right)\right] * 10^{-6},$$ [2.127]

where β_{sc} is a coefficient which depends on type of cement

= 4 for slowly hardening cement, SL

= 5 for normal or rapid hardening cement, N, R

= 8 for rapid hardening high strength cement, RS.

and $\beta_{RH} = -1.55 * \beta_s * RH$ 40% < RH < 99%

$B_{RH} = 0.25$ RH > 99%

where
$$\beta_s * RH = 1 - \left(\frac{RH}{RH_o}\right)^3.$$ [2.128]

f_{cm} is the compressive strength of the concrete in N/mm², and RH is the mean relative humidity of the ambient atmosphere in %, f_{cmo} =10 N/mm² and RH_0 =100%.

The development of shrinkage with time is given in Equations 2.129 and 2.130:

$$\beta_s(t - t_s) = \left(\dfrac{\dfrac{t - t_s}{t_1}}{\beta_{sh} + \dfrac{t - t_s}{t_1}} \right)^{0.5}$$

[2.129]

$$\beta_{SH} = 350 * \left(\dfrac{h}{h_o} \right)^2 \beta,$$

[2.130]

where (t-t$_s$) is the duration of drying or swelling in days, h = 2A$_c$/u (A$_c$ is the cross section of the structural member in mm^2), u = perimeter of the structural member in contact with the atmosphere in mm, h$_o$ = 100 mm and t$_1$ = 1 day.

2.10.6 Gardner Lockman GL 2000 Model

Gardner and Lockman proposed this model following the factors: a) relative humidity, b) average compressive strength, c) concrete member size, d) water to cement ratio, e) cement type, f) modulus of elasticity of concrete at the age of loading, g) concrete age at drying and h) concrete age at loading. This model is calibrated for compressive strength in the range of 2320 psi to 11890 psi, with volume to surface ratio larger than 0.76. The creep coefficient in this model is dependent on volume to surface ratio, age of drying, age of concrete at loading, and relative humidity.

The definition of the creep coefficient chosen is based upon the modulus of elasticity of the concrete at age of loading.

$$\text{Total strain} = \text{shrinkage strain} + \dfrac{\text{Stress}}{\text{Elastic modulus}} \, (1 + \text{creep coefficient}),$$

where Specific creep = Creep coefficient x elastic strain.

Compliance = (1+ creep coefficient) x elastic strain.

E$_{cmto}$ = mean modulus of elasticity.

For analysis purpose, the mechanical properties of mature concrete are considered as the functions of the uniaxial compressive strength. Equation 2.131is proposed for design purposes:

$$E_{cmt} = 3500 + 4300 * f_{cmt}^{0.5} \text{ (MPa)},$$ [2.131]

where E_{cmt} = mean modulus of elasticity at age t, and f_{cmt} = mean concrete strength at age t. If the experimental result for the development of concrete strength over time is not available, Equation 2.132 can be used:

$$f_{cmt} = f_{cm28} * \frac{t^{(\frac{3}{4})}}{a + b * t^{(\frac{3}{4})}}.$$ [2.132]

Here, a and b are the factors, depend upon the type of cement.

Shrinkage:

The following equation can be used to measure the shrinkage at time t from the concrete shrinkage data at 40% relative humidity with correction factors for ambient relative humidity: a) strength at the end of curing, b) duration of curing, c) member size.

It is assumed that the strain increased indefinitely that is why the ultimate shrinkage strain is not assumed. Shrinkage strain at any time $\varepsilon_{sh}(t, t_c)$ is calculated using Equation 2.133:

$$\varepsilon_{sh}(t, t_c) = \varepsilon_{shu}\beta(h)\beta(t - t_c),$$ [2.133]

where ε_{shu} is the ultimate shrinkage strain, $\beta(h)$ is the correction term for the effect of humidity, and $\beta(t - t_c)$ is the correction term for the effect of time of drying. The ultimate shrinkage ε_{shu} is given by Equation 2.134:

$$\varepsilon_{shu} = 900 k (\frac{4350}{f_{cm28}})^{\frac{1}{2}} \times 10^{-6} \text{ in in.-lb units,}$$ [2.134]

where h = humidity expressed as a decimal

t = age of concrete in days

t_c = age drying commenced, end of moist curing (days)

t_o = age of the concrete loaded (days)

V/S = volume surface ratio

f_{cm28} = concrete mean compressive strength at 28 days (psi)

f_{cmt} = concrete compressive strength when drying commenced (psi)

f_{cmo} = concrete compressive strength when loading commenced (psi)

The correction term for effect the of humidity $\beta(h)$ is given by

$\beta(h) = (1 - 1.18h^4)$.

The time function for shrinkage $\beta(t\text{-}t_c)$ is given in Equation 2.135:

$$\beta(t - t_c) = \left[\frac{(t - t_c)}{(t - t_c) + 77\left(\frac{v}{s}\right)^2} \right]^{\frac{1}{2}} \text{ in in.-lb units.} \qquad [2.135]$$

The compliance equation is composed of the elastic and the creep strains. The elastic strain is the reciprocal of the modulus of elasticity at the age of loading E_{cmto}, and the creep strain is the 28 day creep coefficient $\phi_{28}(t, t_o)$ divided by the modulus of elasticity at 28 days E_{cm28}. The creep compliance is the ratio of creep strain to the elastic strain due to the load applied at the age of 28 days and is given in Equation 2.136:

$$J(t, t_o) = \frac{1}{E_{cmto}} + \frac{\phi_{28}(t, t_o)}{E_{cm28}}. \qquad [2.136]$$

The 28 day creep coefficient $\phi_{28}(t,t_o)$ is calculated using Equation 2.137:

$$\phi_{28}(t,t_o) = \phi(t_c)\left[2\frac{(t-t_o)^{0.3}}{(t-t_o)^{0.3}+14}+(\frac{7}{t_o})^{0.5}\left(\frac{(t-t_o)}{(t-t_o)+7}\right)^{0.5} +2.5(1-1.086h^2)\left(\frac{(t-t_o)}{(t-t_o)+77(\frac{v}{s})^2}\right)^{0.5}\right].\qquad [2.137]$$

The creep coefficient includes three terms. The first two terms are required to calculate the basic creep, and the third term is for the drying creep; $\phi(t_c)$ is the correction term for the effect of drying before loading. If $t_o = t_c$. $\phi(t_c) = 1$.

2.11 Conclusion

Cracking due to shrinkage is one of the major problems of concrete. The cause of the cracking include shortcomings in materials, design practice and construction technique. Designers should be careful to specify materials to ensure long-term performance of the structure. The result of standard testing can help with adequate tool to select materials for durability. Sensibly choosing the materials can eliminate some of the cracking problems. Full scale testing can be performed to examine the behavior of structure under sustained loading. This test results can be incorporated with the design practice which will make the structure more durable and require less maintenance.

CHAPTER 3

MATERIALS AND EXPERIMENTAL METHODS

3.1 Introduction

In this chapter the mix proportions of the concrete used for the creep and shrinkage test and the variation in the mix design are discussed. ASTM standard tests performed to analyze the material properties and ACI guideline to make the sample are also described. ACI 211.1 standard specification was followed to prepare the test specimens. Mix design of the geopolymer concrete, sample preparation, curing and storing the test specimens was in accordance to the ASTM C192.

3.2 Concrete Mixture Evaluation

Concrete mixtures were selected from different activator solution to fly ash ratio and for different target strength of the hardened concrete. These parameters were selected to see the effect of sustained load on the concrete. Compressive strength of the concrete varied in ranges between 4000 psi to 8000 psi. No admixture was used to make the samples. The total amount of coarse and fine aggregate was constant for different mix design to see the effect of geopolymerization on the short and long term properties of GPC. All the mixes showed more than an 8 inch slump and the air content was below 4%. Cylinders were kept on a vibrating table for 30 seconds to remove any entrapped air bubble inside it. A total of 6 different GPC and 1 OPC concrete mixture were evaluated.

The OPC mix was used as a control sample to monitor the creep property from the testing frame and adjusting the setup for the test. The detailed mix proportions for these seven mix design is presented in Tables 3.1, 3.2, and 3.3.

3.2.1 Mix Proportion of Concrete

Concrete mixtures were selected from the specific strength range using the particular mix design of the activator solution and fly ash type. The range of designed compressive strength of concrete varied from 4000 to 8000 psi at three days. Class F fly ash was used for the design of concrete cylinders. The only parameter varied to obtain the designed strength was the activator solution to fly ash ratio. Mix design was selected from the preliminary test. The detailed mix proportion for the six mixtures is presented in Table 3.1 to 3.3.

Table 3.1 Mix design of GPC with the variation in AS/FA ratio.

Raw	Mix Design (lb/yd^3)			
Fly Ash DH	943	943	943	943
Pea Gravel	1464	1464	1464	1464
River Sand	1213	1213	1213	1213
Silicate N	198	255	311	368
Hydroxide 14	132	170	207	245
AS/FA	0.35	0.45	0.55	0.65

The second set of mix design was prepared to observe the effect of the extent of geopolymerization. In this test program, the aggregate to fly ash ratio was kept constant.

Table 3.2 Mix design of GPC with the variation in compressive strength.

Raw Material	4000 Psi (lb/yd^3)	Raw Material	8000 Psi
Fly Ash DH	999	Fly Ash DH	999
Pea Gravel	1486	Pea Gravel	1486
River Sand	1032	River Sand	1032
Silicate N	197	Silicate D	197
Hydroxide 10	132	Hydroxide 14	132

OPC mix design was prepared to see the capacity of the loading frame and to use it as a control sample. The mix proportion was selected to get a concrete mix with design strength of 8000 psi.

Table 3.3 Mix design of high strength OPC.

Material	Working Mix Design (lb/yd^3)
Cement	1166
Pea Gravel	1464
River Sand	1062
Water	350
W/C	0.3

This particular mix design was prepared to make a set of samples consisting of cylinders, beams, prism, ring, and cube. OPC samples were prepared and stored according to ASTM C31.

3.2.2 Mix Ingredients

The mix ingredients used in producing the GPC mixtures are described in the following paragraphs. Fly ash was activated with the alkaline solutions and normal coarse and fine aggregates were used as filler material.

Fly ash: The fly ash used in this study was collected from the Dollet Hills powerplant company. Chemical analysis of the fly ash is given in Table 3.4:

Table 3.4 Chemical analysis of fly ash (mass %).

Oxides	Mass (%)
SiO_2	61.23
Al_2O_3	19.20
Fe_2O_3	7.27
CaO	5.64
MgO	2.23
Na_2O	1.11
K_2O	1.28
TiO_2	0.97
SO_3	0.29
LOI	0.06

Coarse aggregate: Only one type of gravel is used throughout this study. Normal pea gravel was used. The gradation of the aggregate is displayed in Table 3.4. This aggregate was used from the same batch of supply to make all the samples to avoid any kind of discrepancy in the experimental plan. Figure 3.1 shows the sieve analysis of coarse aggregate. Sieve analysis of the coarse aggregate is given in Table 3.5.

Table 3.5 Sieve analysis of coarse aggregate.

Sieve #	Sieve Size (mm)	Mass of Sieve (gm) A	Mass of Sieve + Agg (gm) B	Mass of Agg. Retained (gm) B-A	% of Mass Retained (Rn)	Cumm. Of % Retained ($\sum$Rn)	% Finer (100 - $\sum$Rn)
1.5"	37.5	548.6	548.6	0	0	0	100
1"	25.4	840.4	891.4	51	2.13	2.13	97.86
1/2"	12.9	547.1	1830.2	1283.1	53.75	55.89	44.11
# 4	4.75	510.9	1561.8	1050.9	44.02	99.91	0.08
# 8	2.36	474.8	475.4	0.6	0.025	99.94	0.06
Pan	-	366.9	368.3	1.4	0.058	-	-
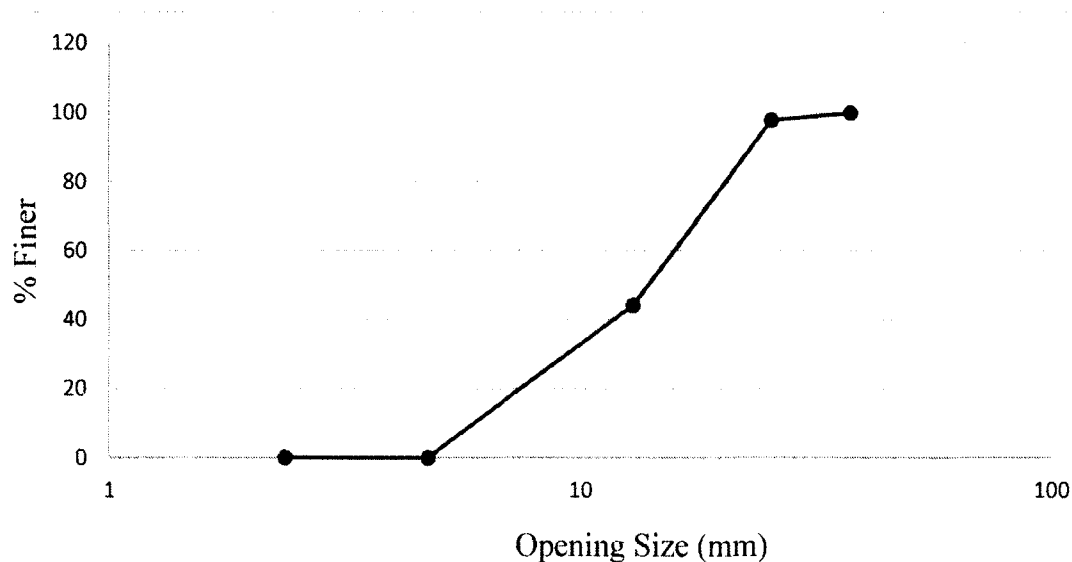
Figure 3.1 Sieve analysis of coarse aggregate.

Fine aggregate: The material was transported from the same source as the coarse

aggregates. The fine aggregate was used in SSD condition before it was mixed with the

other mix ingredients in the production of concrete. Fineness modulus of the fine

aggregate was 2.31 and the specific gravity was 2.64. Sieve analysis of the fine aggregate

is presented in Table 3.6:

Table 3.6 Sieve analysis of fine aggregate.

Sieve #	Sieve Size (mm)	Mass of Sieve (gm) A	Mass of Sieve + Agg (gm) B	Mass of Agg. Retained (gm) B-A	% of Mass Retained (Rn)	Cumm. Of % Retained d ($\sum$Rn)	% Finer (100 - $\sum$Rn)
3/8"	9.50	642.50	642.50	0.00	0.00	0.00	100.00
# 4	4.75	511.00	511.60	0.60	0.04	0.04	99.96
# 8	2.36	474.70	507.50	32.80	2.17	2.21	97.79
# 16	1.18	414.30	517.40	103.10	6.81	9.02	90.98
# 30	0.60	529.80	864.90	335.10	22.13	31.15	68.85
# 50	0.30	390.00	1275.90	885.90	58.51	89.66	10.34
# 100	0.15	503.70	649.70	146.00	9.64	99.30	0.70
Pan	-	366.80	377.40	10.60	0.70	-	-
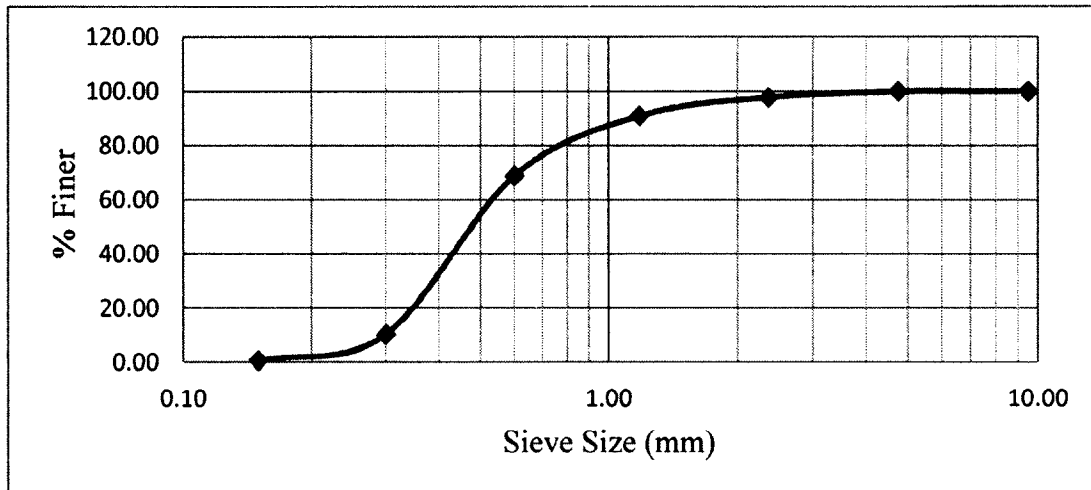
Figure 3.2 Sieve analysis of fine aggregate.

Water: Tap water was used throughout the experiments in an attempt to mimic the field conditions. Normal temperature water obtained from the laboratory was used to produce the concrete mixtures. Temperature of the water was 64° F.

Sodium hydroxide: Different concentration of hydroxide solution was used in this experiment. The concentrated 50% alkaline solution was converted to 14 molar and 12 molar solutions.

Sodium silicate: Silicate N and silicate D was used in this experiment to see the effect of creep and shrinkage. Silicate D is a more concentrated solution which gives more strength to the GPC, and silicate N is a less dense solution than silicate D. Silicate D contains a large amount of solids; therefore more reactive material will be available to participate in the reaction and that is why silicate D provides better compressive strength.

3.3 Manufacturing the Concrete Specimens

For each batch two cubic feet of fresh concrete was produced. Tests were conducted to assure the target slump as well as the air content of the GPC. A small

mixing machine was used for this purpose. Six 6"x12" cylinders and two ring specimens and the two prism specimens were produced from each batch. A mix design spreadsheet which includes mix proportion by weight of all ingredients was generated. Samples of the coarse and the fine aggregate were dried overnight to calculate their in situ moisture content. Absorption was calculated and extra water was added to ensure the slump of the mix.

3.3.1 Concrete Mixing Procedure

The mix design was chosen based on a previous study and preliminary tests were carried out to obtain a formulation suitable for handling necessary changes in the fresh mix behavior due to the unique characteristics of the geopolymer concrete. The activator solution was adjusted depending on the consistency of the mix. Well graded sand and pea gravel were used as fine and coarse aggregate, respectively. The fly ash to activator solution ratio was 1 to 3 and the coarse to fine aggregate ratio was 1. The mixing sequence was chosen to promote the first phase of geopolymerization (dissolution of silicate and aluminates species). Mixing was carried out as follows:

(1) The aggregate and sand were mixed for 60 seconds

(2) Silicate added and mixed for 30 seconds

(3) Fly ash was added and mixed for 30 seconds

(4) NaOH solution was added and mixed for another 30 seconds.

For each batch, fresh properties of concrete were tested to make sure that the target slump, flow as well as air content was achieved. Gravity mixing machine was used for this purpose. With this amount of the concrete mix, cylinders were made to test the compressive strength and elastic modulus of at different ages. After the mixing and

testing procedures are completed the fresh concrete was placed into a 6 x 12 and 4 x 8 in plastic cylindrical molds. Among six specimens, two were used for compressive strength, two were loaded and observed for total deformation from the creep frame, and two were kept unloaded to use as a control to indicate deformations due to causes other than load. All specimens went through the same curing and storage treatments as the loaded specimen. After consolidation a trowel was used to finish the surface of all concrete specimens. The tops of cylinders were then covered with plastic lids in order to avoid any moisture loss due to evaporation.

All specimens were allowed to cure in the mixing room environment during the first 24 hours (ASTM C192), then all molds were removed and specimens were properly labeled and then moved to a storage room.

3.4 Curing Conditions for Concrete Specimens

The concrete specimens for the compressive strength test, split tensile strength test, and elastic modulus test were cured in an oven at 140° F for 24 hours. After curing, those samples were allowed to stay under standard environmental condition (50% RH and 72° ± 2° F).

3.5 Tests on Fresh Concrete

The concrete mix were tested to ensure that the samples are being manufactured with desired slump, setting time, density, air content and other fresh properties. Listed in Table 3.7 are the ASTM standard tests performed to see the fresh properties of GPC.

Table 3.7 List of the tests done on fresh concrete.

Test	Setting time	Density	Air content	Slump	Temperature
Standard	ASTM C403	ASTM C138	ASTM C173	ASTM C143	ASTM C1064

3.5.1 Setting Time Test

To perform the setting time test, ASTM C403 was followed. Setting time was obtained only for the mortar portion of the concrete. Initial and final setting time were determined according to the standard. Figure 3.3 shows setting time test.

Figure 3.3 Measuring setting time with Vicat apparatus.

3.5.2 Air Content Test

Air content of the concrete was measured following the ASTM C173. Air-meter was utilized to find the air content of the concrete. No air entraining agent was used to increase the entrained air in the concrete. The mold was made with aluminum and the surface of the mold was coated with the non-reacting paint so that the geopolymer did not react with it. Water was inserted inside the mold to make them air tight. The mold was

tapped with rubber mallet to make sure that no void remained inside. Air content test is

shown in Figure 3.4.
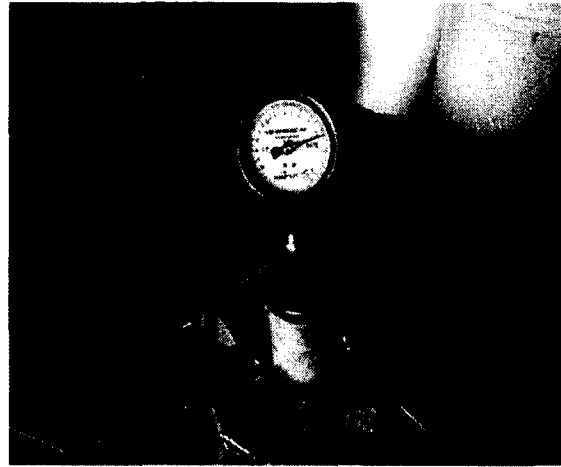
Figure 3.4 Air content measurement.

3.5.3 Unit Weight Test

The unit weight of the concrete was measured following ASTM C138. The same

container for the air content test was utilized to measure the unit weight of concrete. The

volume of the container was known. It was filled with freshly mixed concrete and leveled

with the plainer. The weight of the empty container and the container filled with concrete

was measured separately. The unit weight was calculated using the following equation:

$$\text{Unit weight} = \frac{M_f - M_e}{V},$$

where M_f = weight of the container full with concrete

M_e = weight of the empty container

V = volume of the container.

3.5.4 Slump Test

Slump of the concrete was measured following ASTM C138. The slump cone was first wiped with water and then filled with three layers of concrete. Each layer of concrete was compacted with the 25 blow of the tamping rod. After filling the mold completely with concrete, it was removed and the slump was measured. Measured slump was reported in the unit of inch. Figure 3.5 shows the slump test of 8000 psi OPC and GPC.
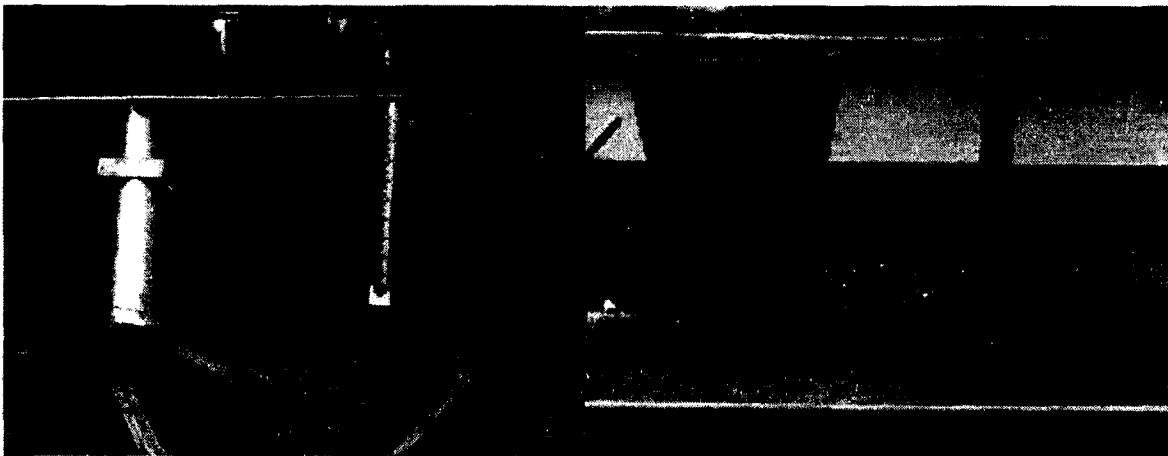
Figure 3.5 Measurement of slump 8000 psi OPC (left) and GPC (right).

3.5.5 Temperature Test

Temperature of the concrete was determined following the ASTM C1064 standard. Thermometer used to check the temperature was acquired from the Humboldt standard equipment. Freshly mixed concrete was kept in a container and the thermometer was inserted inside it to measure the temperature.

3.6 Tests on Hardened Concrete

A list of the tests performed on the hardened concrete is given in Table 3.8:

Table 3.8 List of the tests done on the hardened concrete.

Test	Compressive Strength	Splitting Tensile Strength	Elongation	Elastic Modulus	Shrinkage	Creep
Standard	ASTM C39	ASTM C496	ASTM C157	ASTM C469	ASTM C1581	ASTM C512

3.6.1 Compressive Strength Test

The compressive strength test was run in accordance with ASTM C39. Figure 3.6 shows the setup for the compressive strength test. The testing machine used was a M-test quarto machine with a maximum load capacity of 400,000 lb. Tests were run according to the standard which indicates that the load rate should be 35 psi/sec. Three 4 x 8 in (101.6 x 203.2 mm) cylindrical specimens per batch per curing condition were tested for analysis. Before testing, the cylinders were capped with sulfur so that two end surfaces were made even to support the applied load uniformly. Compressive strength was determined at the age of 1, 3, 7, 14, 28, and 56 days. The compressive strength of the specimen was calculated using the following equation:

Compressive strength $f_c = \dfrac{P}{A}$,

where P = ultimate load attained during the test in pounds (lb), and

A = loading area in square inches (in^2).
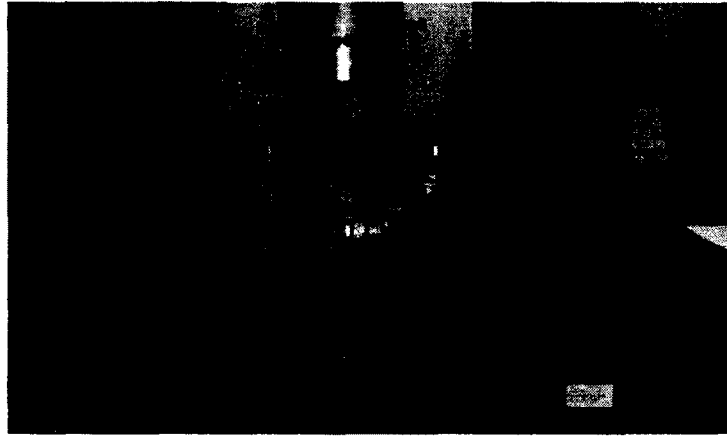
Figure 3.6 Compression test.

Among the three replicate specimens per condition, one specimen was first tested to determine its ultimate compressive strength so that the modulus of elasticity test could be run at 40% of the ultimate strength of the concrete. The modulus of elasticity test was then run on the two remaining specimens to get the results. The average 1 day compressive strength test result of all geopolymer mixes investigated in this study are summarized in Table 3.9.

Table 3.9 Average compressive strength of the cylinders after curing.

GPC Mix ID	AS/FA	Total Load (Kip)	Breaking Stress (psi)
GP35	0.35	144.20	5100
GP45	0.45	127.23	4500
GP55	0.55	113.01	4000
GP65	0.65	106.03	3750
GP4000	0.50	113.01	4000
GP8000	0.50	212.06	7500
OPC	0.30	226.20	8000

3.6.2 Splitting Tensile Strength Test

The splitting tensile strength test was run in accordance with the procedures following ASTM C496. Three 4 x 8 in (101.6 x 203.2 mm) cylindrical specimens per condition were used for this test. The test setup is shown in Figure 3.7. Splitting tensile strength of the specimen was calculated using the expression below:

Splitting tensile strength, $f_t = 2P/\pi l d$. Where

P = maximum applied load

l = length of the cylindrical specimen; and

d = diameter of the cylindrical specimen.
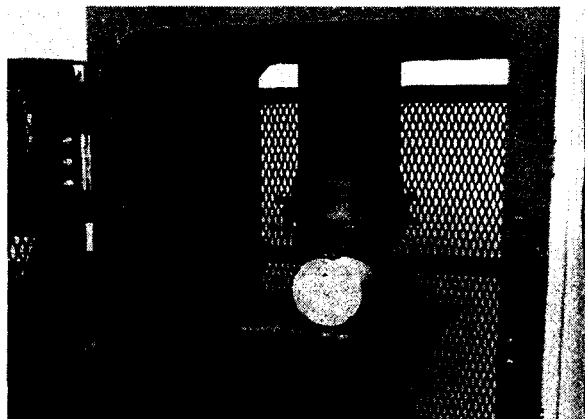
Figure 3.7 Splitting tensile strength test.

The average splitting tensile strengths at various ages of curing times of the fourteen concrete samples both GPC and OPC are displayed in Table 3.10.

Table 3.10 Splitting tensile strength at different age of concrete.

Mix Number	W/C AS/FA	fc 1Day (Psi)	Splitting tensile strength at different ages of concrete (Psi)					
			3	7	14	28	56	91
GP35	0.35	5100	532	537	543	543	544	545
GP45	0.45	4500	485	490	494	495	496	497
GP55	0.55	4000	448	452	457	457	458	458
GP65	0.65	3750	429	433	437	438	439	439
GP4	0.5	4000	457	462	466	467	467	468
GP8	0.5	7500	645	652	658	659	660	661
OPC	0.3	8000	750	757	765	775	786	793

It can be seen from the test result that the splitting tensile strength has a defined relation with the compressive strength of the cylinders. The water cement ratio plays a very important role in the case of both types of concrete. The extent of geopolymerization plays an important role in the case of strength of the GPC specimen, which is later affiliated with the increment of amorphous content increase in the GPC [49].

3.6.3 Elastic Modulus Test

The average elastic modulus values at various curing ages of the concrete mixes evaluated are displayed in Table 3.11.

Table 3.11 Modulus of elasticity of concrete cylinders from nondestructive test.

Mix Number	W/C AS/FA	FA/Agg C/Agg	EM at different ages of concrete (Ksi)					
			3	7	14	28	56	91
GP35	0.35	0.35	3871	3909	3948	3952	3960	3964
GP45	0.45	0.35	3526	3561	3596	3600	3607	3611
GP55	0.55	0.35	3256	3288	3321	3324	3331	3334
GP65	0.65	0.35	3119	3150	3181	3184	3191	3194
GP4	0.50	0.35	3324	3357	3390	3394	3400	3404
GP8	0.50	0.35	4694	4740	4788	4793	4802	4807
OPC	0.30	0.46	5454	5508	5563	5569	5580	5585

It can be seen from this study that the elastic modulus of the GPC sample varies from 3000 Ksi to 5000 Ksi.

3.6.4 Free Shrinkage Test

Square prism specimen with dimensions of 2 x 2 x 11.25 in. (50 x 50 x 286 mm) was used in the free shrinkage test in accordance with ASTM C157 method. Figure 3.8 shows the samples and the device for the test. Elongation of the specimen was measured with the elongation meter. The gage reading of the device was a millionth of an inch. To make the specimen for the elongation test, the same mix from the batch for each test set was used. First, the mold was carefully sprayed with Teflon so that the material did not stick to the surface of the mold. The metal stud at the two ends of the mold was inserted carefully so that it does not touch any releasing agent. After the concrete mixing, the fresh concrete was placed into the mold in two equal layers vibrating each layer for 30 seconds by placing the molds over a vibrating table. Specimens were kept in ambient

condition for one day and heat cured in the oven at a temperature of 140° F (60° C) for

another 24 hours.
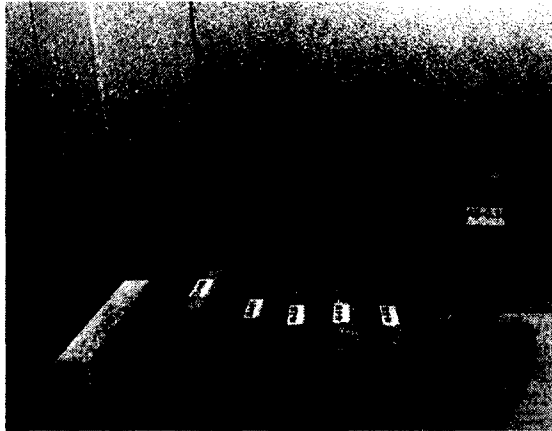
Figure 3.8 Free shrinkage test.

3.6.5 Restrained Shrinkage Test

This test was performed following the ASTM C1581. Foil strain gages were used

to measure the strain on the surface of the steel inner ring. The outer ring was used with a

PVC two part mold with a hinge system [50]. Data acquisition system was utilized to

collect the data from the strain gage system. The raw data obtained from the data

acquisition system was plotted to measure the day of cracking. Detailed arrangement for

the restrained shrinkage test is described in the methodology part.

3.6.6 Creep Test

In this method, 6 x 12-in (152.4 x 304.8-mm) cylindrical concrete specimens are

cast, and the free shrinkage of the concrete specimens was measured by means of a

Whittemore gage. Pairs of gage points with a gage distance of 10 in. (254 mm) were

placed in each test concrete specimen. A Whittemore gage is used to measure the change

in distance between the gage points due to drying shrinkage. A gage point positioning

guide was used to mark the gage point where the metal studs will be located. Each pair of

stud was placed at an angle of 120° apart. Figure 3.9 shows the concrete cylinders with

the gage points attached on them after the molds have been removed. More description is

stated in the next chapter.
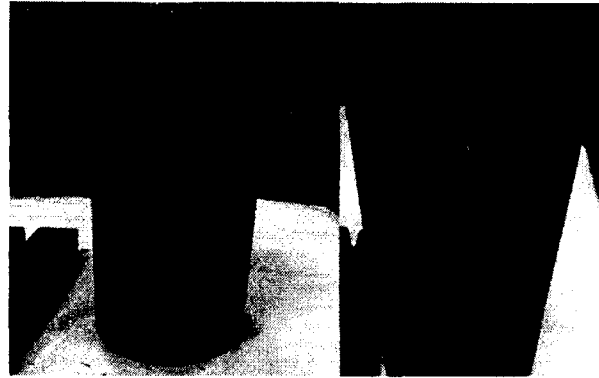
Figure 3.9 Brass stud attached to the concrete cylinder.

A Whittemore gage was used to measure the change in the distance between the

gage points as the concrete cylinder shrinks [51]. The Whittemore gage has a resolution

of 0.0005 in. Three sets of measurements were taken from each specimen and can be

expressed as follows:

$$\varepsilon_{sh} = \frac{1}{3}\sum_{i=1}^{3}\frac{(l_i - l_o)}{l_o}, \qquad [3.1]$$

where l_i = measured distance between i^{th} pair of gage points

l_o = original distance between i^{th} pair of gage points measured immediately after

demoulding.

CHAPTER 4

APPARATUS DESIGN AND TESTING PROCEDURE

4.1 Introduction

This chapter describes the design of the shrinkage and creep test apparatus following ASTM C1581 and ASTM C512. Mold for the preparation of the sample was guided by the specification given in the standard. Temperature and humidity of the storage chamber was strictly maintained throughout the entire testing period due to the sensitivity of the test to these parameters.

4.2 Design Requirements of Shrinkage Test Apparatus

The shrinkage test apparatus was prepared following ASTM 1581. The mold was prepared with a metal pipe section as the inner ring and a PVC two-part outer ring. Strain gages were attached to the inner metal ring to calculate the shrinkage strain caused by the drying of concrete. Data acquisition system was used to calculate the deformation occurred in the strain gage and the stress in concrete was also analyzed from this data. Ring specimens are more commonly used because of the benefits that they can easily be cast and the end effects are removed providing an axi-symmetric geometry [52]. The following are the design requirement for the shrinkage test apparatus:

- If the thickness of the steel is too large, no measurable deformation occurs in the steel. Such test setups have provided qualitative evaluations, but have not established

a simple procedure to routinely quantify the restrained characteristics of the material

[53].

- The steel strain is measured by the foil strain gage, which provides an accurate

  assessment of the time to cracking.

- Cracking of the test specimens are indicated by a sudden decrease in compressive

  strain in the steel ring. The measured strain provides the basis for quantifying the

  restrained shrinkage behavior of the concrete specimen.

- Strain gages were placed at mid height of the steel annulus, where the average strain

  is measured.

- Thickness of the steel was 0.5 inch and the concrete wall's thickness was maintained

  1.5 inch for all specimens [54].

4.2.1 Manufacturing the Outer and Inner Mold

The steel ring for the inner part of the mold was prepared from the steel pipe

section of the standard size. Dimension of the steel ring was selected following the

ASTM C1581. Mold used for the restrained shrinkage test is shown in Figure 4.1.

Figure 4.1 Manufacturing the inner steel ring and outer PVC split mold.

Thickness of the steel ring was 0.5 in and the inside diameter of the ring was 12

in (30.48 cm). The steel pipe was cut according to the specified height given in the

standard. The edge of the ring was grinded with fine sand paper. The inner and outer

surfaces of the steel ring were cleaned using the sand blasting apparatus to remove any

oil and grease. The steel pipe used to prepare the inner mold was obtained from the

industrial quality 75 Ksi steel welded joint pipes.

4.2.2 Attaching the Strain Gages to the Inner Ring

The steel ring obtained from the pipe section was further prepared to put the foil

strain gage to the inner surface. Two strain gages were put on the surface 180° apart.

First, the steel was ground with the coarse sand paper, and then the surface was polished

with fine sand paper. Strain gages were one inch long and half an inch wide. Attaching

the foil strain gage to the steel ring is shown in Figure 4.2. The steel surface below the

strain gages were then rubbed with isopropyl alcohol, a conditioner and a neutralizer.

Special glue was used to stick the gages to the surface of the ring.

Figure 4.2 Strain gage installation to the inner steel ring.

Once the strain gages were attached to the surface of the steel ring, the end of the gages was welded with the wire to connect to the data acquisition system. The wire end was tested with a voltmeter to check the connection to ensure proper data collection from the strain gages. Once the connections were made, the ring was placed on a vibration free table to prevent interruptions.

4.2.3 Data Acquisition System

The data acquisition system used to collect the strain data was set to read the strain from each ring at an interval of 3 minutes. This time interval was selected from the standard test procedure. Data obtained from the computer was collected and analyzed using the gage constant to convert the voltage data to the strain data. Figure 4.3 shows the arrangement for the restrained shrinkage test.

Figure 4.3 Preparing the ring specimen.

Data collection from the acquisition system was stopped when the crack formed at the outer surface of the concrete propagated to the inner ring, and there was no change in the reading obtained from the strain gages.

4.2.4 Environmental Chamber

The rate of shrinkage can change due to temperature and relative humidity. It is very important to keep concrete specimen in a controlled environment to measure the shrinkage accurately. For this test an environment chamber (Figure 4.4) with dimensions 30 x 15 x 8 ft was made with thick insulated aluminum walls including the door.
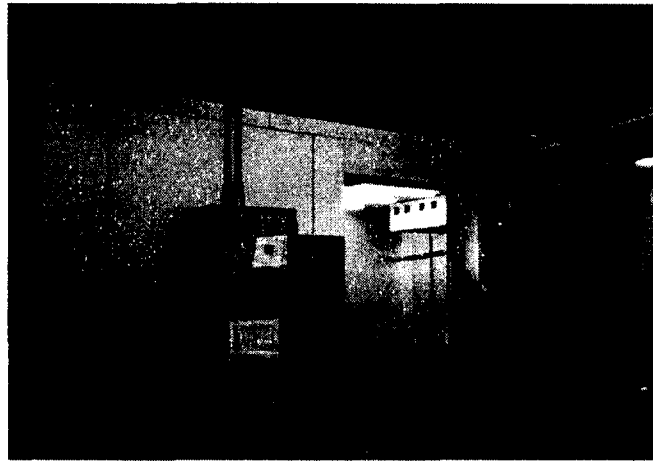
Figure 4.4 Temperature and humidity controlled chamber.

This chamber helped to keep the specimen at the right temperature and humidity without too much stress on the mechanical devices. There was an arrangement to read the actual temperature and humidity by the digital panel from outside the chamber. For this experiment the environment chamber was kept at a constant temperature of $73\pm3^\circ$ F and a relative humidity of 50 ± 4 [55].

4.2.5 Strain Data Calculation

Each sample was equipped with two strain gages. In order to record the strain reading at the same time for three months of testing, the data acquisition system is essential. Data logger used was manufactured by Hewlett Packard and they contain 96 channels for strain readings. This also allows multiple mixes to be recorded at the same

time. Every three days the data was collected from the data logger to a computer. The file obtained from the data acquisition system was processed through the data logger software and a spreadsheet was used to plot the strain over time. These strains were also monitored to see whether there is a trend of cracking in any of the ring specimen. Cracking strain capacity on the other hand was also determined by the elastic modulus test and splitting tensile strength test. The following equation was used to determine the cracking strain:

$$\varepsilon_t = \frac{\sigma_t}{E}. \qquad\qquad [4.1]$$

E = Elastic modulus

ε_t = Cracking strain

σ_t = Tensile splitting strength.

4.3 Design Requirements of Creep Test Apparatus

The following are the requirements to satisfy the design setup for the creep test.

- The load frame should be designed in a way so that the maximum load can be applied on the specimen for a long time without any changes in it.

- Relaxation of the spring and the deformation of the bearing plate should not cause a load reduction of more than 2% of the load capacity of the frame.

- Several specimens can be stacked for simultaneous loading so that more reading on the deformation can be taken. In this way reliability of the result will increase by taking the average of all measurements.

- Measures should be taken to align the specimens properly to prevent any bending load on the cylindrical specimens.

4.3.1 Design of Creep Apparatus

For this experimental work, the maximum capacity of the creep apparatus was determined according to the maximum compressive strength of the concrete. Parts for this apparatus were selected in such a way that it can maintain a constant sustained load for at least one year.

4.3.2 Determination of the Maximum Capacity of the Creep Apparatus

Maximum compressive strength of the concrete used in this study was 8000 psi. ASTM C512 says that the load applied on the cylinder for the creep test should be 40% of the maximum compressive strength of the cylinder. So the load capacity of the frame should be the surface area times the maximum stress applied on the cylinder, which is 3200 psi. The maximum load was 3200*28.274 = 90.5 kip.

4.3.3 Design of Springs

Five sets of railway locomotive suspension spring (Figure 4.5) were used for each frame. Load capacity for each set of spring was 21,300 lb. For the larger spring the outside diameter of the outer coil (OD) = 5.5"

Full height (FH) = 8.52"

Bar = 1-7/32"

Solid capacity = 15,959 lbs.

For the inner smaller spring the diameter of outer coil (OD) = 2.9375"

FH = 8.52"

Bar = 11/16"

Solid capacity = 5,386 lbs.

With five sets of springs, the load capacity was 5*21300 = 106,500, which is well above 90,464 lb. A solid work drawing of the creep frame model is shown in Figure 4.6.
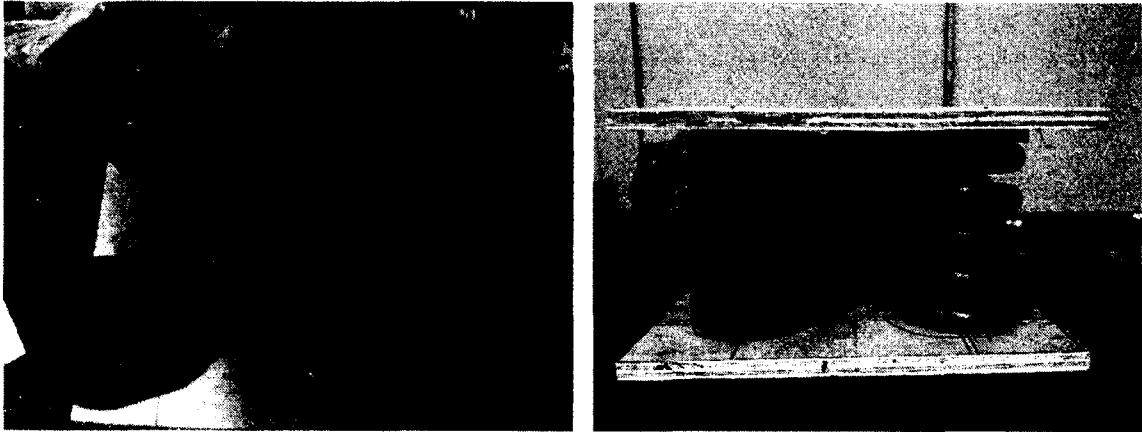
Figure 4.5 Railroad spring for sustained load.
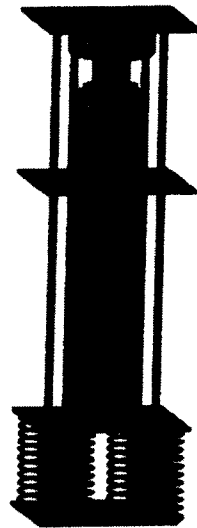
Figure 4.6 3-D view of the creep frame.

4.3.4 Design of Gage Point Positioning Guide

Gage point studs were put in the concrete cylinder at 120° apart. Three pairs of gage points with a gage distance of 10 inches were placed in each test specimen. A gage-

point positioning guide was made to position the gage points on the plastic cylinder mold. By inserting a 6 x 12 cylinder mold into the gage point positioning guide and tightening the six screws on the guide was the procedure to mark the position of the studs with the gage distance of 10 inches and 120° angle along the periphery of the specimen [56]. The initial gage length for the studs is very important because the high resolution of the strain measuring the device allows it to move only 0.25 in.

4.3.5 Design of Header Plate

To design the header plate, the finite element analysis software ANSYS was used and checked with the maximum deformation in the plate due to that load. From the analysis, it was found that the maximum deformation in the plate was less than 0.00064 in at the center of the plate. Thus a header steel plate with a thickness 1.5 in was selected to make the frame for testing. Figure 4.7 shows the stress in the plate and the maximum deformation.
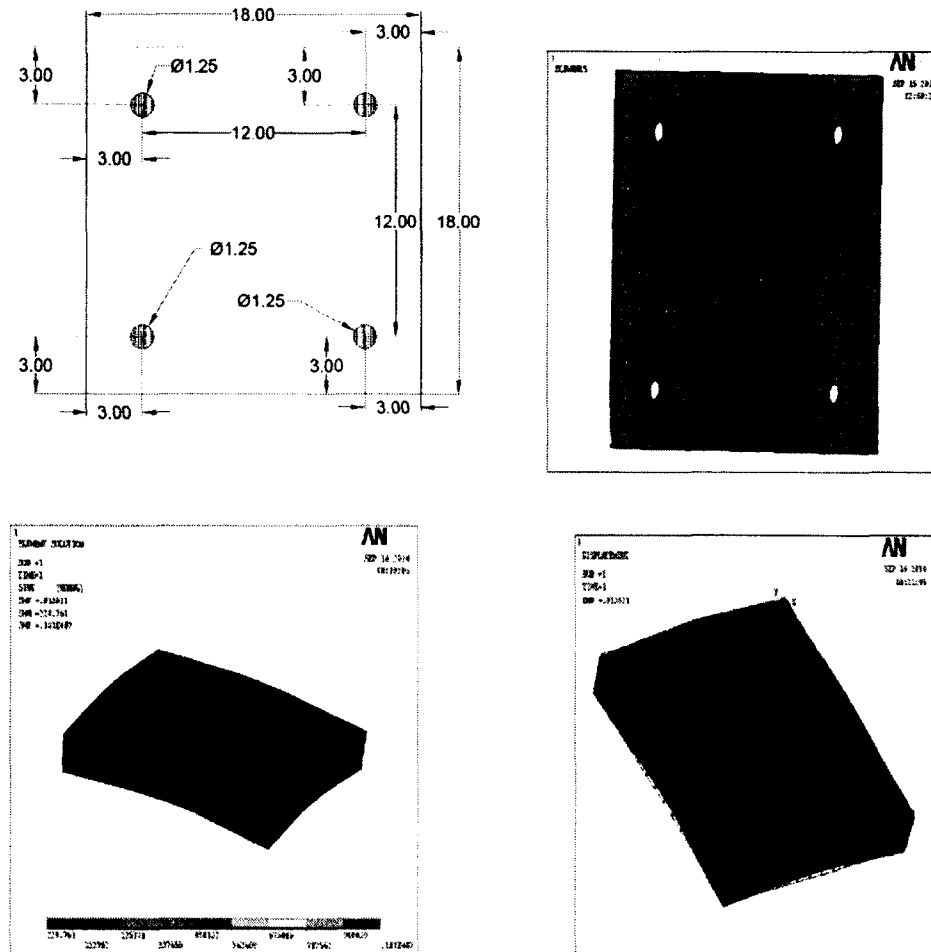
Figure 4.7 AutoCAD drawing (top left), mesh of header plate (top right), and ANSYS analysis of the header plate (bottom left and right).

For this analysis a solid metal plate with the original dimensions which is 18 x 18 x 1.5 inch was modeled with the proper end restrain. The maximum load from the highest compressive strength test setup, which is 90,000 lb was applied vertically to the surface of the metal plate and the ANSYS program was run to see the deformation in the plate. It was checked for surface deformation.

4.3.6 Selection of Hydraulic Jack

A bottle hydraulic jack was selected for this experimental setup (Figure 4.8). The load capacity of the hydraulic jack was 50 tons. With this jack the load was applied to the cylinder header plate. The maximum load needed to apply for the 8000 psi concrete was 90,000 lb.

Figure 4.8 Hydraulic jack to load the specimen.

The capacity of the hydraulic jack was selected according to the maximum stress requirement. When the desired load reached, stress on the test cylinders was fine-tuned with the help of the air valve attached to the hydraulic jack and the load cell calibrated with a data acquisition system.

4.4 Calibrating the Load Cell

The load cell was calibrated with the data acquisition system to monitor the stress applied on the creep testing frame. Compressive load applied on the load cell was plotted against the voltage change in the acquisition system and a linear fit was obtained as the

load was increased. This calibration curve was later used to find the desired load on the test samples. Figure 4.9 shows the process of load cell calibration with the help of MTS machine and data acquisition system.
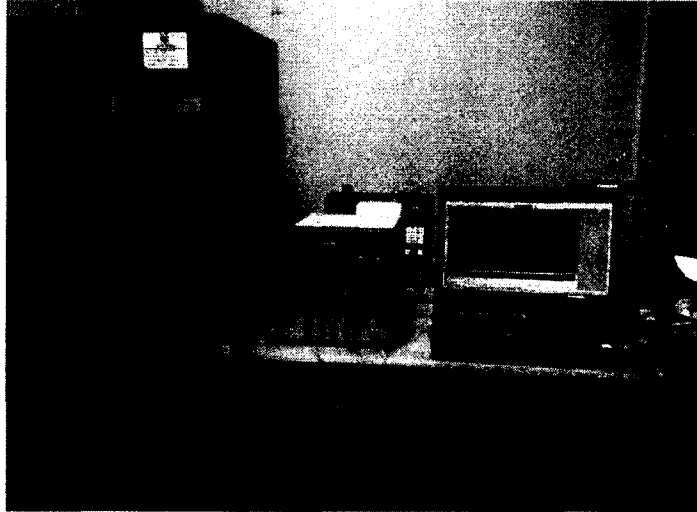
Figure 4.9 Calibration of the load cell.

The voltage amplitude shown on the monitor corresponded with a concentric compressive load. Several data points were obtained by varying the load on the compression machine to feed the information to the data logger software to calculate the calibration equation for the load cell.

4.5 Testing Procedure

Concrete cylinders were ground with the grinding machine shown in Figure 4.10 to make the load bearing surface smooth. Four discs were used for each creep frame.
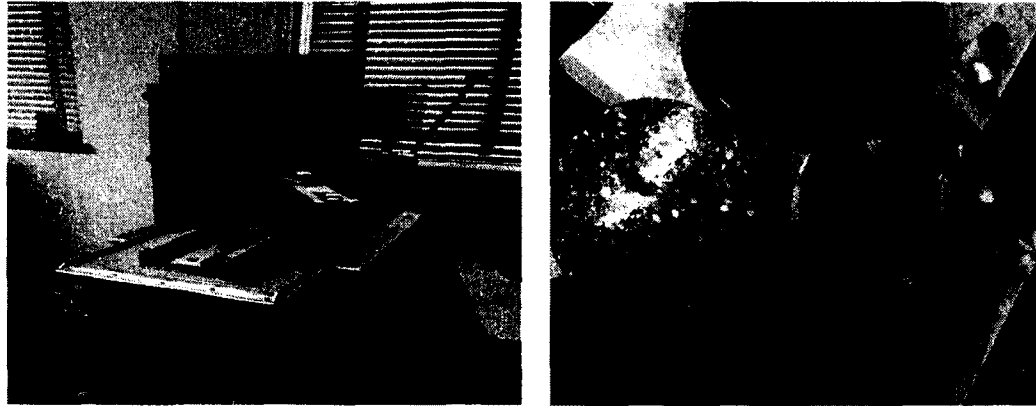
Figure 4.10 Manufacturing and polishing the spacer concrete disc.

Three concrete cylinders were stacked and separated by steel disks. Alignment frame was utilized to make the cylinders in a perfectly vertical position. This cylinder was placed on the top of the plate above the spring system and the header plate was placed above it. Above the header plate the cylinder center position was marked to put the load concentrically with the hydraulic jack. This system helped to avoid any kind of eccentric load applied on the cylinders [57]. The concrete column made by the three cylinders was centered and vertical. Loaded specimen in the creep frame is shown in Figure 4.11.

When the concrete cylinder was centered, the nut below the header plate was loosened and kept below the plate at least 1.5 in and the upper nuts were tightened so that the plate kept the cylinder column in position. The hydraulic jack was set and its position was aligned with the concrete column. A circle was drawn at the top of the header plate

to make the hydraulic jack co-axial with the cylinder to avoid any kind of eccentric loading. The frame was pre-loaded with about a load of 450 lb to set the header plate on top of the cylinder. Then the top four nuts were tightened. Initial data was taken at this condition to record the initial gage length. The load was applied to the top of the header plate gradually till it reached the target load.
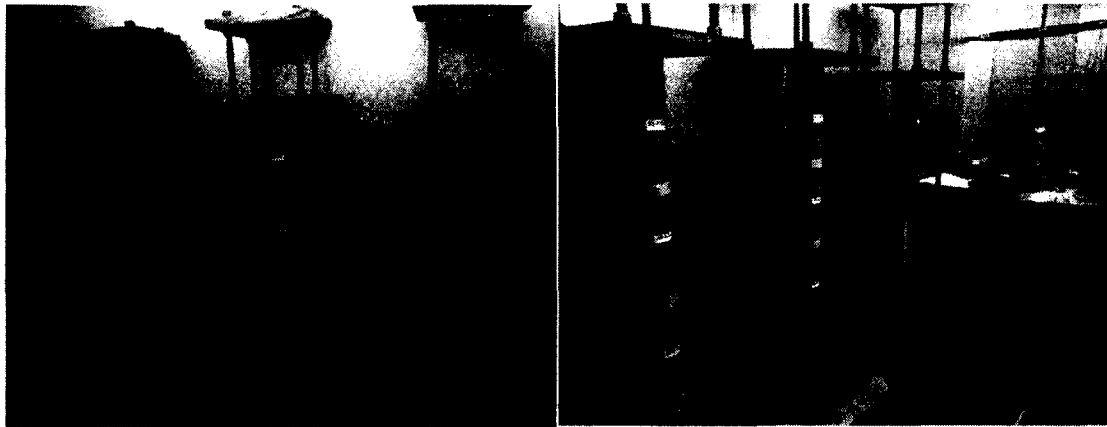
Figure 4.11 Creep frame for testing concrete specimen.

4.6 Summary on the Performance of the Creep Apparatus

The creep apparatus designed in this research work was guided by the ASTM C512. The entire standard requirement was followed throughout the experimental process. Deflection in the metal plates was assumed to be zero. The mechanical gage used for this experiment to measure the strain in the cylinder was with a precision of 0.00001 in. It was well calibrated and gave a satisfactory measurement. Experimental results indicate that the creep test apparatus designed in this research was effective and satisfactory.

CHAPTER 5

MECHANICAL STRENGTH AND

CHEMICAL COMPOSITION

5.1 Introduction

This chapter presents the results of the mechanical testing for the concrete specimen that were used for the creep test. Testing was performed to determine the relationship between the compressive strength and the flexural strength of the concrete. An empirical equation was developed to find the relation among the chemical component of the material to the mechanical strength of the GPC. Regression analysis was done to find the relationship among the elastic modulus, unit weight and the compressive strength of the concrete. This study is based on the analysis of 60 FA samples collected from power generating stations around the United States and from different countries.

The database of FA samples is partitioned into two individual sets, the first consists of 50 samples for data analysis and modeling, and the second consists of the 10 remaining samples for validation purposes. The first set has 28 samples that are classified as type F ash and 22 classified as type C, according to ASTM C618. The second set consists of 6 type F and 4 type C Fly Ash stockpiles. The 60 samples were analyzed via XRF and XRD to obtain their chemical and crystallographic composition. The samples were further analyzed using the Topas software to determine the amount of crystalline

phases found in the samples to facilitate calculations presented later in this study. The result of the XRD quantitative analysis was utilized to find the reactive portion.

5.2 Objective of the Analysis:

The objective of this part of the research work is to enrich a database with the inclusion of the test results to provide the true functional relationship between the FA characteristics and the properties of GPC through the development of the empirical models. This model will predict the fresh and hardened properties of the GPC using the chemical, crystallographic, and physical characteristics of FA. This study will assist with the prediction of important characteristics of the GPC. Discerning the relationship between the physical, chemical, and crystallographic characteristics of FA and the mechanical properties of the GPC is a significant step towards a large scale production of the GPC with reasonably consistent properties [58]. This study will also help to make a correlation between the mechanical behaviors of the GPC based on the effect posed by using different sources of FA. This prediction equation will help the designer select the particular FA source, or in some instances their element percentage, to achieve certain desired mechanical and fresh mix properties. The early age mechanical properties of the GPC can be used to find the creep and shrinkage behavior with the help of empirical equations.

5.3 Curing

In order to attain the maximum potential in terms of strength, geopolymer are typically cured under a slightly elevated temperature (up to $60°$ C). Elevated temperature helps to accelerate the formation of the geopolymer binder which ultimately contributes to the strength. Hardjito showed that the maximum compressive strength of the GPC can

be reached after 48 to 96 hours when cured at 60° C. In this research work, samples are cured at 60° C for three days before the compressive and flexural strength test. On the other hand, aggressive thermal curing (70° C to 80° C) can be detrimental, which can cause excessive loss of water during geopolymerization, possibly resulting in cracking and shrinkage [59].

5.4 Statistical Modeling

Regression analysis is a technique often used for studying the effect of more than one variable or regressor in a particular response or set of responses. Among the multivariate analysis methods, multiple linear regression is the tool used to model the changes of a dependent variable or response when the independent variables or regressor varies. The general form of the linear multiple regression is shown in Equation 5.1:

$$y = \beta_0 + \beta_1 x_1 + \beta_2 x_2 + \ldots\ldots\ldots + \beta_k x_k + \varepsilon, \qquad [5.1]$$

where y is the response and ε represents the error of the model. The parameters β_i, i = 0, 1, 2... k, are the regression coefficients and x_i are the regressors. The parameter β_i corresponds to the expected change in the response y per unit change in x_i when the rest of the regressors are kept constant. This is an effective method to analyze the information obtained in this study, discern the complexity of the existing relationships, and provide an empirical approximation of the underlying mechanism of FA activation and GPC properties [60].

5.4.1 Ordinary Least Square (OLS) Method

OLS is a common technique used to estimate the regression coefficients. This technique is based on minimizing the sum of square difference between the observations y_i and straight line, i.e. the residual square error. However, OLS has some drawbacks as it

estimates typically a low bias but a large variance, which can result in poor prediction accuracy. It lacks variable selection capabilities, as in many cases when there are a large number of regressors. Often it is desired to keep only the regressor that has the most significant impact in the response and drop the ones that have low impact. This method facilitates the interpretation of the relationship being modeled [61]. The most noticeable attempts to improve OLS have been the development of subset selection methods and Ridge regression. Subset selection, as the name implies, helps to select the best subsets of a given dataset. However, it is a discrete process where regressors are either retained or dropped from the model, depending on their influence. Small changes in the data can produce significantly different models; thus, it can be highly variable [62]. On the other hand, in Ridge regression the coefficients are continuously shrunk through a tuning parameter or penalization, allowing for a more stable process, but variables cannot be set to zero. For this reason, Ridge regression produces models that are hard to interpret [63].

5.4.2 Least Angle Shrinkage and Selection Operator

The LASSO method for estimating the regression coefficients in linear regression models was introduced by Tibshirani (1996) to improve accuracy and interpretation of the OLS technique. It is a penalized least square method that has the capability to shrink coefficients and set others to zero depending on their effect on the response. Instead of focusing on subsets, LASSO defines a continuous shrinking operation that selects the best predicting subsets and optimizes its coefficients at the same time. Tibshirani (1996) demonstrated that this technique outperforms Ridge regression and subset selection, especially for data with a small to moderate number of moderate size effects. Although the LASSO method has shown success in many situations, it is limited in the following

cases: (1) the number of regressors p is greater than the number of observations n. This method can select at most n variables before it saturates; (2) there is a group structure among the predictions with a high pair-wise correlation. In this case, LASSO arbitrarily chooses one variable from the group and drops the rest; and (3) the regressors are highly correlated. In the presence of multicollinearity, the accuracy of the model can be considerably reduced [64].

5.5 Procedure

Fly ash samples were tested for their Loss on Ignition (LOI) and moisture content according to ASTM C114. These samples were also tested for the specific gravity (SG) following ASTM C188. Chemical analysis of the fly ashes was performed following the ASTM C311. Setting time for the fly ashes with the mortar mix was measured using the Vicat apparatus. Geopolymer were tested for compressive strength for different cubes with the mortar mix and the concrete cylinders. Different fly ashes required different amounts of activator solution to achieve similar consistency. Flow number varied between 105-115 mm on the flow table. Mechanical tests have been performed for compressive strength following ASTM C39 and ASTM C469 for elastic modulus and Poison's ratio. The concrete beam test was performed for flexural strength following ASTM C78. Test procedures are shown in Figure 5.1. Particle size distribution (PSD) of the fly ashes was done using the Microtrac Flex 3500 machine. The particle size distribution curve obtained from the analysis is shown in Figure 5.3.
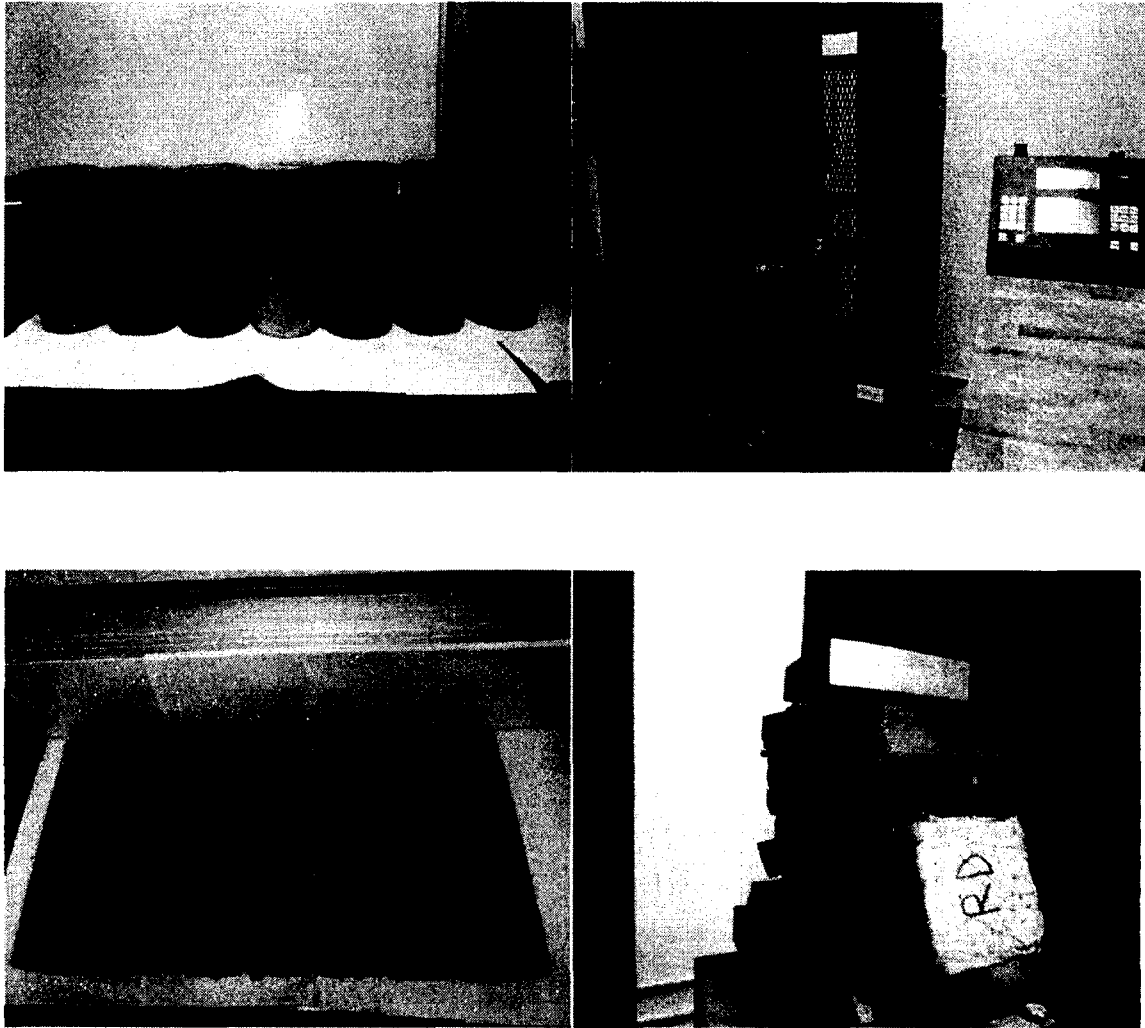
Figure 5.1 Samples for mechanical strength test (top left), elastic modulus test of the GPC cylinders (top right), GPC beam (bottom right), and flexural strength test of beam sample (bottom right).

5.6 Effect of Curing Time

Both curing time and curing temperature influence the compressive strength of geopolymer concrete. Longer curing time improves the polymerization process, resulting in higher compressive strength. The rate of increase in compressive strength is rapid during the first 24 hours of curing time, beyond 24 hours the gain in strength is only moderate. As heat curing is recommended for low-calcium fly ash based geopolymer

concrete, adding slag can be a solution to gain strength for class F fly ash based GPC.

Test results with class F fly ash and slag blended together is shown in Figure 5.2.
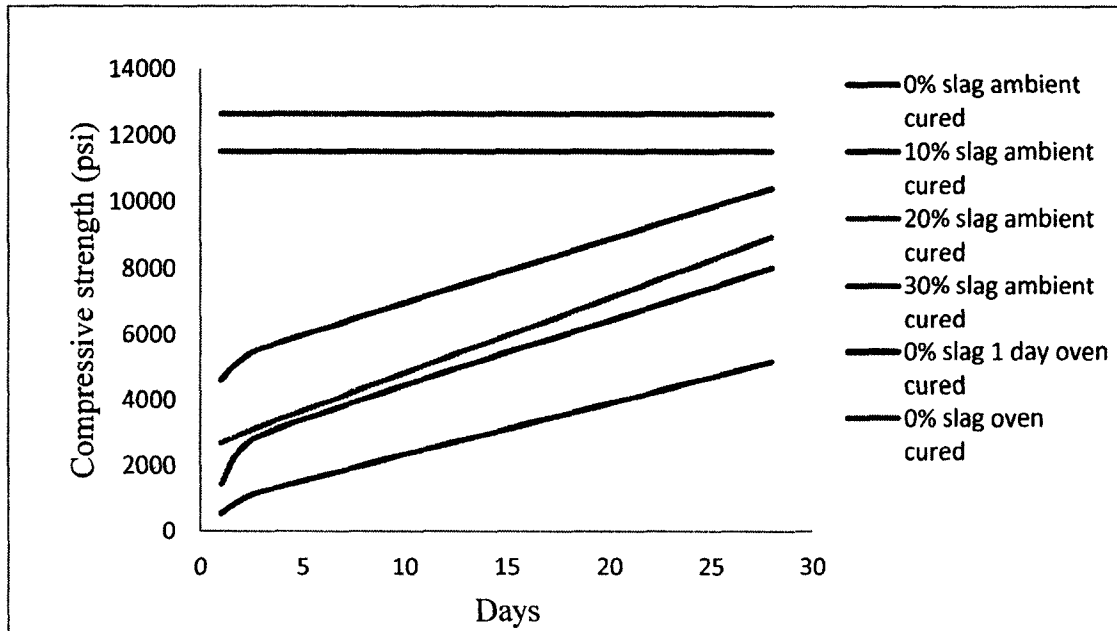
Figure 5.2 Effect of slag on curing.

These tests have been performed for Dollet hills fly ash with mortar cubes of 2 x 2

in. This test was performed to facilitate ambient curing in order to observe the effect of

slag. Test specimens for mechanical strength were prepared with heat curing. It can be

observed from the graph that there is no strength gained after the concrete is heat cured.

The sample with slag showed strength gain when it was ambient cured.

5.7 Particle Size Distribution

The particle size distribution curves of selected samples are shown in Figure 5.3.

A summary of the physical properties of the FA samples including specific surface area

and mean particle size is given in Table 5.1. It can be seen from the graph that among

these eight fly ashes BY sample has the finest particle and PD sample has the coarsest

particles. From the particle size distribution test it was observed that WS sample has the smallest d50, which is 9.5 μm, and PD has the largest d50 with 45.06 μm. WS and BY have the highest specific surface as 1.223 and 1.02 m²/g and PD has the smallest specific surface area as 0.088 m²/g.
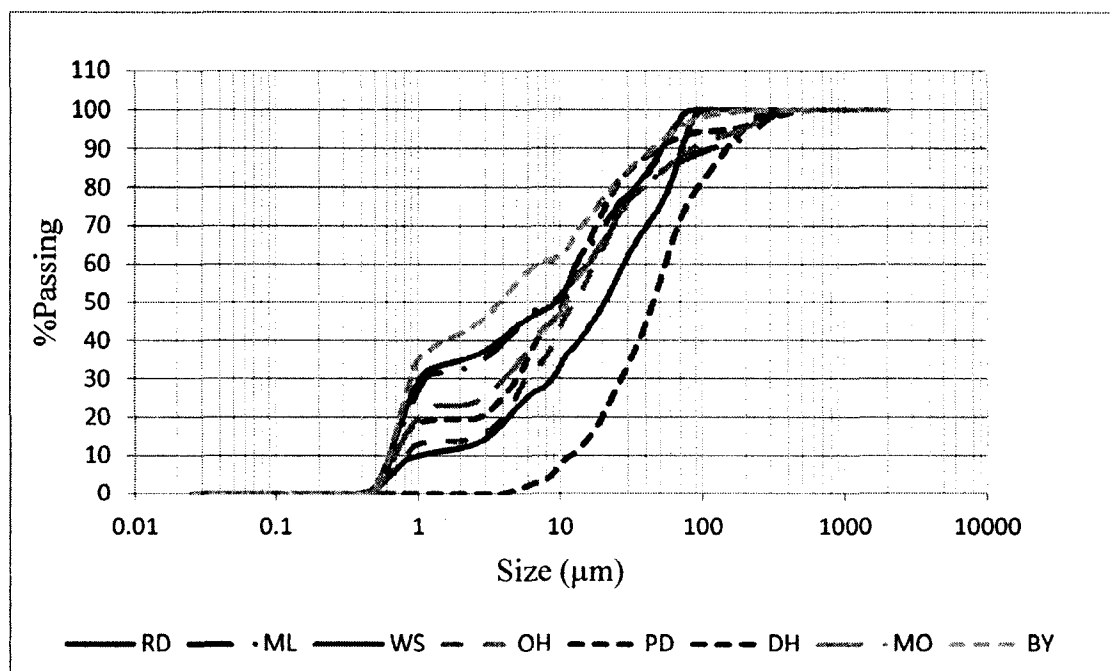
Figure 5.3 Particle size distribution of some selected FA sample.

5.8 Chemical Analysis

Chemical analysis was performed following ASTM C311 using the XRF machine. Data obtained from the test results are shown in Table C-1 of Appendix C.

5.9 Materials and Methods

The current study is based on the analysis of 60 samples. These fly ash samples were analyzed to find the moisture content, loss on ignition and chemical properties. The activator solution used for all samples was the same. The total sample was divided into two sets, the first for analysis and model building, and the second for validation purposes.

All tests were performed under the same conditions using the same filler material. Test parameters were selected from the preliminary tests results.

5.9.1 Materials

Coarse and fine aggregate used were the same throughout the entire testing process. An activator solution consisting of sodium silicate and sodium hydroxide was used with the same concentration and adjusted for the consistency of the mix. Fly ash samples were tested for the LOI and PSD to determine the activator solution's ratio and setting time, as these two criteria can be predicted based on the observation of the chemical components following the standard test ASTM C618. Tests have been performed following the same procedures and the same conditions suggested by the previous work performed by Ivan Dyaz loya [65].

5.9.2 Methods

Samples were analyzed chemically via X-ray Fluorescence (XRF) following ASTM D4326. A qualitative and a quantitative phase analysis were performed by X-ray diffraction (XRD) of the fly ash, as well as on geopolymer paste made from each of the fly ash samples. The fresh geopolymer paste was cured for 3 days at 60°C then crushed and grinded for analysis. Each fly ash sample was spiked and thoroughly mixed with 10% Corundum crystal that was used as an internal standard. The mixture was then put onto a zero background holder and placed into an Analytical X'Pert Pro diffractometer using Cu radiation at 45 KV/40 mA. Scans were run over the range of 10° – 80° with a step size of 0.01580 and a counting time of 800 seconds per step. Once the pattern was obtained, the phase was identified with the Topas software. Particle size distribution (PSD) analysis was conducted using a Microtrac Flex S5300 laser-based equipment with

a measuring range between 0.024 μm and 2816 μm. Samples were suspended in Isopropyl alcohol and run through the necessary cycles of reading and dispersing using ultrasound to obtain a realistic analysis. The mix design was chosen based on a previous study by Hardjito and Rangan [66]. Preliminary tests were carried out to obtain a formulation suitable for handling necessary changes in the fresh mix behavior due to the unique characteristics of each fly ash sample. The activator solution was a 14 M NaOH solution and Sodium Silicate (45% by weight and SiO_2 to Na_2O ratio of 2:1) with a 1:1 ratio. Fly ash to activator solution ratio was adjusted depending on the fly ash source to obtain a uniform consistency. Well graded sand and pea gravel (0.5" diameter round stone) was used as a fine and course aggregate, respectively. Fly ash to aggregate ratio was 1 to 3 and the course to fine aggregate ratio was 1 to 4.

5.10 Characterization of FA, GPP and GPC

Samples were analyzed to get the chemical composition using the XRF and XRD methods. Particle size distribution was obtained to monitor the physical characterization. The setting time was tested to find the initial setting time for the geopolymer paste. Moisture content was determined by drying the fly ash in the oven. Fly ash was burnt in the high temperature furnace to get the LOI percentage. Initial tests were performed to estimate the activator solution ratio for individual fly ash samples. Activator solution to FA ratio varies depending on the FA. The same mixer and mixing sequence was utilized to conduct the experiments throughout the study. The fresh mixture was cast into a 15 x 30 cm cylindrical mold to be tested as per ASTM standard C39 for compressive strength and ASTM C469 for static modulus of elasticity and Poisson's ratio.

5.10.1 Chemical Composition

Silica and alumina are the main precursors for the formation of geopolymer network and calcium oxide has significant influence in the chemical structure of the binder; however, these values cannot be taken from the XRF analysis without taking into consideration their crystalline arrangement since they represent absolute totals regardless of their reactivity [67]. Previous studies showed that the crystalline part of FA stays nearly inert, while the amorphous component is the reactive one throughout the geopolymerization reaction. Therefore, the amount of silica, alumina, and calcium oxide in a crystalline arrangement was not taken into account in the analysis, and it was assumed that only the amorphous components participated in the geopolymerization reaction.

5.10.2 Crystallographic Analysis

From the crystallographic analysis, it was determined that the main crystalline phase present in the fly ash consists of quartz and mullite and the rest is made of amorphous materials. During the polymerization process, some of the crystalline part dissolves to create more of a glassy phase, which increases the compressive strength of the resulting GPC. All samples are predominantly amorphous, containing relatively small amounts of quartz and mullite. Amorphous compounds are easier to dissolve than crystalline compounds during the first step of geopolymerization (dissolution of species), yielding higher amounts of reactive SiO_2 and Al_2O_3 which combine during the transportation/coagulation phase of the polymeric reaction.

5.10.3 Particle Size Distribution and Specific Surface Area

Particle size distribution is one of the most important properties impacting the reactivity of FA and the resulting GPC [68]. Geopolymeric reaction, like hydration in cement, occurs mostly at the surface of the particles. As a smaller particle has more surface area, thus those FA consisting of finer particles show higher reactivity. Researchers have highlighted the importance of powdered PSD with respect to their application in concrete [69]. The powder in the concrete has the highest percentage of surface area with respect to the other solids (sand and gravel) in the mix. Therefore, its packing characteristics have a significant impact on the fresh and hardened properties of the resulting GPC.

5.10.4 Data for Statistical Analysis

Preliminary studies showed that the crystalline part of FA stays nearly inert, while the amorphous component is the reactive one throughout the geopolymerization reaction. The amount of silica, alumina, and calcium oxide in a crystalline arrangement was not taken into account in the prediction equation, and only the amorphous component was considered to be participating in the polymerization process. In order to get the reactive percentage of the precursor's element, the crystalline form was subtracted from the total percentage of each element found in the fly ash sample via XRF. Each crystalline form was composed of one or more elements in the form of oxides, e.g., quartz is composed of 100% SiO_2 and mullite is composed of 71.79% Al_2O_3 and 28.21% SiO_2. To illustrate the process, assume the XRF analysis for a given fly ash yielded 38.80% SiO_2 and 43.34% Al_2O_3.

Step 1: Crystalline percentage present in the FA sample was obtained following XRD analysis. The fly ash was found to contain 12.25% quartz and 5.17 % mullite.

Step 2: The chemical composition of the phase was identified. Quartz contains 100% SiO_2 and mullite contains 71.79% Al_2O_3 and 28.21% SiO_2.

Step 3: The total content of non-reactive silica, alumina, and calcium oxide (labeled as $NSiO_2$ and NAl_2O_3) was calculated using Equations 5.2 and 5.3:

$$NRSiO_2 = \frac{12.25*100 + 5.17*28.21}{100} = 13.71\% \qquad [5.2]$$

$$NRAl_2O_3 = \frac{12.25*0 + 5.17*71.79}{100} = 3.72\%. \qquad [5.3]$$

Step 4: The non-reactive silica, alumina, and calcium oxide are subtracted from the total to obtain the reactive components labeled as $RSiO_2$ and RAl_2O_3:

$$RSiO_2 = Total\ SiO_2 - NRSiO_2 = 38.80 - 13.713 = 25.09\% \qquad [5.4]$$

$$RAl_2O_3 = Total\ Al_2O_3 - NRAl_2O_3 = 43.34 - 3.715 = 39.63\%. \qquad [5.5]$$

Using the reactive percentage of the elements rather than the absolute total is expected to increase the accuracy of the prediction model.

5.11 Relationship between FA Characteristics and Compressive Strength of GPC

Statistical analysis software, R, was used to determine the relationship among the regressors $RSiO_2$, RAl_2O_3, RCaO, LOI, and d50 with the significant maximum compressive strength values as the response. Subset selection was performed using the LEAPS package and coefficient optimization was performed using the LASSO algorithm.

The model to exhibit the highest R^2 value with five regressor variables is shown in Equation 5.6:

$$f_c^{'} = 31.3024 + 0.5326\,RSiO_2 + 0.4475\,RAL_2O_3 + 0.3232\,RCaO \qquad [5.6]$$
$$- 0.7351\,d50 - 0.8643\,LOI,$$

where f_c' is the compressive strength of GPC after three days of thermal curing at 60° C. The adequacy of the Equation 5.6 was further analyzed using the residual analysis. The assumption of least square technique is based on normality; the prediction and confidence interval depend on this assumption. A normal probability plot is shown in Figure 5.4. The parameters d50 and LOI both show a negative sign as they have a detrimental effect on the compressive strength. Fly ash with a larger d50 indicates lower total particle surface [70]. Regression analysis software R was used to analyze Equation 5.6. Plot obtained from the analysis is shown in Figure 5.4. It was observed from the graph that the data points follow a normal distribution curve. A second set of data was analyzed to improve the R squared value of the prediction curve with the removal of the outliers. That second equation was also validated with experimental data obtained from a set of arbitrary FA samples.
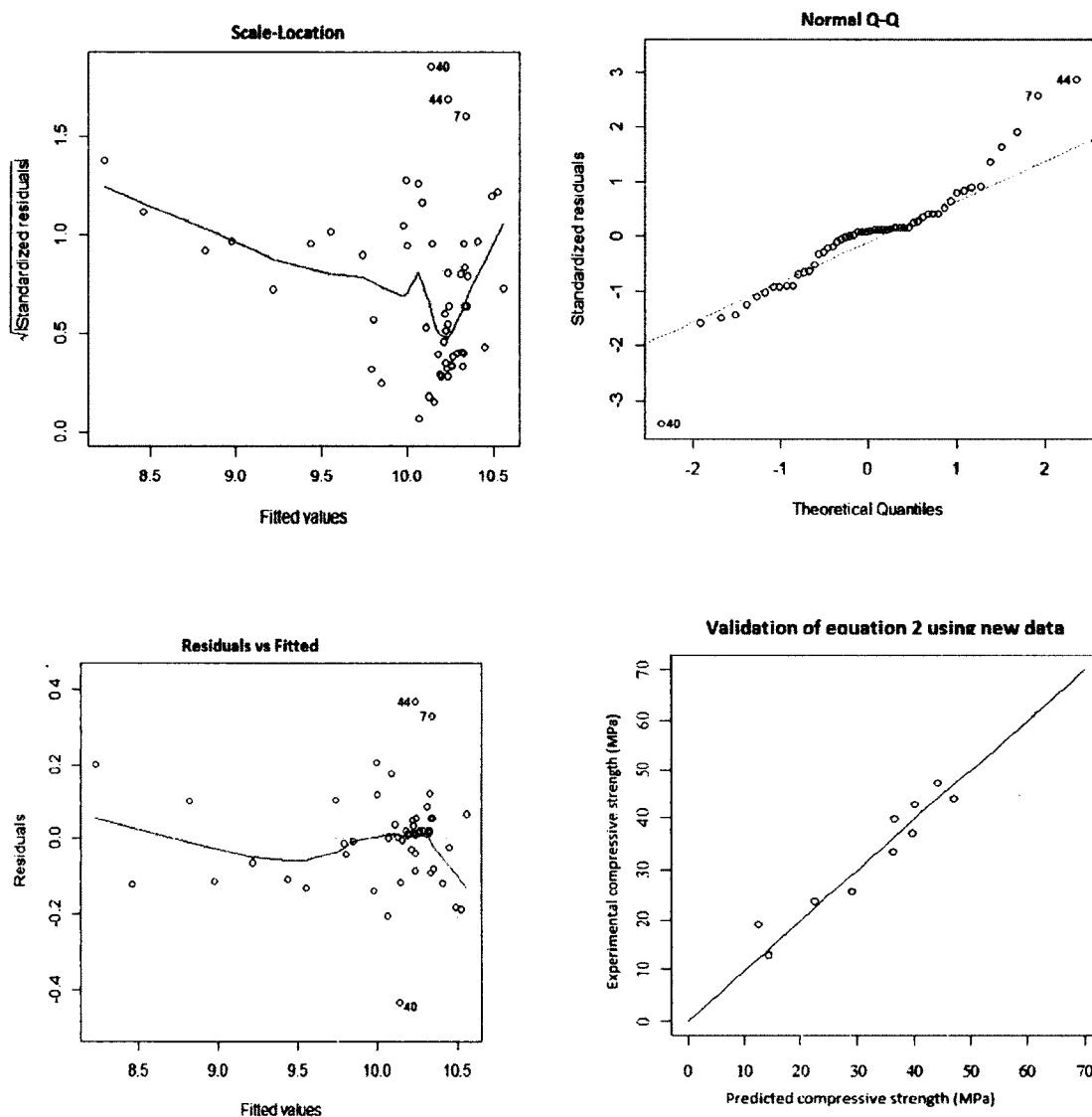
Figure 5.4 Analysis of Equation (5.2). Residual vs Fitted (top left), normal probability (top right), standard residual vs Fitted (bottom left), and validation curve from the experiment (bottom right).

A lower total particle surface indicates less extensive geopolymerization as the formation of the geopolymer binder occurs only at the surface of the FA particles. A previous study showed that LOI in the form of fine carbon may have a greater impact in concrete than FA with high LOI in the form of larger carbon particles [71]. This

phenomenon was observed when some FA, having higher LOI contents, showed low liquid demand and moderate compressive strength.

5.11.1 FA Characteristics and Density of GPC

Density of the GPC is strongly correlated with the specific gravity of the fly ash stockpile. The regression model found from the analysis was:

$$w = 2675 - 2145 * \frac{1}{SG^2}(kg/m^3).$$ [5.7]

Here, w represents the density of the GPC as per ASTM C138 and SG is the specific gravity of the fly ash following ASTM C188. The graphical representation of the equation is shown in Figure 5.5. FA with low specific gravity demands more liquid to fill larger voids due to less dense packing; when the liquid evaporates, it results in a larger pore volume, and thus lowers the density of the GPC.
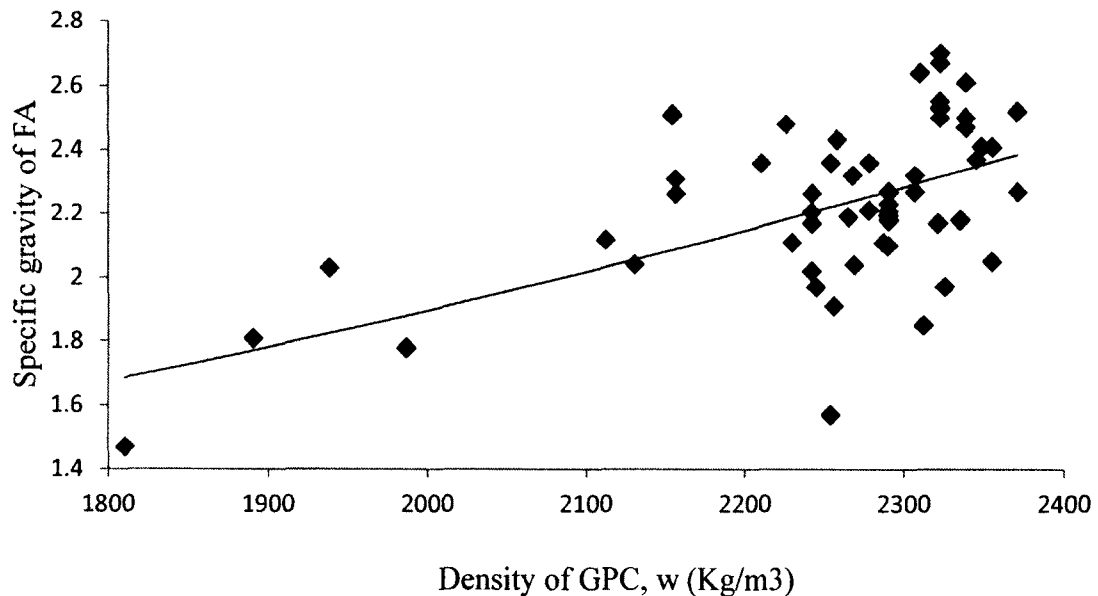
Figure 5.5 FA specific gravity vs. density of the GPC.

5.11.2 FA Characteristics and Setting Time of GPP

Previous test results showed that the setting time of the GPC is strongly influenced by the calcium content in FA. This premise remained true throughout this study. It was observed that the setting time decreased as the RCaO content increased in a manner similar to an exponential decay curve. This could be attributed to the calcium present in the mixture reacting with the silicate and aluminate monomers dissolved from the source material forming CSH and CASH. The hydration of these compounds results in increased alkalinity, which in return promotes further dissolution of silicate and aluminate from the source material, and an increased rate of polycondensation or geopolymerization. The presence of calcium enhances the geopolymerization process and lowers the setting time [72]. A scatter plot of GPC setting time vs reactive CaO content is shown in Figure 5.6.
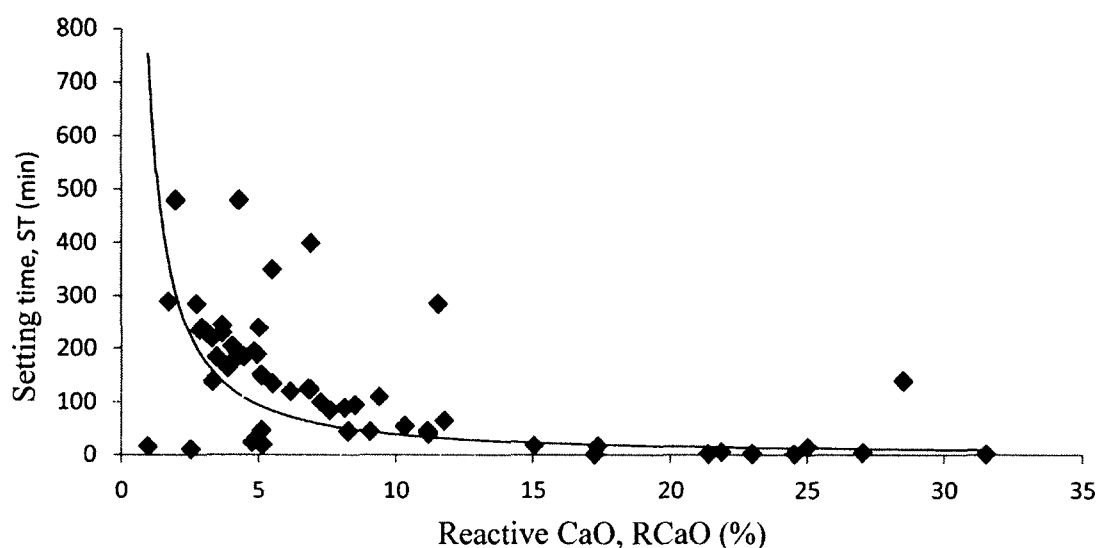
Figure 5.6 Reactive CaO vs. setting time graph.

Figure 5.6 suggests that RCaO and setting time are inversely related. However, geopolymer setting time is a complex process and other factors are also likely to influence it.

5.12 Analysis of Mechanical Properties of GPC

5.12.1 Compressive Strength vs Flexural Strength

Regression analysis suggests that the relationship between the compressive and flexural strength of geopolymer concrete can be expressed approximately by the following expression:

$$f_r = 0.64\sqrt{f'_c} \ (MPa), \hspace{3cm} [5.8]$$

where f_r is the flexural strength and f_c' is the compressive strength after three days of thermal curing at $60°$ C. The model labeled as Equation (5.8) provides R^2 value of 0.934. This equation seems to predict the flexural strength accurately using the compressive strength values despite the fact that the observations were recorded from different batches. It is worth noting that this experimental model for GPC is similar to the equation proposed by the American Concrete Institute in the Building Code 318-08, Section 8.5.2.3 to estimate the modulus of rupture for use in the calculation of deflection (ACI 2008):

$$f_r = 0.62\sqrt{f'_c} \ (MPa). \hspace{3cm} [5.9]$$

The relationship between the two parameters agrees well with the expression proposed by Ivan Diaz *et al*:

$$f_r = 0.68\sqrt{f'_c} \ (MPa). \hspace{3cm} [5.10]$$

5.12.2 Compressive Strength vs. Static Elastic Modulus

A regression model representing the correlation between static elastic modulus and compressive strength is presented in Figure 5.7. The equation obtained from the analysis is shown in Equation 5.11:

$$E_c = 771.4 f_c^{'0.929} \ (MPa), \qquad [5.11]$$

where E_c is the static elastic modulus and f_c' is the compressive strength. The R^2 value for this model is 0.926. ACI 318 (2008), Section 8.5.1, suggests the expression for computing the modulus of elasticity for normal weight concrete as:

$$E_c = 4733\sqrt{f_c'} \ (MPa). \qquad [5.12]$$

The relationship obtained between these two parameters in the regression model analyzed by Ivan Diaz *et al* was:

$$E_c = 580 f_c' \ (MPa). \qquad [5.13]$$

Equation 5.14 was given to relate the static elastic modulus of geopolymer concretes of various densities with their respective compressive strengths:

$$E_c = 0.039(w)^{1.5} \sqrt{f_c'} \ MPa. \qquad [5.14]$$

A similar equation is given in ACI 318 (2008), Section 8.5.1, which is derived from short term tests of OPC concrete ranging in density from 1,442 to 2,483 kg/m³ as:

$$E_c = 0.043(w)^{1.5} \sqrt{f_c'} \ MPa. \qquad [5.15]$$

Similar equation derived by Ivan Diaz was:

$$E_c = 0.037(w)^{1.5} \sqrt{f_c'} \ MPa. \qquad [5.16]$$

As the geopolymer data set is growing, the equations derived for geopolymer concrete are converging towards the equations listed in ACI 318 (2008) for Ordinary Portland Cement concrete. A 3-D plot for Equation 5.10 is shown in Figure 5.7.
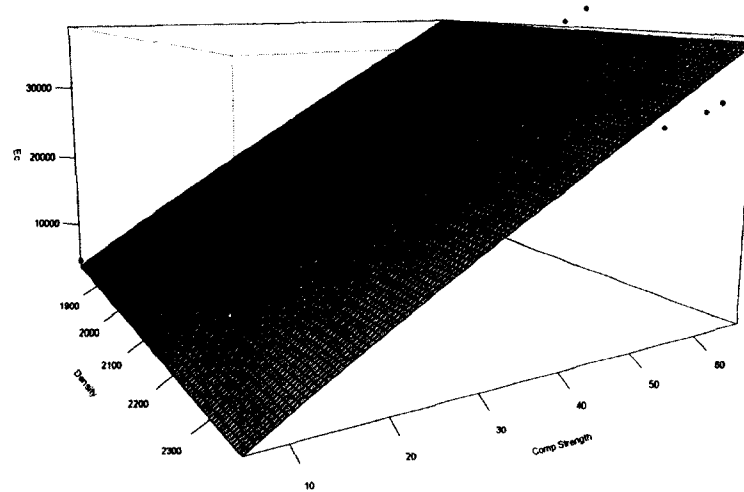
Figure 5.7 3-D plot for the validation of Equation 5.10.

5.13 Validation of the Prediction Equation

Table 5.1 contains the summary of the statistical results of the samples used for validation purposes. O represents the observed compressive strength, P the compressive strength predicted by the equation, and E the percentage of error between observed and predicted values for compressive and flexural strength, and elastic modulus. Results show that error percentages lie within 5% for compressive strength and flexural strength and within 10% for elastic modulus.

Table 5.1 Error percentages between the observed (O) and predicted (P) compressive strength values for compressive and flexural strength, and elastic modulus.

Sample	Compressive strength f_c' (MPa)			Flexural strength f_r (MPa)			Elastic modulus E_c (MPa)		
	O	P	E (%)	O	P	E (%)	O	P	E (%)
2 C	52.28	49.88	4.59	4.72	4.62	2.12	34377	31571	8.16
9 C	52.81	51.29	2.88	5.27	4.65	5.76	41878	38059	9.12
32 C	39.45	42.04	6.57	4.45	4.01	9.89	23519	25802	9.71
7 F	47.55	44.86	5.66	5.57	5.41	2.88	29475	29488	0.04
30 F	36.79	37.65	2.34	4.56	3.88	14.91	24724	25128	1.63
27 F	52.57	51.54	1.96	4.17	4.64	11.27	29089	31986	9.96
45 F	46.97	48.98	4.28	4.87	4.38	10.06	28015	29899	6.72
51 F	35.87	34.67	3.35	4.04	3.83	5.20	28691	25408	11.44
59 F	41.36	45.72	10.54	4.53	4.12	9.05	25478	27499	7.93
33 F	41.93	43.61	4.01	4.65	4.34	6.67	24995	27083	8.35
Avg E			4.61			7.76			7.30

5.14 Discussion of Mechanical Properties

It has been observed during this study that the flexural strength of the GPC increases with the compressive strength, following a certain pattern. The elastic modulus is influenced by the density and compressive strength of the concrete. Compressive strength of the GPC is correlated with a number of factors; in this study, a relationship among the parameters was established. The aggregate was the same for all samples, so the change in the mechanical properties was due to the variation of the geopolymer paste. The elastic modulus of the GPC increased as the density of the concrete increased, and the trends were found similar to equations listed in the ACI 318 (2008) for Ordinary Portland Cement concrete. Poisson's ratio values range from 0.11 to 0.21, with an average of 0.15.

CHAPTER 6

SHRINKAGE RESULTS

6.1 Introduction

This chapter presents the result from shrinkage tests on the geopolymer concrete

mix on the six different mix designs. Both restrained and free shrinkage test was

conducted to see the age of cracking and free shrinkage strain of geopolymer concrete.

Tests were performed to evaluate the effect of various factors on the shrinkage behavior.

Statistical analysis was done to establish the relationship between compressive strength at

the age when shrinkage test was started and shrinkage strain at its ultimate value reached.

An empirical equation was generated relating elastic modulus and compressive strength

with the shrinkage of GPC [73]. A theoretical model was developed and compared with

existing empirical models to see the effectiveness of prediction equation.

6.2 Restrained Shrinkage and Early Age Behavior

GPC mixes were tested under restrained conditions. Structural elements made of

concrete subjected to a restrained state in most cases. Because of that it is important to

test the material in a restrained condition. In this experimental process, two different mix

criteria for the GPC were examined: the first one was with the AS/FA ratio and the

second one was the ultimate strength of the GPC. Strength of the GPC was designed with

the densities of the basic mix design ingredients and keeping the AS/FA ratio constant.

Each concrete batch was used for the pouring of two restrained shrinkage rings that were heat cured for one day. The outer ring was removed after the curing has taken place and kept connected to the data acquisition system with the strain gages attached to the inner surface of the steel ring.

The cracking behavior of a particular mix is very important and the influence of changing certain parameters is important. The day a particular specimen cracks can be used to compare which mix performed better under restrained shrinkage conditions. Mixes that take a longer time to crack are considered to perform better. The number of cracks formed and the length of the cracks as well as the cracking area are also an indication of the performance of the mix. The pattern of cracking is also important. Usually, a ring will start cracking from the outer surface near either the top or bottom, and then the crack will continue to move inward toward the ring over time. This cracking rate at which crack propagates and moves toward the steel ring depends on the mix proportions. It is possible that the crack will not propagate fully to the ring [74].

As soon as the crack reaches the ring there is a compressive pressure that is relieved on the steel ring. Rings were monitored daily for surface cracks and these cracks were recorded and plotted on crack maps. The following pages show the records of the crack maps. The mix dates are shown along with cracking days.

6.2.1 Shrinkage Coefficient from Graph Plot for Restrained Shrinkage Test

Each ring was equipped with two strain gages. These strain gages were connected to the data acquisition system. Data obtained from the acquisition system was gathered every seven days from the device and plotting was done on the excel sheet. The graph obtained from the acquisition system was used to interpret the days to appear the first

crack on the concrete. The shrinkage coefficient was obtained from the graph. Prediction equation obtained from the system using the regression equation is shown in Equation 6.1. Coefficients obtained from the experimental data is given in Table 6.1.

$$\varepsilon = \alpha\sqrt{t} + K,$$ [6.1]

where ε = net strain in/in

α = strain rate factor for strain gage on the test specimen (in/in)

t = elapsed time in days

k = regression constant.

Table 6.1 Regression coefficients obtained from restrained shrinkage test.

Specimen	α (1x10^{-5})	K (1x10^{-5})
GP 35	3.75	2.36
GP 45	4.84	0.81
GP 55	5.67	0.74
GP 65	6.82	0.35
GP 4000	5.53	0.32
GP 8000	3.94	2.93
OPC 8000	6.81	0.22

6.2.2 Material Property Development and Drying Shrinkage Calculation

Chapter 5 discusses the experimental results obtained from the mechanical tests and the elastic modulus tests that were performed to have a better understanding of the property of the hardened material. Since these experimental results correspond to measured properties at specific times, regression functions were developed to provide a method that could represent the time dependent material properties at different ages of the concrete [75].

Elastic modulus of the specimen was calculated from the control specimen using the nondestructive test utilizing an e-meter.

6.2.3 Modulus of Elasticity as a Function of Time

Similar to free shrinkage the elastic modulus was also represented as a time-dependent property using a regression function that fit a hyperbolic curve. Elastic modulus measurements are represented using Equation 6.2:

$$E_c(t) = 0.039(w)^{1.5} \sqrt{f_c'(t)} \, MPa. \tag{6.2}$$

By using a nonlinear regression equation, the function for the compressive strength $f_c(t)$ was determined. With this regression equation an elastic modulus prediction curve was generated. It can be seen that the lower AS/FA mix design has higher strength and higher stiffness than the mix with higher AS/FA ratio. Elastic modulus was also calculated from the non-destructive test from the control sample.

6.2.4 Determination of Actual and Instantaneous Degrees of Restraint

The degree of restraint provided by the steel ring was computed for each batch of mix designed for the test. The geometry of the steel ring, free shrinkage, and steel ring strain were considered. At the same time, an instantaneous degree of restraint for each mixture R_{ins} was determined by replacing the modulus of elasticity of concrete E_c into the calculation instead of the effective modulus of elasticity (E_{eff}). The instantaneous degree of restraint is the degree of restraint at a particular time prior to any relaxation effect taking place.

The actual degree of restraint is higher than the instantaneous degree of restraint reflecting the decrease in modulus of elasticity of the concrete due to internal changes from inside the concrete [76]. The actual degree of restraint quickly attains a constant or

long term value due to the modulus of elasticity stabilization. The calculated values of the initial degree of restraint for the AS-0.65 concrete are approximately 50% for the 0.5 in steel. This value is 45% for the GP-8000 concrete. These restraint values are used to calculate the effective modulus of elasticity of concrete for each mixture. The magnitude of the effective modulus of elasticity relative to the modulus of elasticity of the concrete being a measure of stress relaxation induced in the concrete under restraint. Stress relaxation is likely a combination of micro cracking and viscoelastic deformation. The long term value of the actual degree of restraint can be used to calculate the modulus of elasticity with a rearrangement:

$$E_{eff} = E_s.z - \left(\frac{E_s.z}{R_{actual}} \right) = E_s.z - \left(\frac{R_{actual} - 1}{R_{actual}} \right), \qquad [6.3]$$

where
$$z = \frac{1 - (\frac{R_{is}}{R_{os}})^2 \left(1 + v_c\right) \left(\frac{R_{oc}}{R_{os}} \right)^2 + \left(1 - v_c\right)}{1 - (\frac{R_{oc}}{R_{os}})^2 \left(1 + v_s\right) \left(\frac{R_{is}}{R_{os}} \right)^2 + \left(1 - v_s\right)}. \qquad [6.4]$$

The maximum tensile or residual stress generated within the concrete ring specimens was quantified. The measured modulus of the steel, strain of the steel ring, and the geometry of the steel ring were all considered in the computation. It can be seen that the highest stress generated in the 0.35 AS/FA concrete at the end of 17 days. Here, 0.65 AS/FA and the GP-4000 mix showed a lower level of stress development. Differences in stress levels may be due to variability in the restrained ring data for the concrete specimens. An examination of the concrete strain data was made and determined that the variability of 3 $\mu\varepsilon$ should be considered. This is inferred that the stress levels may have a deviation of 0.2-0.5 MPa, depending upon the variability of the mix design.

6.2.4 Determination of Stress Relaxation and Maximum Residual Stress

In addition to calculating the residual stress that developed within the concrete ring specimens, the amount of stress relaxation was determined from the test, too. To calculate these values, logarithmic equations were used to fit the average strain measured in the steel rings for each mixture [77]. The maximum elastic stress $\Delta\sigma_{elastic-max}$, and the maximum residual stress $\Delta\sigma_r = R_{ic}$ were considered. The average residual stress in a restrained specimen at time t, σ_{actual}^{avg}, is given by Equation 6.5:

$$\sigma_{actual}^{avg}(t) = \left(\varepsilon_{sh}(t) - \varepsilon_{st}(t)\right)E_{eff}(t).$$

[6.5]

Here, E_{eff} is the effective modulus of elasticity of the concrete.

ε_{sh} is the free shrinkage of concrete. From Equation 6.5 we get:

$$\sigma_{actual}^{avg}(t) = R_{inst}(t)\varepsilon_{sh}(t)E_{eff}(t).$$

[6.6]

The same way average elastic stress $\sigma_{elastic}^{avg}$ is given by Equation 6.7:

$$\sigma_{elastic}^{avg}(t) = R_{inst}(t)\varepsilon_{sh}(t)E_c(t).$$

[6.7]

Now the ratio of the two Equation 6.6 and 6.7 gives:

$$\frac{\sigma_{actual}^{avg}(t)}{\sigma_{elastic}^{avg}(t)} = \frac{E_{eff}(t)}{E_c(t)}.$$

[6.8]

Given that the actual and elastic stress distribution through the thickness of the concrete ring is nonlinear, the average stresses in the equation are determined using the expressions for the stresses as functions of the radius of the ring [78]. To determine $\sigma_{actual}^{avg}(t)$ in this test, the previous equation was integrated over the thickness of the concrete, as shown in Equation 6.9:

$$\sigma_{actual}^{avg} = \frac{1}{R_{OC} - R_{IC}} \int \sigma(\theta)(r)dr.$$

[6.9]

Combining Equations 6.6 through 6.9 we get:

$$\sigma^{avg}_{actual}(t) = \frac{B}{R_{oc} - R_{Ic}} \cdot \varepsilon(t) \left[(R_{oc} - R_{ic}) + R^2_{oc} \left(\frac{1}{R_{ic}} - \frac{1}{R_{oc}} \right) \right].$$ [6.10]

In Equation 6.10:

$$B = E_s \cdot \frac{R^2_{os} - R^2_{is}}{2\left(R^2_{oc} - R^2_{os}\right)}.$$ [6.11]

The average elastic stress is calculated from Equations 6.12 and 6.13:

$$\sigma^{avg}_{elastic} = \frac{1}{R_{OC} - R_{IC}} \int \sigma_{elastic}(r) dr \text{ and}$$ [6.12]

$$\sigma^{avg}_{elastic}(t) = \frac{1}{R_{oc} - R_{ic}} \left\{ A \varepsilon_{sh}(t) \left[(R_{oc} - R_{ic}) + R^2_{oc} \left(\frac{1}{R_{ic}} - \frac{1}{R_{oc}} \right) \right] \right\},$$ [6.13]

where

$$A = \frac{E_c}{\frac{E_c}{E_s} C_{1R} + C_{2R}} \times \frac{R^2_{os}}{R^2_{oc} - R^2_{os}}.$$ [6.14]

Initially, the material is in the plastic state where there is substantial relaxation. For this reason the E_{eff}/E_c starts near zero. The sharp increase in E_{eff}/E_c at early ages is attributed to the aging of the concrete. This indicates that the aging of concrete is dominating the behavior of restrained concrete specimens. From the point where the E_{eff}/E_c is maximum and onward, the stress relaxation begins to dominate, driving E_{eff}/E_c to decrease steadily over time.

6.2.5 Tensile Creep Coefficient Determination from the Ring Test

Creep coefficient C_r is conveniently defined as creep strain ε_{cp} divided by elastic strain ε_e. The following equations give detailed explanations of how creep coefficients are determined from the restrained ring specimen test [79].

Shrinkage strain measured from the concrete (ε_{sh}) and steel (ε_{st}) can be related to the elastic (ε_e) and creep strain (ε_{cp}) and is shown in Equation 6.15:

$$\varepsilon_{sh}(t) - \varepsilon_{st}(t) = \varepsilon_e + \varepsilon_{cp}(t).$$
[6.15]

From the definition of elastic modulus we get:

$$\sigma_{actual}^{avg}(t) = E_c(t)\varepsilon_e = E_{eff}(t)\{(\varepsilon_e + \varepsilon_{cp}(t))\}.$$
[6.16]

From the definition the tensile creep coefficient (C_r) is given by:

$$C_r(t) = \frac{\varepsilon_{cp}(t)}{\varepsilon_e},$$
[6.17]

Combining Equations 6.16 and 6.17 we get:

$$E_c(t)\varepsilon_e = E_{eff}(t)[\varepsilon_e + C_r(t)\varepsilon_e].$$
[6.18]

This equation can be written as:

$$E_c(t) = E_{eff}(t)[1 + C_r(t)].$$
[6.19]

Equation 6.19 can be rewritten as:

$$\frac{E_{eff}(t)}{E_c(t)} = \frac{1}{1 + C_r(t)}.$$
[6.20]

Rearranging Equation 6.20 we get:

$$C_r(t) = \frac{E_c(t)}{E_{eff}(t)} - 1.$$
[6.21]

Substituting, we get:

$$C_r(t) = \frac{\sigma_{elastic}^{avg}}{\sigma_{actual}^{avg}} - 1.$$
[6.22]

This equation gives the tensile creep coefficient as a function of time. A similar phenomenon was observed from all mix designs. The creep coefficient decreases as the age of the concrete increases very rapidly. The high C_r values at early ages attributed

primarily to the viscoelastic deformation of the concrete due to a very low elastic modulus. As the concrete dries with time, greater induced stresses are imposed on the system, causing stress relaxation in the form of micro cracking and viscoelastic deformation [80]. As relaxation occurs over time, the creep value steadily increases with time.

6.2.6 Prediction of Residual Tensile Stress

Regression equation was used to calculate the tensile stresses in the concrete. To generate a relation between E_{eff}/E_c, the initial degree of restraint (R_i) and time (t), the following equation is obtained:

$$\frac{E_{eff}(t)}{E_c(t)} = 0.387 R_i^{-0.56} - 0.005t,$$ [6.24]

where R_i is expressed as:

$$R_i = \frac{1}{1 + \frac{A_c E_c}{A_s E_s}}.$$ [6.25]

The predicted residual stress σ_r is given by:

$$\sigma_r(t) = R_i \, \varepsilon_{sh}(t) E_{eff}(t).$$ [6.26]

Combining Equation 6.25 and 6.26 we get:

$$\sigma_r(t) = R_i \, \varepsilon_{sh}(t)[E_c(t).(0.375 R_i^{-0.575} - 0.005t)].$$ [6.27]

The actual restrained system ε_{sh} must be used to calculate the residual tensile stress. The ring specimens had the same surface to volume ratio for all samples. When the stress data is obtained, a close pattern in the plot is observed for all samples, which justify the prediction equations.

6.3 Results and Analysis of Shrinkage Test

Six different mix designs were analyzed for this testing program. Test specimens were heat cured. For heat cured specimen, data reading was started after it had been cured for 24 hours. These specimens were checked with their compressive strength gain at that time to correlate their strain. The cracking behavior due to the parameters of aggregate to sand and activator solution to fly ash is shown in Table 6.2 to 6.4.

Table 6.2 Cracking day for Group 1 Mixes.

Group 1: Activator solution to fly ash ratio			
	F/A	AS/FA	Cracking day
GP 35	0.35	0.35	86
GP 45	0.35	0.45	67
GP 55	0.35	0.55	55
GP 65	0.35	0.65	42

Table 6.3 Cracking day for Group 2 Mixes.

Group 2: Design strength			
	SH(M)	SS	Cracking day
GP 4000	10	N	48
GP 8000	14	D	72

Table 6.4 Cracking day for Group 3 Mixes.

Group 3: Control Mix Design			
	W/C	C/A	Cracking day
OPC 8000	0.30	0.46	41

Each of the specimens was monitored daily for surface cracks and these cracks were measured and placed on crack maps.

6.4 Environmental Conditions for the Restrained Ring Test

Test samples were stored in an environment chamber with a constant temperature (23° C $\pm$ 2° C) and humidity (50% $\pm$ 2%). The air-conditioning unit and the heater were used to control the temperature and the humidifier to control the humidity in the room. The evaporation rate for the different ring specimen was assumed to be uniform causes the controlling unit was away from the table where the samples were kept.

6.4.1 Quantifying Stress Relaxation Using the Ring Test

With the residual stress in the ring specimen, the amount of stress relaxation is also quantified. For these calculations, logarithmic equations were used to fit the average strains measured in the steel rings for each mix design. Maximum residual stresses were determined using the estimated effective modulus of elasticity.

6.4.2 Effects of AS/FA Ratio on Shrinkage Behavior

The test data presented in Tables 6.1, 6.2 and 6.3 show that AS/FA ratio has a substantial effect on shrinkage behavior of concrete mixes. With concrete curing time being the same for all samples, only AS/FA ratio was the influencing factor. The concrete made with higher AS/FA ratio has a higher shrinkage strain than those with lower AS/FA ratio [81].

6.4.3 Effects of Chemical Composition on Shrinkage Behavior

To see the chemical reaction and the degree of geopolymerization, two different mix designs with high and low compressive strengths were considered for this testing program. It is observed from this analysis that the concrete made with 14 (M) NaOH and

D silicate gained some early strength and gave lower strain in shrinkage. On the other hand, concrete with 10 (M) NaOH and N Silicate gave a higher strain as it has a low compressive strength.

6.4.4 Effects of Activator Solution to Fly Ash Ratio on Shrinkage Behavior

Not all the activator solutions take part in chemical reaction process of the geopolymer [82]. In heat cured fly ash based geopolymer concrete, part of the activator solution released during the chemical reaction may evaporate due to the high temperature of the curing process. As the remaining water contained in the micro-pores of the hardened concrete is small, the induced drying shrinkage is also very low. The presence of micro-aggregates in fly ash based geopolymer concrete may also increase the restraining effect of the aggregate on drying shrinkage.

6.4.5 Effects of Coarse and Fine Aggregate on Shrinkage Behavior of Concrete

There was no variation in the coarse and fine aggregate for all test specimens. Locally available pea gravel was used as coarse aggregate and fine sand was used as fine aggregate. It was observed from the study that the micro aggregate formed from the fly ash particle has the larger effect on the total shrinkage, whereas the filler material acted the same way which provided as the perfect material for comparing the other effects of the geopolymerization on shrinkage [83].

6.4.6 Relationship between Compressive Strength and Shrinkage Strain

It was observed from the regression analysis that an empirical equation can be established to find and predict the ultimate shrinkage strain from the compressive strength. Statistical analysis software "R" was used to find this relationship between these

two parameters. The coefficients found from this analysis serves as a reliable parameter to predict the shrinkage strain of the hardened concrete after a certain period of curing.

6.4.7 Relationship between Elastic Modulus and shrinkage Strain

As there is a relationship already established between the compressive strength and the elastic modulus of the concrete, it is predicted that a relationship can be easily found to predict the shrinkage strain of concrete relating the elastic modulus of the same [84].

6.4.8 Restrained Shrinkage Behavior and Cracking Pattern

The cracking behavior of a particular mix is very important. The knowledge of the parameters that changes the certain parameters is also important. The exact day of cracking can be used to compare the various mixes for their performance in the case of restrained shrinkage. Mix design that survives longer without cracking are considered to perform better than those forms crack earlier. The cracking area is also an indication of the performance of a mix. There can be specimens which may crack early but have small cracks, and may not propagate toward the steel ring. Usually, the ring specimens start cracking from the outer surface near either the top or the bottom, and then the crack continues to move inward toward the ring over time [85]. The speed at which the crack propagates toward the steel ring depends on the mix design. It is possible that the crack does not propagate fully towards the ring. When the crack reaches the ring, it causes a release of compressive stress upon the steel ring [86]. The cracking pattern of the specimens tested in this study is shown in Figure 6.1 through Figure 6.7.
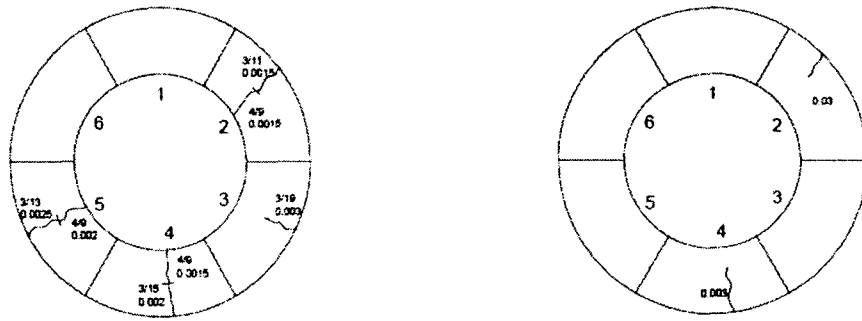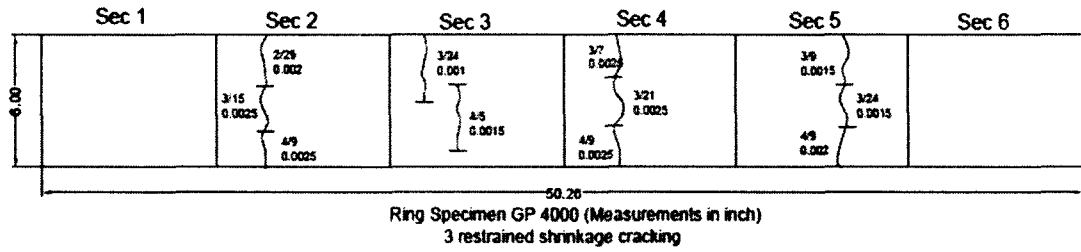
Figure 6.1 Crack map of side, top and bottom view of GP 4000 ring.
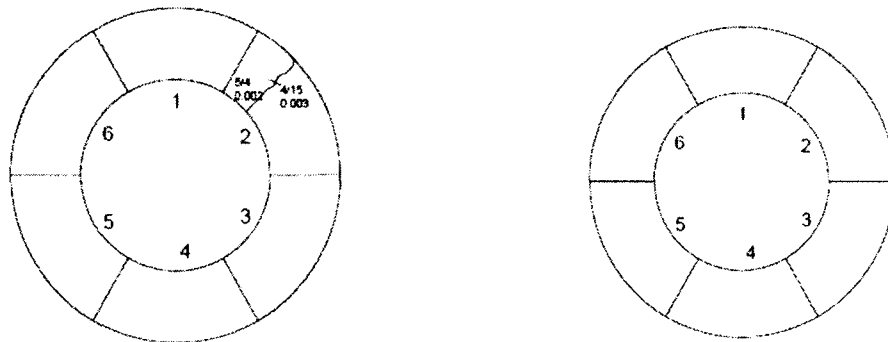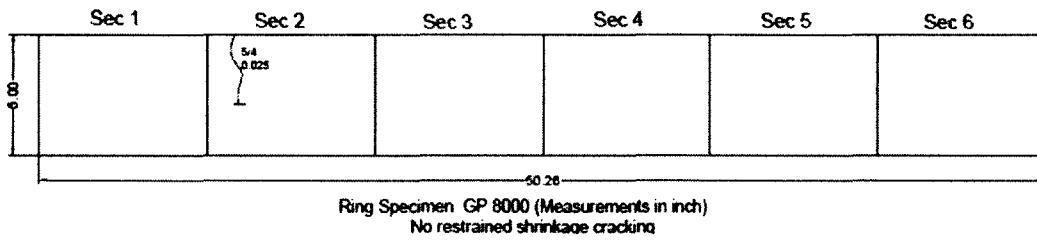
Figure 6.2 Crack map of side, top and bottom view of GP 8000 ring.
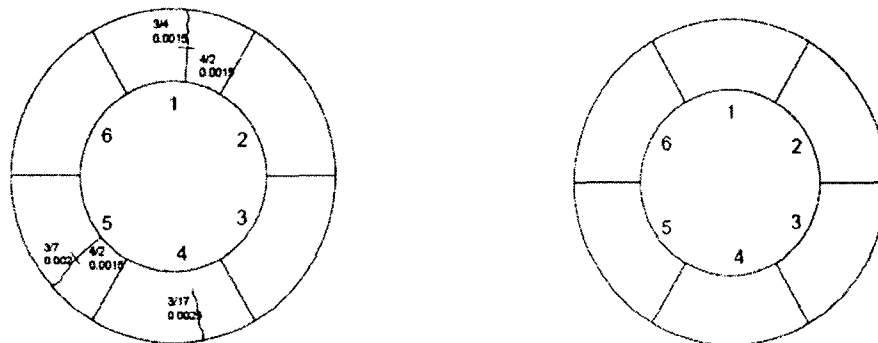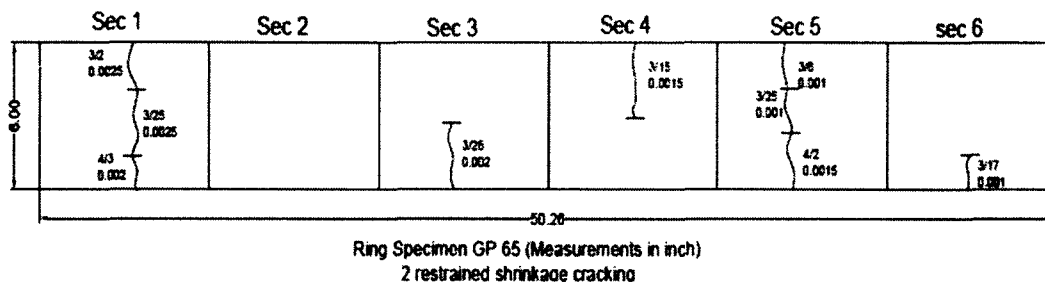
Figure 6.3 Crack map of side, top and bottom view of GP 65 ring.
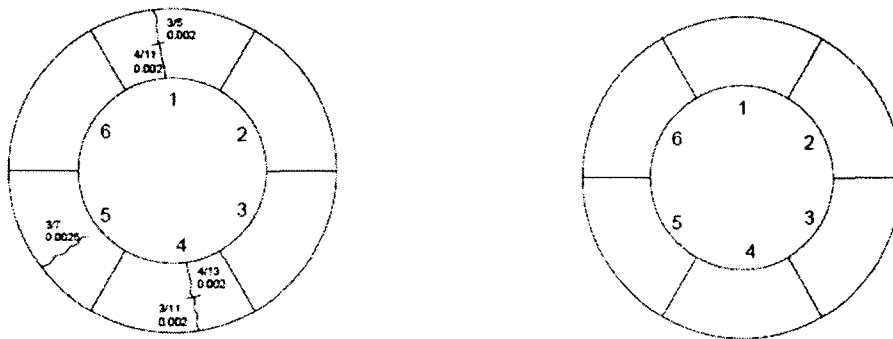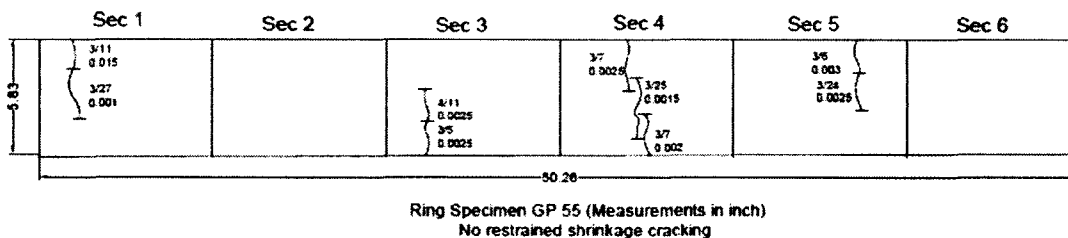
Figure 6.4 Crack map of side, top and bottom view of GP 55 ring.
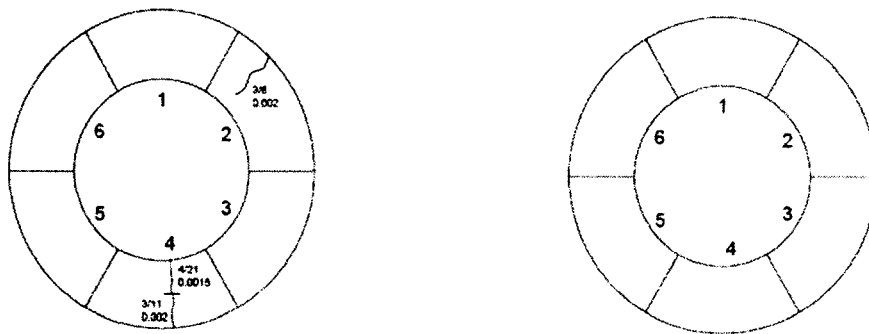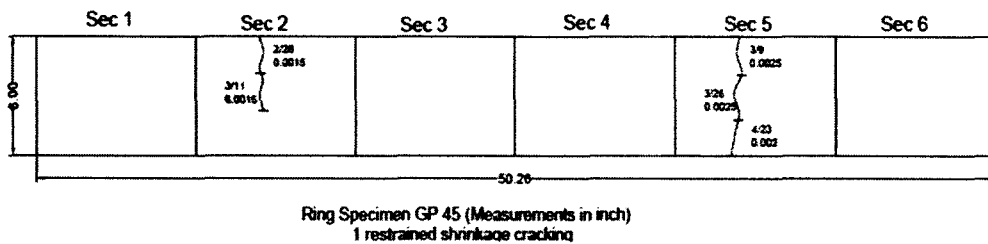
Figure 6.5 Crack map of side, top and bottom view of GP 45 ring.
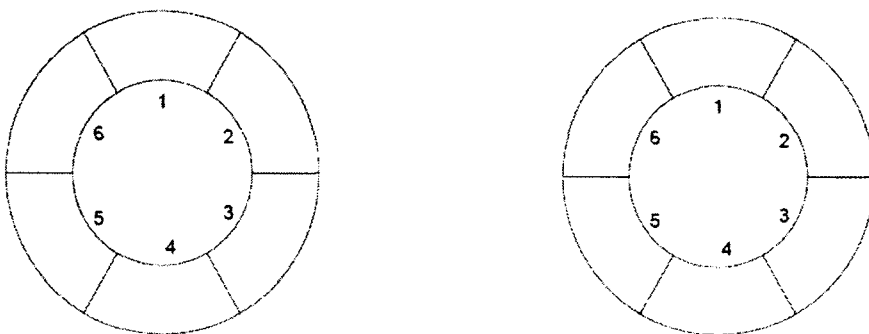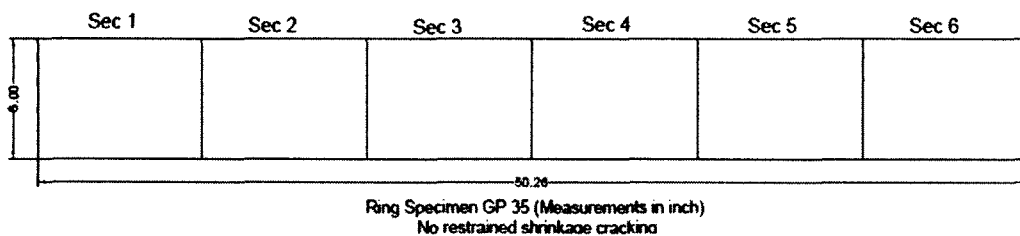
Figure 6.6 Crack map of side, top and bottom view of GP 35 ring.

Sec 1	Sec 2	Sec 3	Sec 4	Sec 5	sec 6

Ring Specimen OPC (Measurements in inch)
2 restrained shrinkage cracking
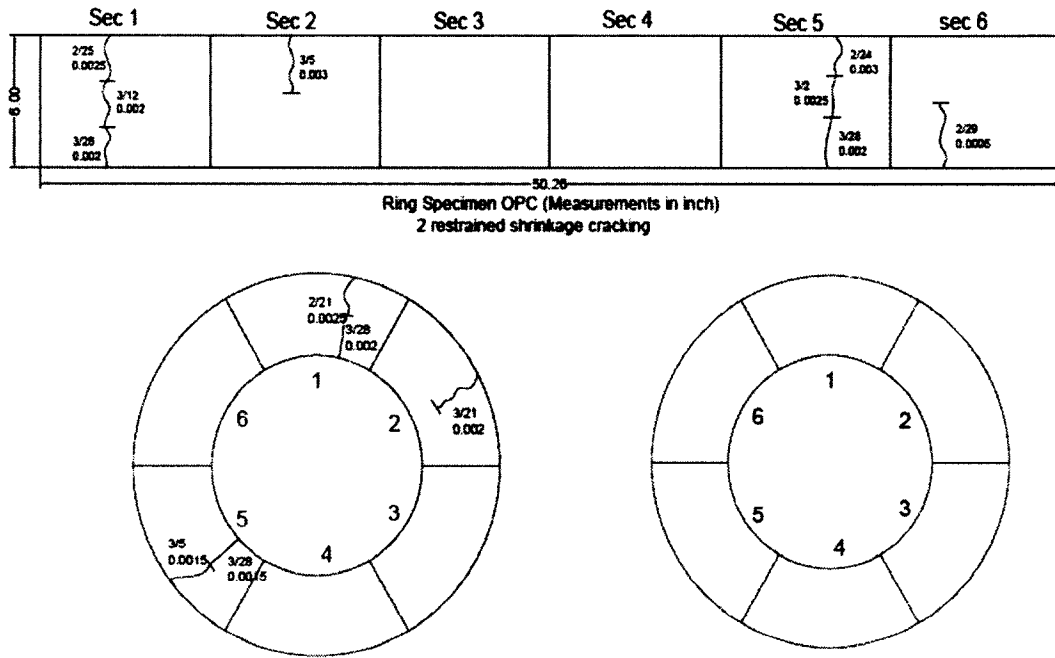
Figure 6.7 Crack map of side, top and bottom view of OPC 8000 ring.

6.5 Free Shrinkage Test Result

Free shrinkage test results were obtained from the prism specimen using the length comparator. The results obtained from the test are shown in the Figure 6.8. It can be seen from the graph that the maximum strain from the GPC sample was more than 500 micro strain and the minimum was around 300 micro strain. This is important data to use in combination with the total strain to find the basic and drying creep for the corresponding mix design of the GPC.
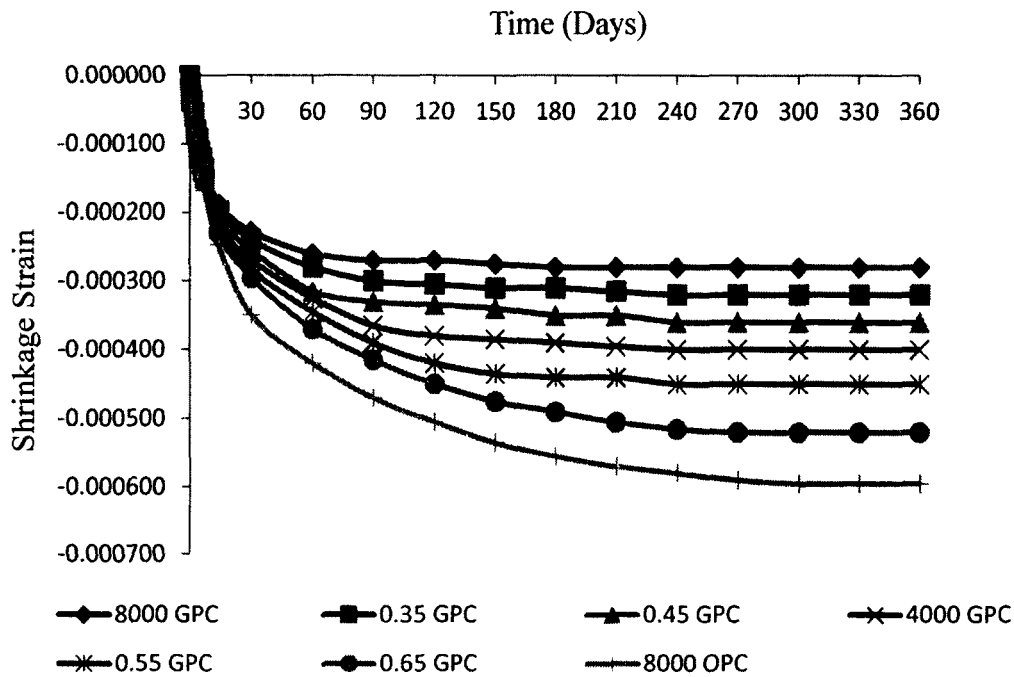
Figure 6.8 Free shrinkage strain.

6.6 Comparison of Experimental and Theoretical Shrinkage Strain

In this study ACI, Bazant B3, CEB, GL2000, and Sakata models were evaluated on their effectiveness and accuracy in predicting the shrinkage strain of the different GPC mixes. The experimental shrinkage strain results for all GPC mixes investigated in this study were compared to the calculated results obtained by applying the empirical formulas. Summary of the results are shown in Figure 6.9 through Figure 6.14.
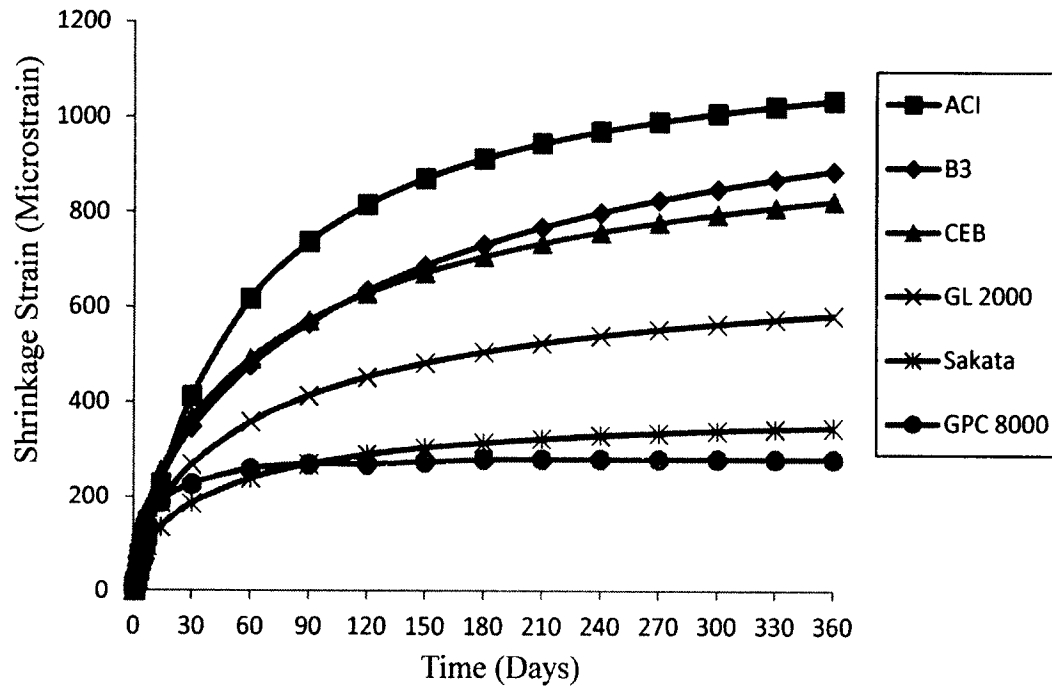
Figure 6.9 Exp. vs. predicted shrinkage strain (GPC 8000).
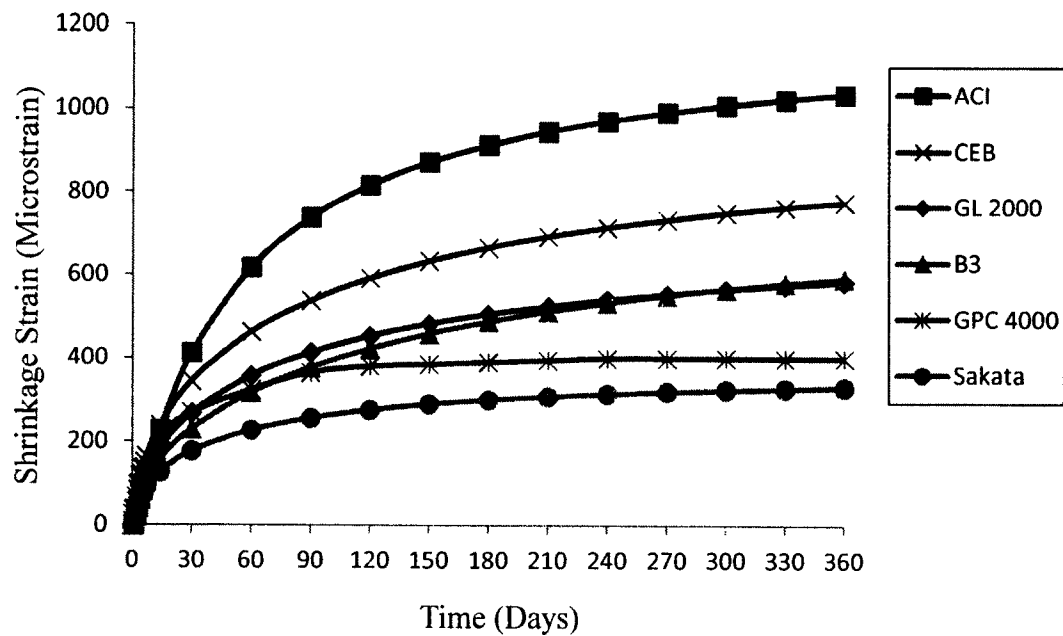
Figure 6.10 Exp. vs. predicted shrinkage strain (GPC 4000).
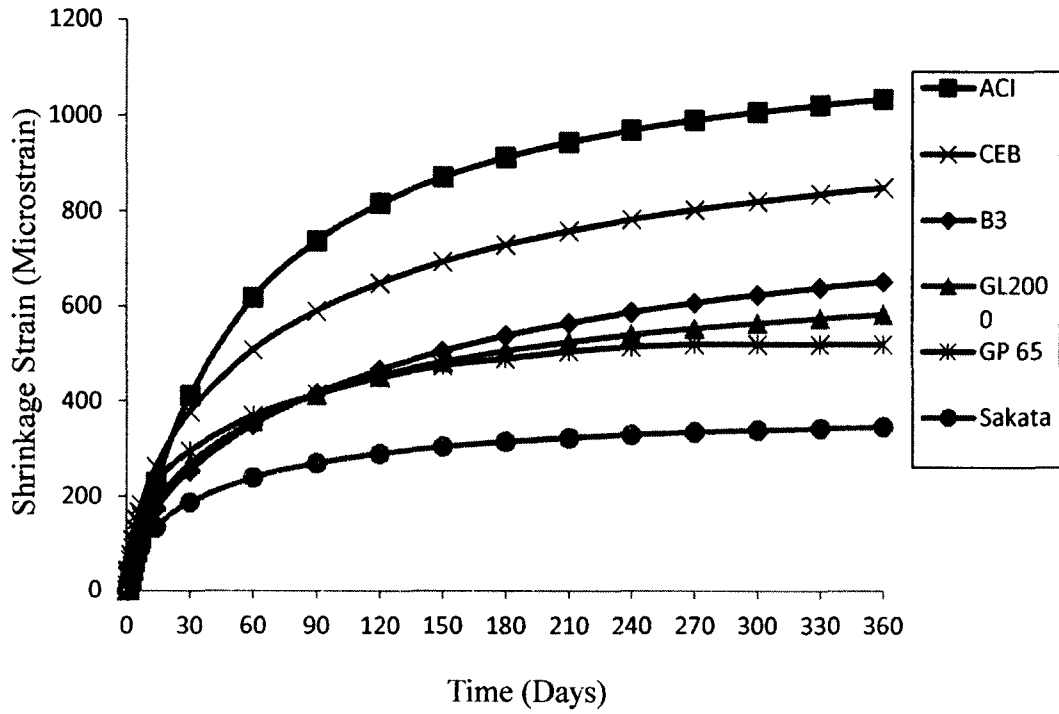
Figure 6.11 Exp. vs. predicted shrinkage strain (GP 65).
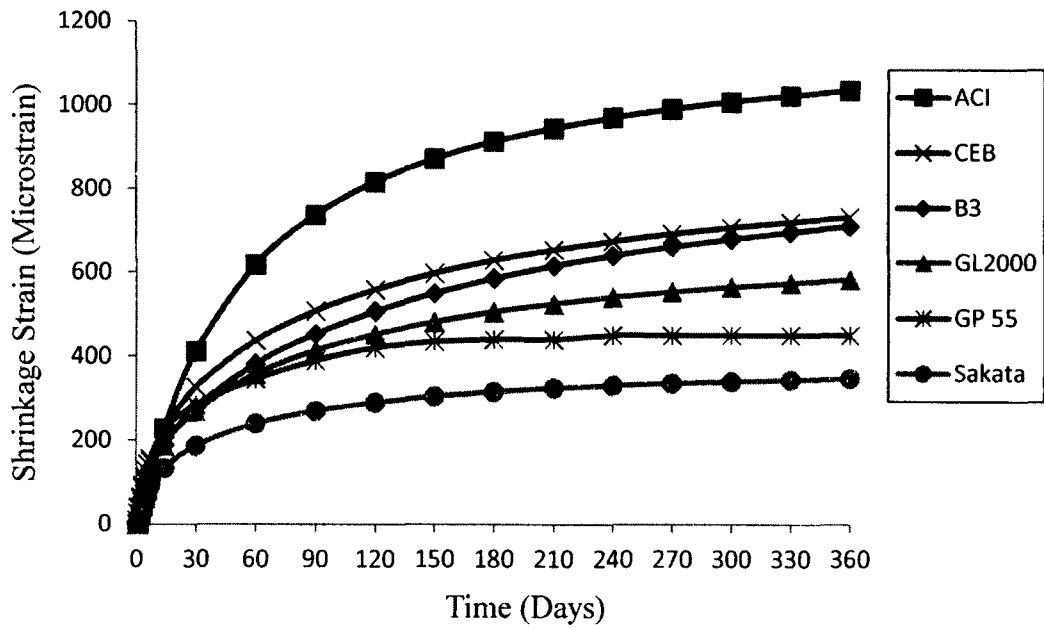
Figure 6.12 Exp. vs. predicted shrinkage strain (GP 55).
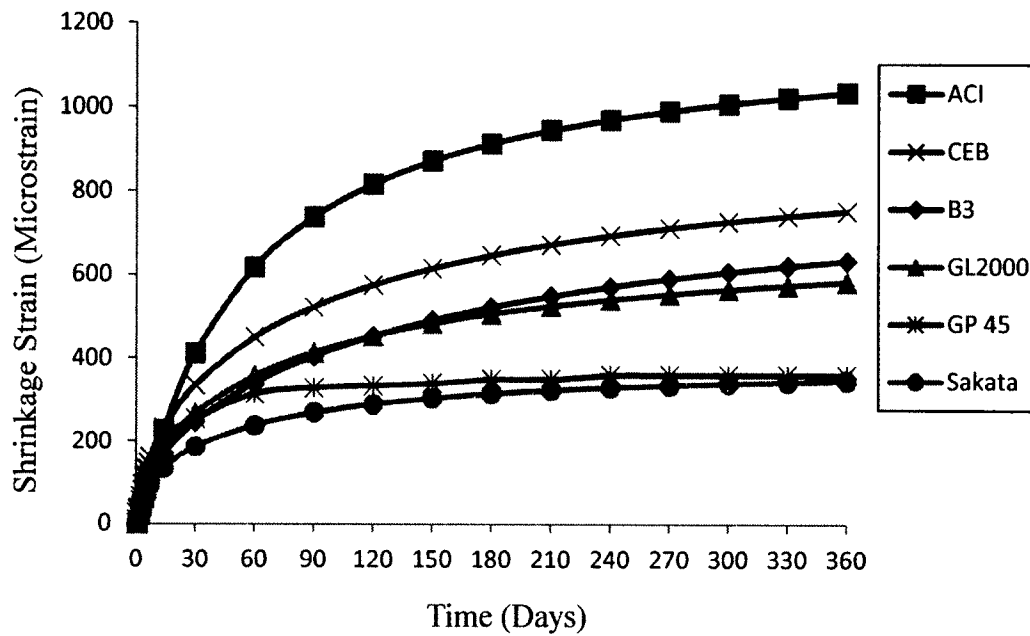
Figure 6.13 Exp. vs. predicted shrinkage strain (GP 45).
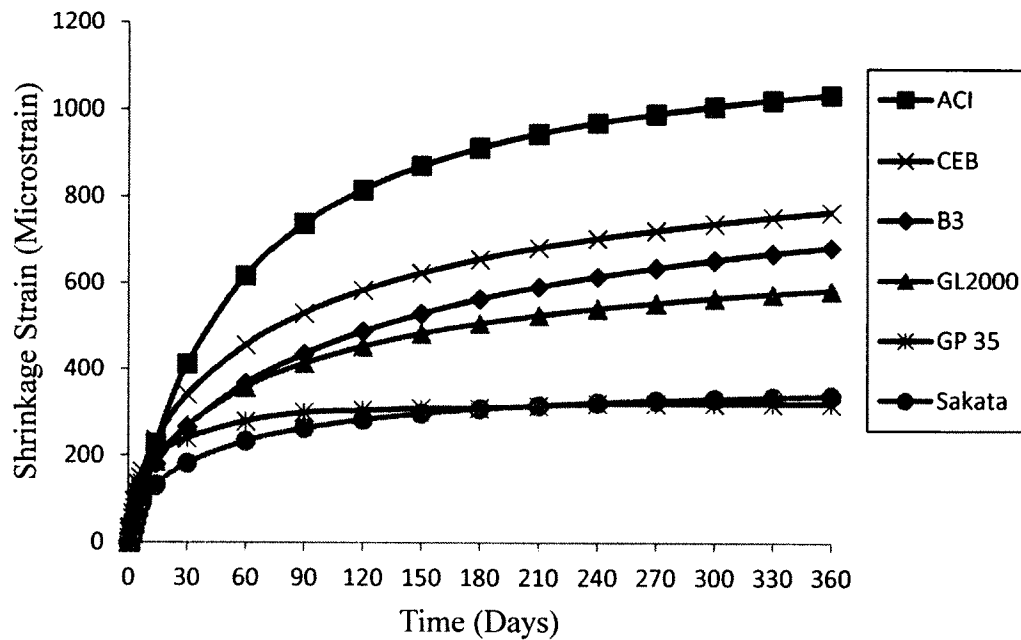
Figure 6.14 Exp. vs. predicted shrinkage strain (GP 35).

From the above data plot, it has been observed that the free shrinkage strain of GPC is less than the data predicted by the empirical equation most of the cases. Among the models used to predict the free shrinkage of the concrete, the Sakata model was very close to the experimental data observed for various GPC samples. Regression analysis also shows the same pattern which indicates that a model can be built to predict the free shrinkage of the GPC following the existing concrete shrinkage model.

CHAPTER 7

CREEP TEST RESULTS

7.1 Introduction

In this chapter, the results from the creep specimens were analyzed for the calculation of creep coefficient and creep compliance. The effect of various factors on creep behavior of concrete was analyzed. From the existing creep model, the creep pattern was predicted and compared with the experimental values. A new creep model was proposed to predict the geopolymer concrete creep more accurately.

7.2 Analysis and Test Results

The creep behavior of fly ash based geopolymer concrete was studied for the six different mixes. The details of these mixtures are given in Table 3.3. The test specimens were 6 x 12 in cylinders. Samples were cured at 60° C for 24 hours in a dry oven. The control OPC sample was moist cured for 7 days. The creep tests commenced on the day after curing the concrete and the applied load was 40% of its crushing strength on that day. Test specimens were named accordingly by their curing condition and the mix design. Table 4.2 presents the loading day compressive strength and the applied sustained stress of the creep specimens. It must be noted that the curing condition and the curing temperature was the same for all GPC samples.

7.3 Strength Gain Effect on Creep Behavior of Geopolymer Concrete

A test program was designed to see the strength gain of the GPC with various mix designs with time. It has been observed that there is no significant strength change that occurs for the GPC as the EM also remains unchanged. This phenomenon is true for the GPC with different AS/FA and different target compressive strength. The mix with concentrated hydroxide and silicate had creep strain at three months over 20 percent less than those having less aggressive activator solution (12 molar and N Silicate). This was because of less amount of polymerization in the later mix. It is observed that the aggressive activator solution selection causes more polymerization; thus, the more strength the more dense the concrete and less creep [87]. Also, the curing time and curing temperature plays a significant role in the reaction process. It is assumed that 70% of compressive strength of the geopolymer concrete is achieved in one day of oven curing and over ninety-five percent of its compressive strength is reached in the three days of heat curing.

7.3.1 Loading Condition of Specimen and its Effect on the Creep Behavior

All the specimens were loaded at a stress of 40 percent of its ultimate strength. As seen from Figure 7.1, the specimen with lower strength showed a higher creep strain and a higher creep coefficient [88]. The significant effects of stress level on creep strain can be seen from both the high strength and low strength concrete. For the 0.65 AS/FA ratio and the same amount of fine material content, 0.35 AS/FA content concrete showed 20 percent reduced creep coefficient. For the other mix such as 0.45, 0.55, and 0.65 specimens oven cured for one day and loaded at 40% of their compressive strength was 11%, 17%, and 22% higher than the 0.35% AS/FA content concrete.

7.3.2 Activator Solution Ratio and Air Content Effect on Creep Strain

The main component on creep in the geopolymer concrete is the polymerized fly ash. Effect of activator solution (sodium hydroxide and sodium silicate) ratio on the total strain of the GPC is shown in Figure 7.1. Creep is related to the internal spaces in the concrete after the whole matrix is hardened. As there is theoretically no water in GPC, creep in it is really low. Capillary voids are not formed in the concrete. Creep is highly influenced by the air content in the concrete. Creep is increased as the air content in the concrete is increased. In the case of geopolymer concrete, the main component that is responsible for creep is the polymer paste, which is formed as the polymerization reaction occurred as fly ash particles comes in contact with the activator solutions. Also, voids in the concrete play an important role influencing the creep behavior, because in high stress, the void in the concrete is collapsed and the specimen reduces in size.
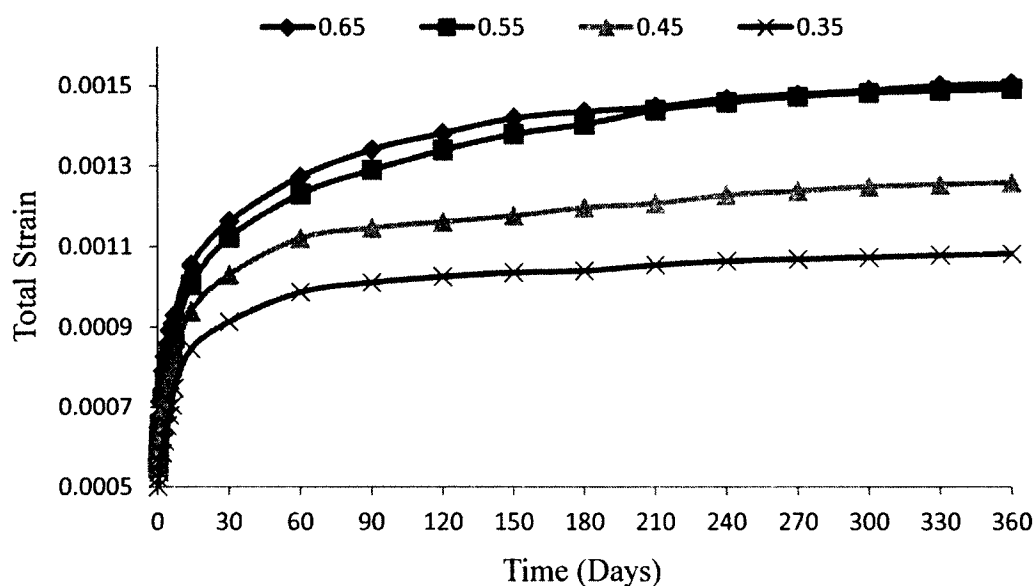
Figure 7.1 Total strain of GPC with different AS/FA ratio.

This is why the activator solution to cementitious material ratio and the air content of concrete plays an important role. This effect was clearly visible from the test result obtained from the research. The five different mix designs with different AS/FA ratio were tested to see the effect of the activator solution ratio on the creep behavior. As these specimens were put on the vibrating table, the air content of the fresh concrete is not completely representative with the void content of the hardened concrete. It can be seen from Figure 7.1 that the total strain for the GP65 is staying at the top of the other GPC mix at the end of 360 days of data collection. Among the other GPC mixes, the GP35 has the lowest total strain. Others samples showed the creep according to the AS/FA ratio, the more the solution content in the concrete, the more the strain value is shown.

7.3.3 Compressive Strength and Creep Strain:

This section discusses the relationship between the concrete compressive strength and the creep strain. Simple linear regression analysis was used to correlate the creep strain with the compressive strength as a function of time. Given the material properties and the fresh properties are kept constant, only the final hardened properties are considered as variables. This is important in the way that the well establishment of a relation between the creep strain and the mechanical strength of the concrete can be a substitution for the creep test. In Figure 7.2 compressive strength of the concrete at 1 day is plotted against the creep coefficient at 90 days for the oven cured concrete at a 40% compressive stress.
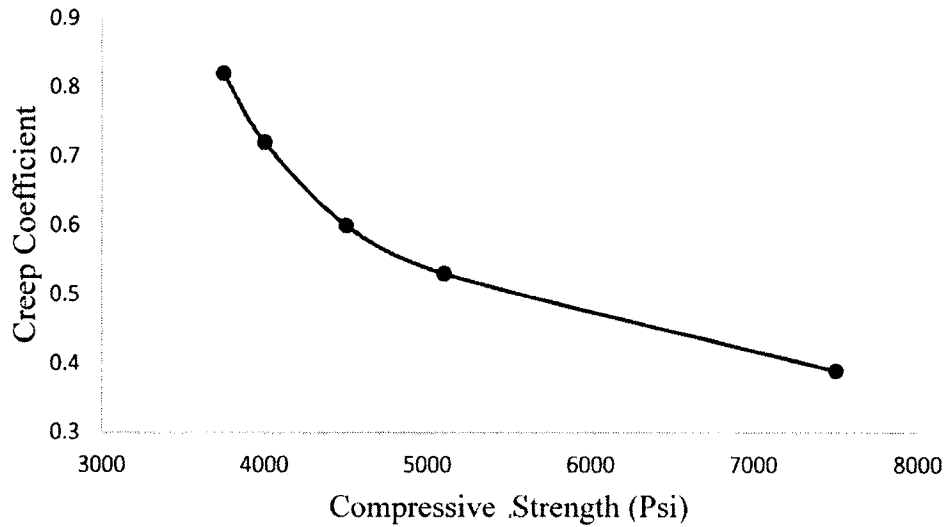
Figure 7.2 Creep coefficient at 90 days.

It is observed from the analysis that the creep strain decreases as the increase of the concrete compressive strength (Figure 7.3). Equation obtained from the regression analysis from this data is:

$$\phi_c = 3656 f_c^{-1.02}$$

[7.1]
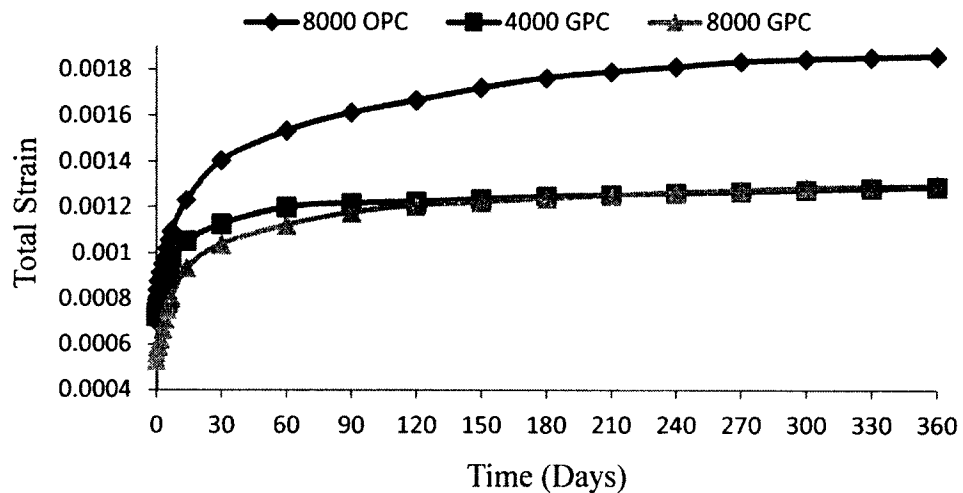
Figure 7.3 Total strain of GPC with different Compressive Strength.

Coefficients are presented in Table 7.1 for a different mix design. The ANOVA analysis shows that the age of curing had no significant effect on the strength and the subsequent creep strain. Thus, the relationship between the compressive strength and creep strain obtained under the stress level of 40% of its ultimate strength can be expressed as one single linear equation regardless of what curing condition was applied to the specimens. Figure 7.4 through 7.7 show the creep strain and total strain of the GPC with different activator solution ratios at different ages of the loaded specimen.
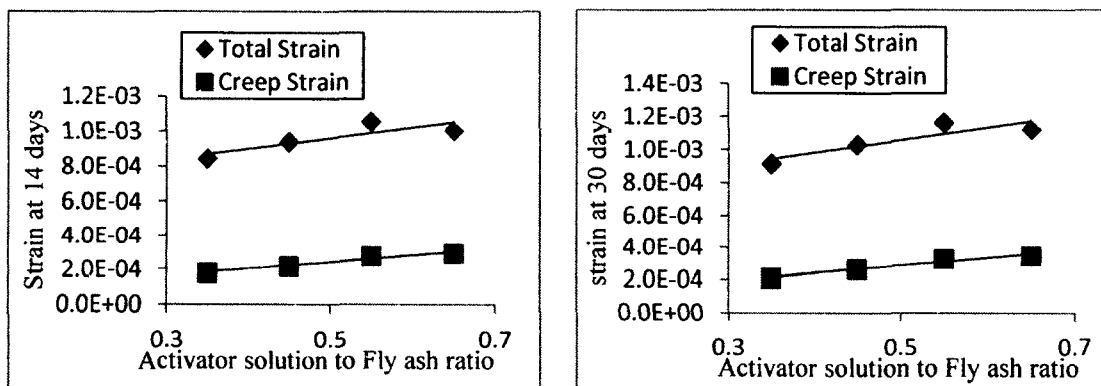
Figure 7.4 Total strain and Creep strain at different age of concrete (15 and 30 Days).
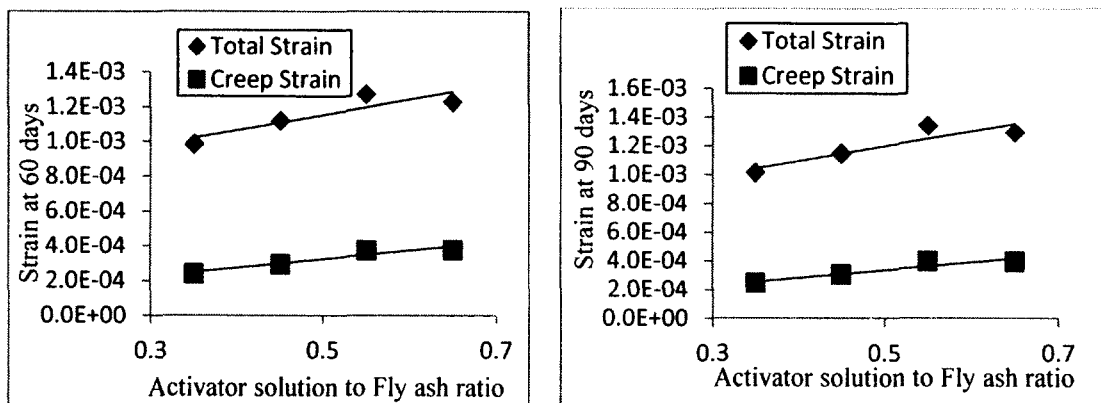
Figure 7.5 Total strain and Creep strain at different age of concrete (60 and 90 Days).
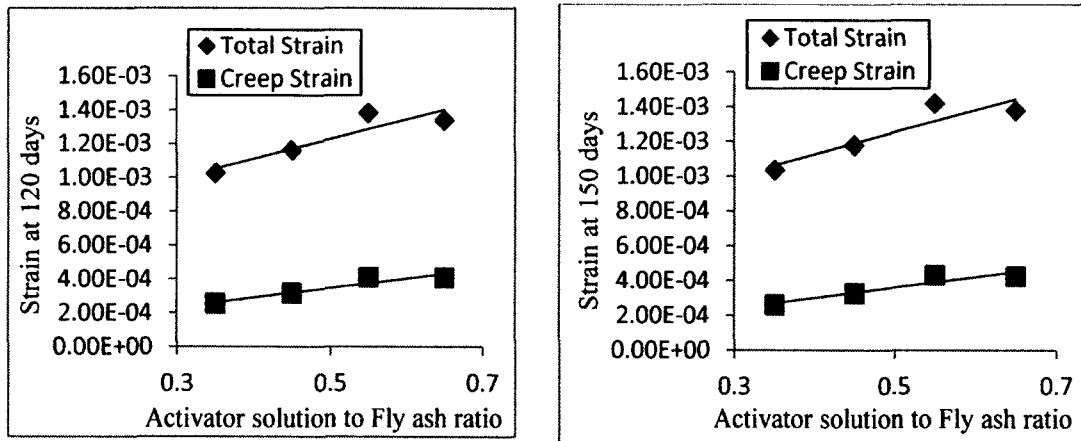
Figure 7.6 Total strain and Creep strain at different age of concrete (120 and 150 Days).
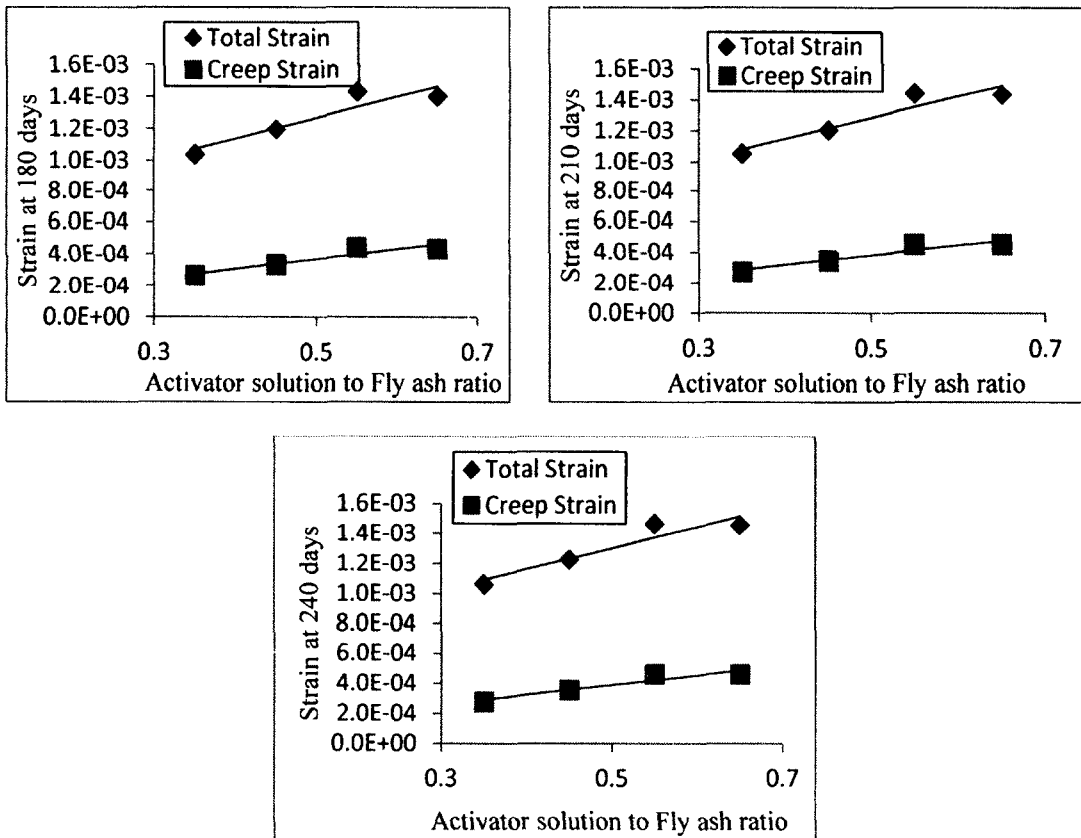
Figure 7.7 Total strain and Creep strain at different age of concrete (180, 210, and 240 Days).

7.4 Definition of Creep Coefficient

Creep coefficient is the ratio of creep strain and elastic strain. This is a very important design parameter for the concrete structure design, which is not only affected by the factors influencing the creep strain, but also by the factor which influences the elastic property of the concrete.

7.4.1 Water Content Effect on Creep Coefficient

The effect of water content is significant on the creep coefficient of the concrete. Figure 7.8 shows the effect of AS/FA ratio on the creep co-efficient of the concrete at different ages. It is observed from the analysis that the creep coefficient increases as the liquid content in the concrete increases.
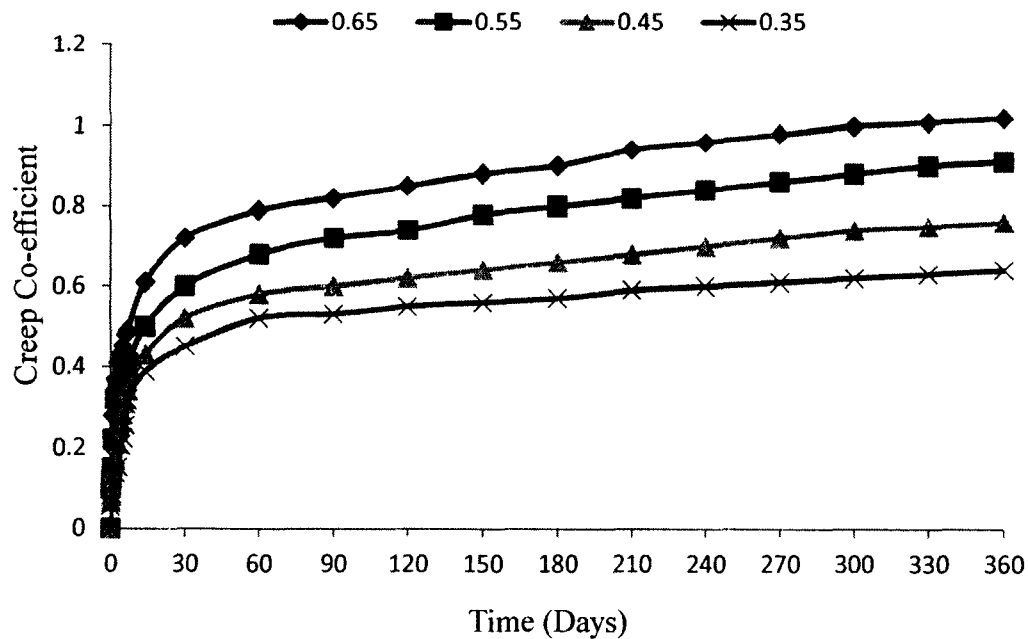
Figure 7.8 Creep coefficient for different AS/FA mix.

7.4.2 Effect of Compressive Strength at Loading Ages on Creep Coefficient

It is observed from the graph shown in Figure 7.9 that the higher the compressive strength of the concrete is at the loading age, the lower the creep coefficient. In the graph,

shown in Figure 7.9, the creep coefficient of the 8000 psi concrete is 15% lower than the creep of the 4000 psi concrete.
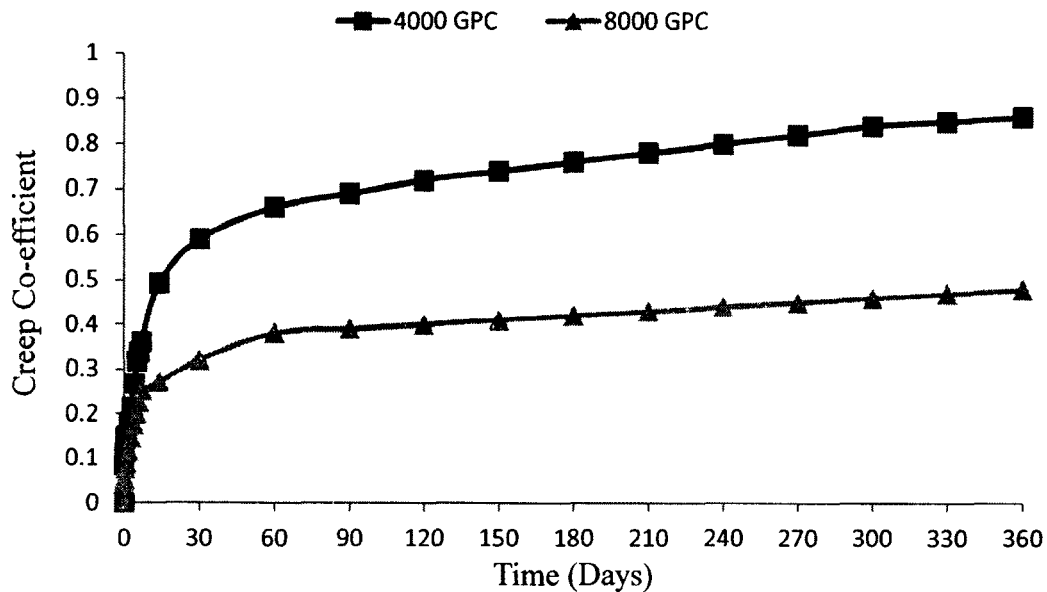
Figure 7.9 Creep coefficient for different strength mix.

It can be seen from Table 7.1 that the compressive strength of the concrete at the loading age is nearly linearly related to the creep coefficient at 90 days. This relation is valid for different loading ages of concrete. To find out how the compressive strength of the concrete at the loading age is related to the creep coefficient at 90 days, the compressive strength at the loading age was plotted against the corresponding creep coefficient at 90 days for specimen loaded at 40% stress.

Table 7.1 Creep coefficient with time.

Time (Days)	8000 OPC	GP4000	GP 35	GP8000	GP 45	GP 55	GP 65
0	0	0	0	0	0	0	0
0.083	0.18	0.09	0.06	0.05	0.065	0.1	0.12
0.25	0.23	0.11	0.07	0.05	0.08	0.12	0.15
0.5	0.36	0.15	0.09	0.08	0.11	0.15	0.2
1	0.42	0.15	0.13	0.09	0.14	0.22	0.28
2	0.45	0.18	0.14	0.12	0.17	0.32	0.37
3	0.47	0.21	0.15	0.15	0.21	0.34	0.41
4	0.48	0.27	0.21	0.18	0.25	0.36	0.43
5	0.52	0.32	0.22	0.20	0.28	0.38	0.45
6	0.55	0.34	0.26	0.23	0.31	0.39	0.48
7	0.58	0.36	0.32	0.25	0.34	0.41	0.49
14	0.68	0.49	0.39	0.27	0.43	0.5	0.61
30	0.8	0.59	0.45	0.32	0.52	0.6	0.72
60	0.9	0.66	0.52	0.38	0.58	0.68	0.79
90	0.95	0.69	0.53	0.39	0.6	0.72	0.82
120	0.98	0.72	0.55	0.40	0.62	0.74	0.85
150	1.02	0.74	0.56	0.41	0.64	0.78	0.88
180	1.06	0.76	0.57	0.42	0.66	0.8	0.9
210	1.08	0.78	0.59	0.43	0.68	0.82	0.94
240	1.10	0.80	0.60	0.44	0.7	0.84	0.96
270	1.12	0.82	0.61	0.45	0.72	0.86	0.98
300	1.13	0.84	0.62	0.46	0.74	0.88	1
330	1.14	0.85	0.63	0.47	0.75	0.9	1.01
360	1.15	0.86	0.64	0.48	0.76	0.91	1.02

As there is a relationship developed between the compressive strength and the elastic modulus, and now a simple linear regression analysis was performed to find out the relation between the creep coefficient and the elastic modulus of the concrete. It was observed that the elastic modulus is correlated with the creep coefficient. The relationship obtained from this data is shown in Equation 7.1:

$$\phi_c = -4E^{-5}E_c + 1.548.$$

[7.1]

7.5 Ultimate Creep Strain Prediction

Creep strain of the concrete decreases with time. At some point, the creep strain will approach a limiting value after an infinite time with the load. A study by Troxel *et al.* indicates that the average value of the creep strain after 30 years is 1.36 times the one year creep strain. From the engineering the practical point of view, it is often assumed that the 30 years creep strain represent the ultimate creep strain. Hence, the ultimate creep strain of the concrete analyzed in this study was determined using the asymptotic Equation 7.2:

$$\varepsilon_c(t) = \alpha.(\frac{t}{t+\gamma})^\beta .$$

[7.2]

This equation is obtained from the ratio of two polynomials. As the time reaches to infinity, the ratio of the two polynomials will be equal to 1. This is why the ultimate creep strain will be equal to α. The relative humidity was controlled at 50% in this study, and 6 x 12 in cylindrical specimens were used for creep tests. The geometric characteristics of the specimen is calculated as:

$$h = \frac{2A_c}{u} = \frac{2 \times \pi \times 3^2}{\pi \times 6} = 3in = 76.2mm .$$

[7.3]

Hence, γ is calculated as follows:

$$\gamma = 150\left[1+\left(1.2\left(\frac{50}{100}\right)^{18}\right)\right]\frac{h}{100}+250 = 294 \leq 1500.$$

[7.4]

Thus, the equation to fit the experimental model becomes:

$$\varepsilon_c(t) = \alpha\left(\frac{t}{t+294}\right)^\beta .$$

[7.5]

Here, $\alpha = 1.36 \times \varepsilon_c(1year)$, and $\beta = 0.5$. Time t is in days.

7.6 Evaluation on Creep Prediction Model

Creep prediction model such as ACI, Bazant B3, CEB, GL2000, and Sakata

models are evaluated in this study. Experimental and theoretical values are plotted in the

graph to see the effectiveness of the equations. Figures 7.10 through 7.15 show the

predicted values and the experimental values.
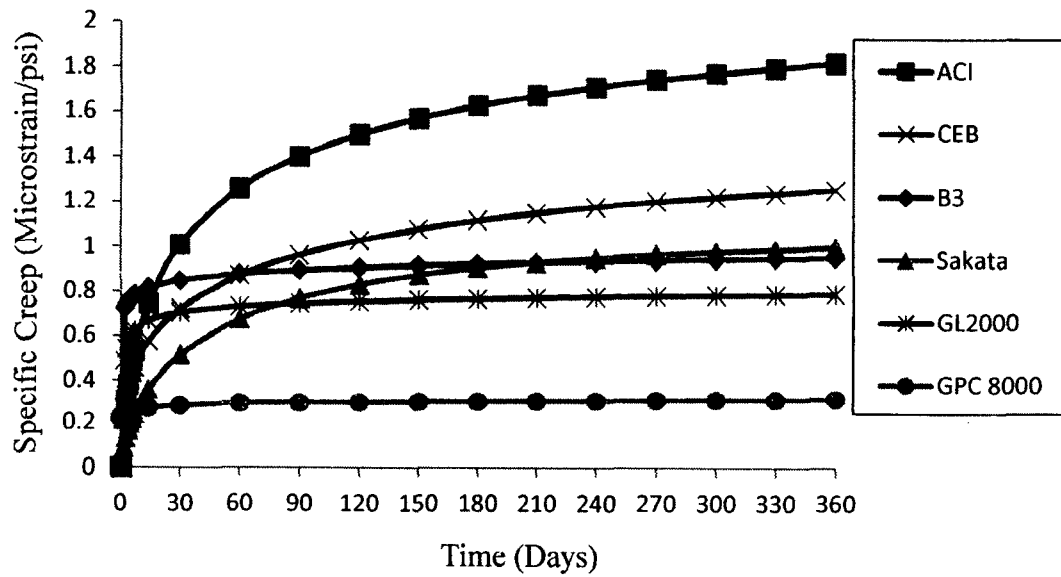
Figure 7.10 Exp. vs. predicted specific creep (GPC 8000).
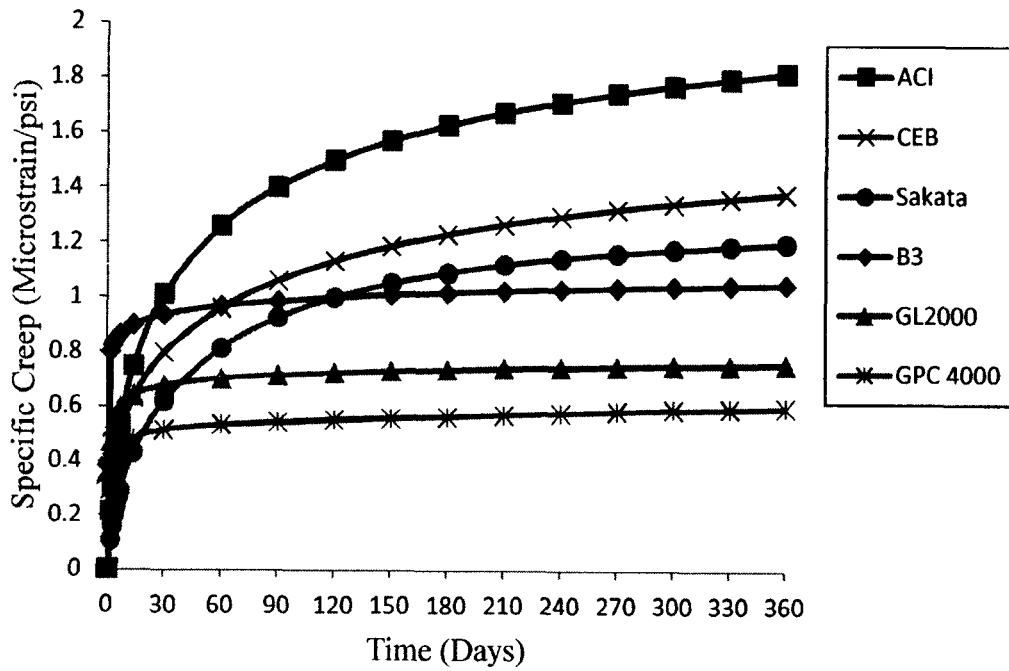
Figure 7.11 Exp. vs. predicted specific creep (GPC 4000).
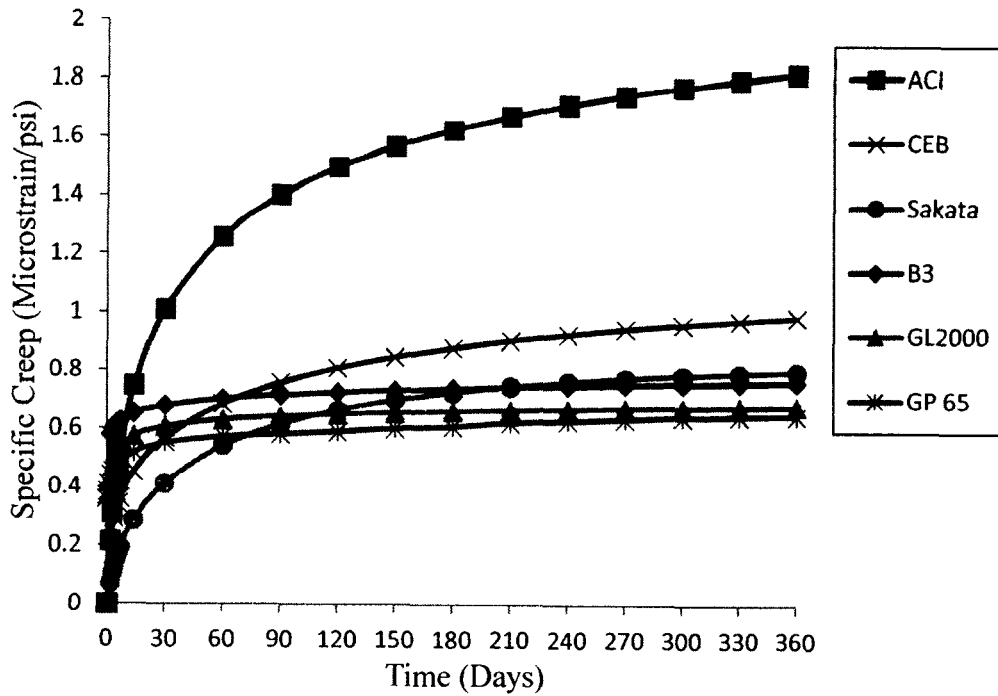
Figure 7.12 Exp. vs. predicted specific creep (GP 65).
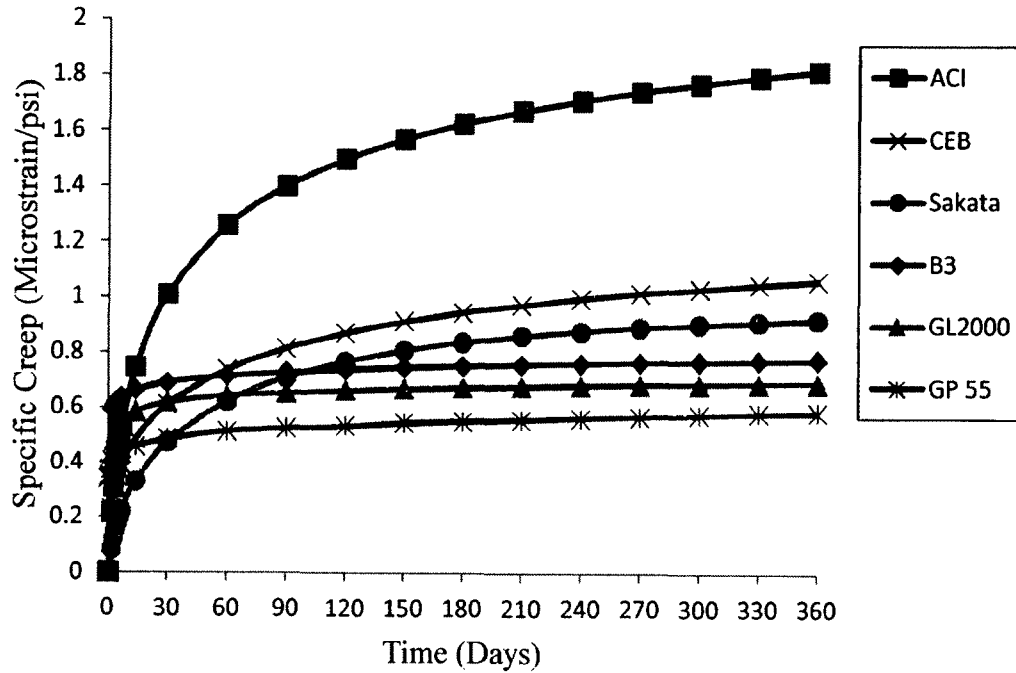
Figure 7.13 Exp. vs. predicted specific creep (GP 55).
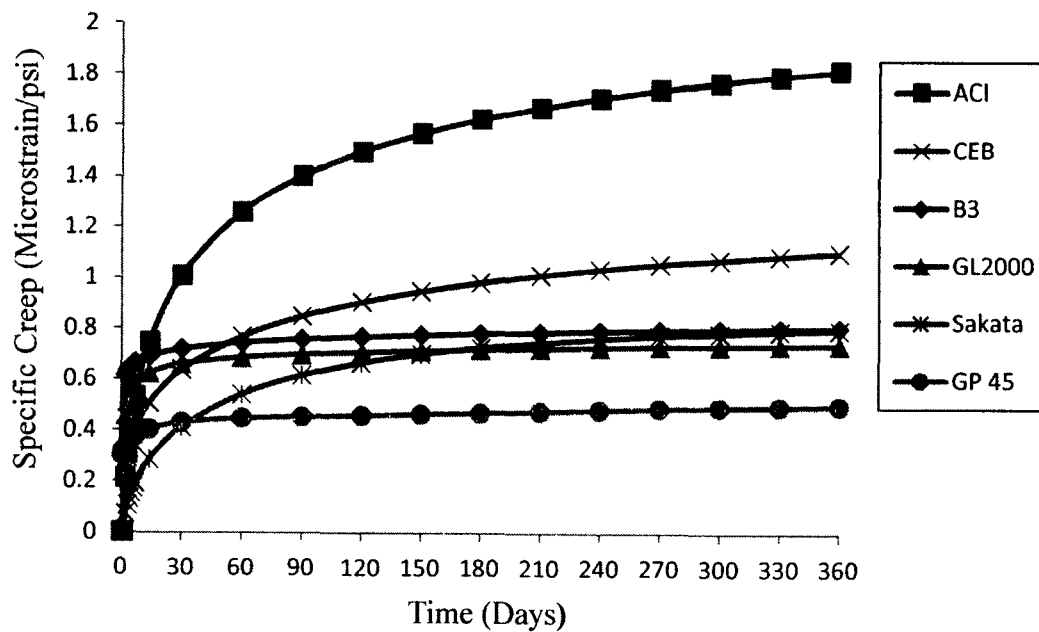
Figure 7.14 Exp. vs. predicted specific creep (GP 45).
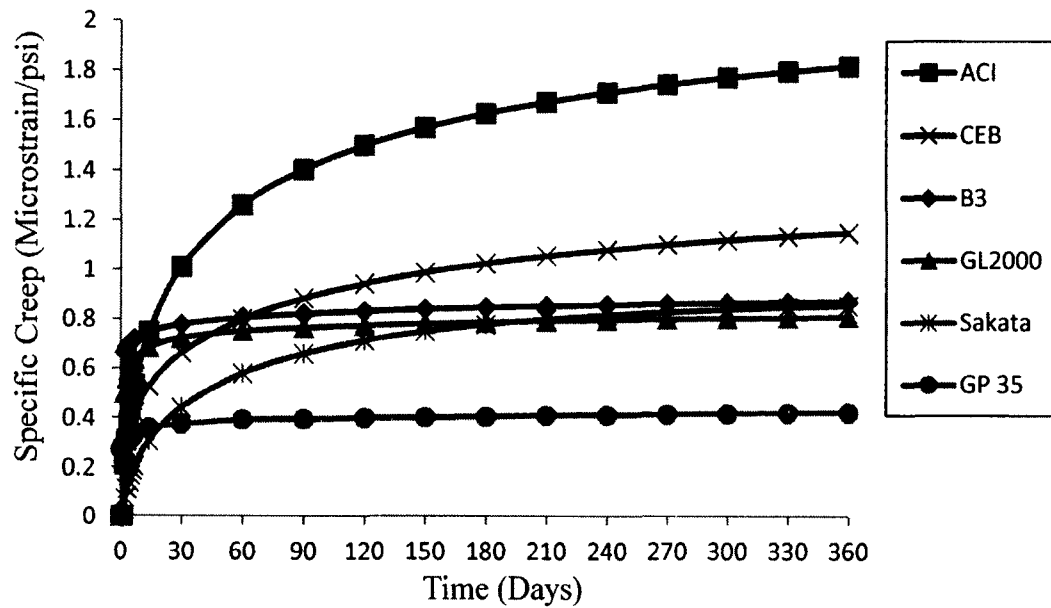
Figure 7.15 Exp. vs. predicted specific creep (GP 35).

Among the theoretical models considered in this study, the GL2000 model has a close relationship with the experimental data. In this study, a model was proposed following the GL2000 model to predict the creep values for GPC. Regression analysis was performed with the experimental data to find the coefficients.

CHAPTER 8

CONCLUSIONS AND RECOMMENDATIONS

8.1 Introduction

This manuscript puts forth the test result and analysis of several mechanical and long term properties of geopolymer concrete. Material used for the sample preparation was selected to guide the concrete mix design. First, the empirical equation was developed to predict the mechanical properties of the GPC using the physical testing process of series of different mix designs of concrete. Compressive strength of the GPC is predicted from the chemical component of the cementitious material. Elastic modulus and flexural strength of the concrete was correlated with the compressive strength and the unit weight of the concrete. A set of regression model is put forth in an attempt to explain the mechanical properties of the GPC.

- Equation 5.2 was found to be the best regression model to predict the compressive strength of GPC. It uses reactive alumina, reactive silica, and reactive calcium oxide as well as loss on ignition and the mean particle size as the regressors. It showed the best fit by predicting compressive strength with an average accuracy of ±7 MPa.

- The density of the GPC was found to be strongly correlated with the specific gravity of the fly ash stockpile. Eq. 5.31 shows the influence of specific gravity of FA on the unit weight of hardened GPC. The relationship between the two variables can be attributed to the packing characteristics of FA.

152

- Relationship between the GPC setting time with the reactive calcium content is shown Figure 5.6. Calcium content in FA has a strong effect on the setting time of the GPC. The effect of reactive calcium content in FA can be explained in two different ways. Firstly, the hydrated products act as nucleation sites that accelerate the setting, and secondly, the hydration of calcium consumes water that raises the concentration of the alkaline solution and accelerates the reaction.

- The relationship between compressive strength (f_c') and flexural strength (f_r') is established for GPC in this study. Eq. 5.4 shows the prediction equation with R^2 value 0.934. It showed to be the best fit by predicting the flexural strength with an average accuracy of ±4 MPa.

- The relationship between compressive strength and modulus of elasticity for GPC was refined in this study using regression analysis and is given in Eq. 5.7. Geopolymer concrete seems to possess a similar mechanical behavior to that of ordinary Portland cement concrete. A similar equation is given in ACI 318 (2008) section 8.5.1. In an attempt to predict elastic modulus of GPC with both compressive strength unit weight of GPC Eq. 5.10 was suggested in this study.

8.2 Design of Shrinkage and Creep Apparatus

In an attempt to calculate the shrinkage of the GPC, the ring mold along with the foil strain gages connected to the data acquisition system was designed following the ASTM C1581. The creep of GPC was measured through a metal frame that was developed following the ASTM C512. The creep frame designed for this test program is capable of applying and maintaining a constant load of up to 125,000 lbs on specimen with accuracy within 1%. The limitation of the creep frame is due to the spring used to

maintain the load. A maximum of three 6 x 12 in cylinders can be stacked in the creep

frame. The bending capacity of the base plate and the header plate was designed using the

finite element analysis. When a maximum load of 125,000 was applied, the deflection of

the 1.5 in thick metal plate was less than 0.0001 in. An efficient surface grinding machine

was utilized to polish the surface of the test specimen to ensure the uniform distribution

of the load.

8.3 Results

The second phase of this test program was designed to understand the long term

properties of the GPC. The main goal for this part of the experiment was to find out the

change in the compressive strength, and the elastic modulus with time. The regression

equation was utilized to find an equation to predict these two properties with time. As

these two mechanical properties are closely related to the long-term behavior of concrete,

it was important to find an equation to predict the values. In an attempt to find out the

shrinkage and creep properties of geopolymer concrete, the creep and shrinkage test setup

was designed and a series of tests was performed to see the shrinkage and creep behavior

of the GPC. Shrinkage and creep behavior of the GPC was plotted in a graph along with

the existing empirical models available for OPC to see which model closely relates with

the experimental data obtained from the test setup. Five different shrinkage and creep

models were compared and those are ACI, B3, CEB, GL2000, and Sakata models. It was

observed from the test procedure that the shrinkage pattern of the GPC closely follow the

SAKATA model, and the creep pattern of GPC was very similar to GL2000 model.

8.3.1 Shrinkage of Fly Ash Based GPC

- From the test result, it was observed that the water content has a significant effect on the drying shrinkage of the GPC. For a mix design with 0.35 AS/FA ratio, it took 86 days and with 0.65 AS/FA ratio, the concrete ring was cracked in only 42 days.

- GPC with higher strength took more days to form the surface crack. The high strength of the GPC prevents the tensile crack formation. The test result obtained from 4000 psi and 8000 psi GPC reflects the hypothesis.

- For the restrained shrinkage test, ASTM C1581 shows that the relationship between the shrinkage strain and time can be presented as Eq. 6.1. Here, "t" is in days. The test result obtained from this study puts forth a table with this coefficient for the shrinkage measurement of the GPC with a different activator solution to fly ash ratio.

- The sand to aggregate ratio had little effect on the mechanical properties or the cracking potential of the mixes. Each of the mixes had an elastic modulus in the range of about 5000 Ksi and a tensile strength in the range of 650 Psi. Every mix in the AS/FA group cracked around 90 days or stopped to put any compression on the inner ring. The free shrinkage at day 90 for each mix was in the range of 350 to 450 micro strain.

- Tensile stress generated by restrained shrinkage of the concrete are significant in the first week after casting and lead to a fracture of the material. The role of the tensile creep in the relaxing shrinkage stress is substantial and reduces the stress.

- The SAKATA model had the closest agreement with the experimental data, and the bounds of the proposed model compared to other available models. The overall

comparison with the available models showed the proposed model in this study has the closest correlation with the experimental data.

8.3.2 Creep of Fly Ash Based GPC

• The compressive strength (f_c') affects the creep of the GPC; the higher the strength the smaller the creep.

• The measured creep strain and instantaneous strain were linearly proportional to the stress applied within the level of stress used for the test (40% of compressive strength). Thus, the measured creep coefficient and creep compliance were not affected because GPC with different strength was used in this study.

• Activator solution to fly ash ratio has a significant effect on the creep behavior of the GPC. The higher the solution to fly ash ratio, the greater the creep coefficient.

• The creep coefficient of the GPC with high strength (8000 psi) was found to be only 60% at the age of 90 days to the low strength (4000 psi) GPC sample. As the degree of geopolymerization controls porosity, and hence the concrete strength, it was validated with this study.

• The effect of utilizing predicted and experimental modulus of elasticity (EM) on the creep prediction equation was studied. It was found that the EM prediction equation can be used with the available empirical model to calculate the creep coefficient of the GPC at different loading age with fair accuracy. Table 3.8 shows the experimental EM of the GPC at different ages. These EM values are in well accordance with the predicted values.

• GL 2000 model (as shown in Figures 7.8 through 7.15) appeared to give a better prediction on the creep behavior of the GPC investigated in this study.

8.4 Recommendation for Future Work

Future research may include the effects of different curing regimes such as steam curing or infrared curing on the short and long term behavior of GPC. Different types of coarse aggregate have different characteristics. Some are better than others. A possible future investigation in this study should be using the same mix design parameters of aggregates from different sources and compare those results to this study. For long term properties, only class F fly ash was considered in this study. Both class F and class C fly ashes can be considered to find the effect of calcium content on the long term properties of the GPC. Though not employed in this research, implementing internal strain gages into the specimens may help verify manual gage length change (Whittemore strain gauge). It can also provide strain measurements for the rapid strain increase experienced during thermal cure and the quick load application process. Mercury intrusion porosimetry (MIP) test can be performed to see the effect of GPC's density on the shrinkage and creep property.

APPENDIX A

EXPERIMENTAL AND CALCULATED DATA

Table A-1 Strain data obtained and calculated from creep test

Mix	Curing Condition	Applied Stress	Strain	2 hour	6 hour	12 hour	24 hour	2 day	3 day	4 day
4000 Psi GPC	1Day Heat Cured	40%	Total	0.00053	0.00056	0.00059	0.00059	0.00062	0.00067	0.00071
			Shrinkage	0.00001	0.00003	0.00004	0.00004	0.00006	0.00008	0.00010
			Elastic	0.00048	0.00048	0.00048	0.00048	0.00048	0.00048	0.00048
			Creep	0.00004	0.00005	0.00007	0.00007	0.00009	0.00010	0.00013
			Creep Coefficient	0.09	0.11	0.15	0.15	0.18	0.21	0.27
			Creep Modulus	2.87E+06	2.80E+06	2.72E+06	2.71E+06	2.65E+06	2.57E+06	2.46E+06

Strain	5 day	6 day	7 day	14 day	1 Month	2 Month	3 Month	4 Month
Total	0.00076	0.00078	0.00080	0.00094	0.00104	0.00112	0.00118	0.00121
Shrinkage	0.00012	0.00014	0.00015	0.00022	0.00027	0.00033	0.00037	0.00038
Elastic	0.00048	0.00048	0.00048	0.00048	0.00048	0.00048	0.00048	0.00048
Creep	0.00015	0.00016	0.00017	0.00024	0.00029	0.00032	0.00033	0.00035
Creep Coefficient	0.32	0.34	0.36	0.49	0.60	0.66	0.69	0.72
Creep modulus	2.36E+06	2.33E+06	2.29E+06	2.09E+06	1.95E+06	1.88E+06	1.84E+06	1.81E+06

Strain	5 Month	6 Month	7 Month	8 Month	9 Month	10 Month	11 Month	1 Year
Total	0.00122	0.00124	0.00125	0.00127	0.00128	0.00129	0.00129	0.00130
Shrinkage	0.00039	0.00039	0.00040	0.00040	0.00040	0.00040	0.00040	0.00040
Elastic	0.00048	0.00048	0.00048	0.00048	0.00048	0.00048	0.00048	0.00048
Creep	0.00036	0.00037	0.00038	0.00039	0.00039	0.00040	0.00041	0.00041
Creep Coefficient	0.74	0.76	0.78	0.80	0.82	0.84	0.85	0.86
Creep Modulus	1.79E+06	1.77E+06	1.75E+06	1.73E+06	1.71E+06	1.69E+06	1.68E+06	1.68E+06

Table A-1. Continued

Mix	Curing Condition	Applied Stress	Strain	2 hour	6 hour	12 hour	24 hour	2 day	3 day	4 day
8000 Psi GPC	1 Day Heat Cured	40%	Total	0.00072	0.00074	0.00076	0.00077	0.00081	0.00086	0.00089
			Shrinkage	0.00001	0.00002	0.00003	0.00003	0.00005	0.00008	0.00009
			Elastic	0.00068	0.00068	0.00068	0.00068	0.00068	0.00068	0.00068
			Creep	0.00003	0.00004	0.00005	0.00006	0.00008	0.00010	0.00012
			Creep Coefficient	0.05	0.05	0.08	0.09	0.12	0.15	0.18
			Creep Modulus	4.48E+06	4.45E+06	4.36E+06	4.31E+06	4.20E+06	4.10E+06	3.99E+06

Strain	5 day	6 day	7 day	14 day	1 Month	2 Month	3 Month	4 Month
Total	0.00093	0.00095	0.00098	0.00105	0.00113	0.00120	0.00122	0.00122
Shrinkage	0.00011	0.00012	0.00013	0.00019	0.00023	0.00026	0.00027	0.00027
Elastic	0.00068	0.00068	0.00068	0.00068	0.00068	0.00068	0.00068	0.00068
Creep	0.00014	0.00015	0.00017	0.00018	0.00022	0.00026	0.00027	0.00027
Creep Coefficient	0.20	0.23	0.25	0.27	0.32	0.38	0.39	0.40
Creep modulus	3.91E+06	3.83E+06	3.75E+06	3.69E+06	3.56E+06	3.40E+06	3.38E+06	3.35E+06

Strain	5 Month	6 Month	7 Month	8 Month	9 Month	10 Month	11 Month	1 Year
Total	0.00124	0.00125	0.00125	0.00126	0.00127	0.00128	0.00128	0.00129
Shrinkage	0.00028	0.00028	0.00028	0.00028	0.00028	0.00028	0.00028	0.00028
Elastic	0.00068	0.00068	0.00068	0.00068	0.00068	0.00068	0.00068	0.00068
Creep	0.00028	0.00029	0.00029	0.00030	0.00031	0.00031	0.00032	0.00033
Creep Coefficient	0.41	0.42	0.43	0.44	0.45	0.46	0.47	0.48
Creep Modulus	3.33E+06	3.31E+06	3.28E+06	3.26E+06	3.24E+06	3.22E+06	3.19E+06	3.17E+06

Table A-1. Continued

Mix	Curing Condition	Applied Stress	Strain	2 hour	6 hour	12 hour	24 hour	2 day	3 day	4 day
GP 35	1 Day Heat Cured	40%	Total	0.00050	0.00052	0.00054	0.00056	0.00058	0.00062	0.00065
			Shrinkage	0.00001	0.00003	0.00003	0.00004	0.00006	0.00008	0.00009
			Elastic	0.00046	0.00046	0.00046	0.00046	0.00046	0.00046	0.00046
			Creep	0.00003	0.00003	0.00004	0.00006	0.00006	0.00007	0.00010
			Creep Coefficient	0.06	0.07	0.09	0.13	0.14	0.15	0.21
			Creep Modulus	3.67E+06	3.62E+06	3.57E+06	3.44E+06	3.40E+06	3.36E+06	3.21E+06

Strain	5 day	6 day	7 day	14 day	1 Month	2 Month	3 Month	4 Month
Total	0.00068	0.00070	0.00075	0.00084	0.00091	0.00099	0.00101	0.00103
Shrinkage	0.00011	0.00012	0.00014	0.00020	0.00024	0.00028	0.00030	0.00031
Elastic	0.00046	0.00046	0.00046	0.00046	0.00046	0.00046	0.00046	0.00046
Creep	0.00010	0.00012	0.00015	0.00018	0.00021	0.00024	0.00025	0.00026
Creep Coefficient	0.22	0.26	0.32	0.39	0.45	0.52	0.53	0.55
Creep modulus	3.16E+06	3.08E+06	2.94E+06	2.79E+06	2.67E+06	2.55E+06	2.53E+06	2.50E+06

Strain	5 Month	6 Month	7 Month	8 Month	9 Month	10 Month	11 Month	1 Year
Total	0.00104	0.00104	0.00105	0.00106	0.00107	0.00107	0.00108	0.00108
Shrinkage	0.00031	0.00031	0.00032	0.00032	0.00032	0.00032	0.00032	0.00032
Elastic	0.00046	0.00046	0.00046	0.00046	0.00046	0.00046	0.00046	0.00046
Creep	0.00026	0.00027	0.00027	0.00028	0.00028	0.00029	0.00029	0.00030
Creep Coefficient	0.56	0.57	0.59	0.60	0.61	0.62	0.63	0.64
Creep Modulus	2.48E+06	2.47E+06	2.43E+06	2.42E+06	2.40E+06	2.39E+06	2.37E+06	2.36E+06

Table A-1. Continued

Mix	Curing Condition	Applied Stress	Strain	2 hour	6 hour	12 hour	24 hour	2 day	3 day	4 day
GP 45	1Day Heat Cured	40%	Total	0.000554	0.000578	0.000602	0.000620	0.000653	0.000698	0.000733
			Shrinkage	0.000010	0.000027	0.000035	0.000038	0.000056	0.000080	0.000095
			Elastic	0.000510	0.000510	0.000510	0.000510	0.000510	0.000510	0.000510
			Creep	0.00003	0.00004	0.00006	0.00007	0.00009	0.00011	0.00013
			Creep Coefficient	0.065	0.08	0.11	0.14	0.17	0.21	0.25
			Creep Modulus	3.31E+06	3.26E+06	3.18E+06	3.09E+06	3.01E+06	2.91E+06	2.82E+06

Strain	5 day	6 day	7 day	14 day	1 Month	2 Month	3 Month	4 Month
Total	0.000768	0.000799	0.000824	0.000940	0.001031	0.001122	0.001147	0.001162
Shrinkage	0.000115	0.000130	0.000140	0.000210	0.000255	0.000315	0.000330	0.000335
Elastic	0.000510	0.000510	0.000510	0.000510	0.000510	0.000510	0.000510	0.000510
Creep	0.00014	0.00016	0.00017	0.00022	0.00027	0.00030	0.00031	0.00032
Creep Coefficient	0.28	0.31	0.34	0.43	0.52	0.58	0.6	0.62
Creep modulus	2.75E+06	2.69E+06	2.63E+06	2.47E+06	2.32E+06	2.23E+06	2.20E+06	2.18E+06

Strain	5 Month	6 Month	7 Month	8 Month	9 Month	10 Month	11 Month	1 Year
Total	0.001177	0.001197	0.001208	0.001228	0.001238	0.001248	0.001253	0.001258
Shrinkage	0.000340	0.000350	0.000350	0.000360	0.000360	0.000360	0.000360	0.000360
Elastic	0.000510	0.000510	0.000510	0.000510	0.000510	0.000510	0.000510	0.000510
Creep	0.00033	0.00034	0.00035	0.00036	0.00037	0.00038	0.00038	0.00039
Creep Coefficient	0.64	0.66	0.68	0.7	0.72	0.74	0.75	0.76
Creep Modulus	2.15E+06	2.12E+06	2.10E+06	2.07E+06	2.05E+06	2.03E+06	2.01E+06	2.00E+06

Table A-1. Continued

Mix	Curing Condition	Applied Stress	Strain	2 hour	6 hour	12 hour	24 hour	2 day	3 day	4 day
GP 55	1Day Heat Cured	40%	Total	0.00062	0.00065	0.00067	0.00071	0.00079	0.00083	0.00086
			Shrinkage	0.00001	0.00003	0.00004	0.00004	0.00006	0.00009	0.00011
			Elastic	0.00055	0.00055	0.00055	0.00055	0.00055	0.00055	0.00055
			Creep	0.00006	0.00007	0.00008	0.00012	0.00018	0.00019	0.00020
			Creep Coefficient	0.1	0.12	0.15	0.22	0.32	0.34	0.36
			Creep Modulus	2.96E+06	2.91E+06	2.83E+06	2.67E+06	2.47E+06	2.43E+06	2.39E+06

Strain	5 day	6 day	7 day	14 day	1 Month	2 Month	3 Month	4 Month
Total	0.00089	0.00091	0.00093	0.00105	0.00116	0.00127	0.00134	0.00138
Shrinkage	0.00013	0.00014	0.00015	0.00023	0.00028	0.00035	0.00039	0.00042
Elastic	0.00055	0.00055	0.00055	0.00055	0.00055	0.00055	0.00055	0.00055
Creep	0.00021	0.00022	0.00023	0.00028	0.00033	0.00038	0.00040	0.00041
Creep Coefficient	0.38	0.39	0.41	0.5	0.59	0.68	0.72	0.74
Creep modulus	2.36E+06	2.34E+06	2.31E+06	2.17E+06	2.05E+06	1.94E+06	1.89E+06	1.87E+06

Strain	5 Month	6 Month	7 Month	8 Month	9 Month	10 Month	11 Month	1 Year
Total	0.00142	0.00144	0.00145	0.00147	0.00148	0.00149	0.00150	0.00151
Shrinkage	0.00044	0.00044	0.00044	0.00045	0.00045	0.00045	0.00045	0.00045
Elastic	0.00055	0.00055	0.00055	0.00055	0.00055	0.00055	0.00055	0.00055
Creep	0.00043	0.00044	0.00045	0.00046	0.00048	0.00049	0.00050	0.00050
Creep Coefficient	0.78	0.8	0.82	0.84	0.86	0.88	0.9	0.91
Creep Modulus	1.83E+06	1.81E+06	1.79E+06	1.77E+06	1.75E+06	1.73E+06	1.71E+06	1.70E+06

Table A-1. Continued

Mix	Curing Condition	Applied Stress	Strain	2 hour	6 hour	12 hour	24 hour	2 day	3 day	4 day
GP 65	1Day Heat Cured	40%	Total	0.00055	0.00058	0.00062	0.00066	0.00072	0.00077	0.00080
			Shrinkage	0.00001	0.00003	0.00004	0.00004	0.00007	0.00009	0.00011
			Elastic	0.00048	0.00048	0.00048	0.00048	0.00048	0.00048	0.00048
			Creep	0.00006	0.00007	0.00010	0.00013	0.00018	0.00020	0.00021
			Creep Coefficient	0.12	0.15	0.2	0.28	0.37	0.41	0.43
			Creep Modulus	2.78E+06	2.71E+06	2.60E+06	2.44E+06	2.28E+06	2.21E+06	2.18E+06

Strain	5 day	6 day	7 day	14 day	1 Month	2 Month	3 Month	4 Month
Total	0.00083	0.00084	0.00087	0.00100	0.00112	0.00123	0.00129	0.00134
Shrinkage	0.00013	0.00013	0.00016	0.00023	0.00030	0.00037	0.00042	0.00045
Elastic	0.00048	0.00048	0.00048	0.00048	0.00048	0.00048	0.00048	0.00048
Creep	0.00022	0.00023	0.00024	0.00029	0.00035	0.00038	0.00039	0.00041
Creep Coefficient	0.45	0.48	0.49	0.61	0.72	0.79	0.82	0.85
Creep modulus	2.15E+06	2.11E+06	2.09E+06	1.94E+06	1.81E+06	1.74E+06	1.71E+06	1.69E+06

Strain	5 day	6 day	7 day	14 day	1 Month	2 Month	3 Month	4 Month
Total	0.00138	0.00140	0.00144	0.00146	0.00147	0.00148	0.00149	0.00149
Shrinkage	0.00048	0.00049	0.00051	0.00052	0.00052	0.00052	0.00052	0.00052
Elastic	0.00048	0.00048	0.00048	0.00048	0.00048	0.00048	0.00048	0.00048
Creep	0.00042	0.00043	0.00045	0.00046	0.00047	0.00048	0.00049	0.00049
Creep Coefficient	0.88	0.9	0.94	0.96	0.98	1	1.01	1.02
Creep modulus	1.66E+06	1.64E+06	1.61E+06	1.59E+06	1.58E+06	1.56E+06	1.55E+06	1.54E+06

Table A-1. Continued

Mix	Curing Condition	Applied Stress	Strain	2 hour	6 hour	12 hour	24 hour	2 day	3 day	4 day
8000 Psi OPC	1Day Heat Cured	40%	Total	0.00070	0.00076	0.00084	0.00088	0.00092	0.00096	0.00098
			Shrinkage	0.00001	0.00003	0.00004	0.00004	0.00007	0.00010	0.00011
			Elastic	0.00059	0.00059	0.00059	0.00059	0.00059	0.00059	0.00059
			Creep	0.00010	0.00013	0.00021	0.00025	0.00026	0.00027	0.00028
			Creep Coefficient	0.18	0.23	0.36	0.42	0.45	0.47	0.48
			Creep Modulus	4.64E+06	4.43E+06	4.00E+06	3.83E+06	3.77E+06	3.72E+06	3.68E+06

Strain	5 day	6 day	7 day	14 day	1 Month	2 Month	3 Month	4 Month
Total	0.00102	0.00106	0.00110	0.00123	0.00141	0.00153	0.00161	0.00167
Shrinkage	0.00013	0.00015	0.00017	0.00025	0.00035	0.00042	0.00047	0.00051
Elastic	0.00059	0.00059	0.00059	0.00059	0.00059	0.00059	0.00059	0.00059
Creep	0.00031	0.00032	0.00034	0.00040	0.00047	0.00053	0.00056	0.00057
Creep Coefficient	0.52	0.55	0.58	0.68	0.80	0.90	0.95	0.98
Creep modulus	3.58E+06	3.53E+06	3.45E+06	3.25E+06	3.03E+06	2.87E+06	2.80E+06	2.75E+06

Strain	5 Month	6 Month	7 Month	8 Month	9 Month	10 Month	11 Month	1 Year
Total	0.00172	0.00176	0.00179	0.00181	0.00183	0.00184	0.00185	0.00186
Shrinkage	0.00054	0.00056	0.00057	0.00058	0.00059	0.00060	0.00060	0.00060
Elastic	0.00059	0.00059	0.00059	0.00059	0.00059	0.00059	0.00059	0.00059
Creep	0.00060	0.00062	0.00063	0.00065	0.00066	0.00066	0.00067	0.00067
Creep Coefficient	1.02	1.06	1.08	1.10	1.12	1.13	1.14	1.15
Creep Modulus	2.70E+06	2.65E+06	2.62E+06	2.60E+06	2.57E+06	2.56E+06	2.55E+06	2.54E+06

APPENDIX B

R CODES FOR STATISTICAL ANALYSIS

```
--------------------------------------------------------------
```
R code of approach one
```
--------------------------------------------------------------

gpcdata=read.csv("F:/DataSets5ed/Chapter 2/Examples/gpcdata.csv", header = T)
plot(gpcdata)
model1 = lm(fc~RSiO2+RAl2O3+RCaO+D50+LOI, data=gpcdata)
summary(model1)
plot(model1)
predict(model1,data.frame(RSiO2=25,RAl2O3=39,RCaO=6,D50=16,LOI=1),interval="p
rediction")
predict(model1, interval="confidence")
```
```
--------------------------------------------------------------
```
#Standardizing
```
--------------------------------------------------------------

x=as.matrix(cbind(1,gpcdata[,2:6]))
H=x%*%solve(t(x)%*%x)%*%t(x)
dim(H)
eh= diag(H)
hmax=max(eh)
plot(eh) #obs 11,12,28,29,40,41,49
fc <- row.names(gpcdata)
identify(1:54,eh,fc)
hmax
standardize=function(x){
xbar=mean(x)
s=sd(x) #sd(x)*sqrt(length(x)-1)
z=(x-xbar)/s
return(z)
}
z2=apply(gpcdata, 1, standardize)
mean(z2)
var(z2)
dat3=z2
colMeans(dat3)
var(dat3)
```
```
---------------------------------
```
#other diagonistics
#eigen value
```
---------------------------------------
```
#1.) Inspection of the main diagonal of the correlation matrix
cor(gpcdata[,2:6])
#2.) eigensystem of X'X
exx= eigen(t(gpcdata[,2:6])%*%as.matrix(gpcdata[,2:6]))
exx
max(exx$values)/min(exx$values)
```

```
--------------------------------------------------
                      #VIF
--------------------------------------------------
anova(model1)
library (car)
vif(model1)
library(MPV)
PRESS(model1)

          ---------------------------------------------------
                      #Residual Analysis
          ---------------------------------------------------


gg = lm(fc~RSiO2+RAl2O3+RCaO+D50+LOI, data=gpcdata)
ggs = summary(gg)
ggs$sig
x = model.matrix(gg)
lev = hat(x)
#3.) Studentized residuals
stud = gg$res/(ggs$sig*sqrt(1-lev))
plot(stud,ylab="Studentized Residuals",main="Studentized Residuals")
fc <- row.names(gpcdata)
identify(1:54,gg$res,fc) #sort(g$res)[c(1,54)]
#5.) R-student
jack = rstudent(gg)
plot(jack,ylab="Jacknife Residuals",main="Jacknife Residuals")
jack[abs(jack)==max(abs(jack))]  #extracting the maximum R-student residual
plot(gg$fit, gg$res)
plot(gg$fit, rstudent(gg))
gg22=lm(sqrt(fc)~., gpcdata)
plot(gg22$fit, rstudent(gg22))
#4.) PRESS residuals
plot( gg$res/(rep(1, length(gg$res))-lev) )


          ---------------------------------------------------------
                      #Outlier Detection.
          ---------------------------------------------------------
library(faraway)
data(gpcdata)
install.packages("rggobi")
library(rggobi)
g = lm(fc~RSiO2+RAl2O3+RCaO+D50+LOI, data=gpcdata)
plot(g$res,ylab="Residuals",main="Index plot of residuals") #Index Plot of Residuals
fc <- row.names(gpcdata)
identify(1:54,g$res,fc) #sort(g$res)[c(1,54)]
```

```
-------------------------------------------------------
```
#Leverage and Influence
```
-------------------------------------------------------
```

```
library(faraway)
g=lm(fc~RSiO2+RAl2O3+RCaO+D50+LOI, data=gpcdata)
cook = cooks.distance(g)
influence.measures(g)
plot(cook,ylab="Cooks distances")
fc <- row.names(gpcdata)
identify(1:54,cook, fc)
gl = lm(fc~.,gpcdata,subset=(cook < max(cook)))
summary(gl)
summary( g)
```

```
---------------------------------------------------
```
#Interaction
```
---------------------------------------------------
```

```
rm=lm(fc~RSiO2:RAl2O3+RCaO+D50+LOI, data=gpcdata)
summary(lm(fc~RSiO2:RAl2O3+RCaO+D50+LOI, data=gpcdata))
anova(lm(fc~RSiO2/RAl2O3+RCaO+D50+LOI, data=gpcdata))
```

```
---------------------------------------------------
```
#Variable Selection
```
---------------------------------------------------
```

```
#Criterion-Based (adjusted R^2, R^2, Cp)-sometimes called all-subset regression
install.packages("leaps")
library(leaps)
x=gpcdata[,2:6] #matrix of predictors
y=gpcdata[,1]   #response
leap.dat=leaps(x,y, method="Cp")
leap.dat
library(faraway)
Cpplot(leap.dat)
```

```
---------------------------------------------------
```
#Model2
```
---------------------------------------------------
```

```
gpcdata1=gpcdata[-c(1,12,20,35,42,46),]
model2 = lm(fc~RSiO2+RAl2O3+RCaO+D50, data=gpcdata1)
summary(model2)
plot(model2)
anova(model2)
library (car)
vif(model2)
library(MPV)
PRESS(model2)
predict(model2,data.frame(RSiO2=25,RAl2O3=39,RCaO=6,D50=16,LOI=1),interval="p
rediction")
```

APPENDIX C

CHARACTERIZATION OF FLY ASH

Table C-1 Physical test of FA samples

Sample	Particles <45 microns (%)	Calculated surface (m2/cm3)	Mean particle size (microns)	Specific gravity	Specific surface area (m²/g)
1	83.01	2.916	11.36	2.5	1.1664
2	83.80	2.58	12.31	2.53	1.02
3	68.75	1.33	20.87	2.38	0.56
4	63.50	0.57	27.52	2.32	0.25
5	66.17	1.25	22.68	2.27	0.55
6	63.75	1.10	24.93	2.29	0.48
7	61.66	0.98	28.31	2.27	0.43
8	62.97	1.12	29.96	2.23	0.50
9	74.24	2.00	15.17	2.47	0.81
10	71.26	1.08	22.30	2.17	0.50
11	55.39	0.49	40.03	1.78	0.28
12	58.19	0.795	34.57	1.73	0.46
13	58.02	0.588	36.73	1.82	0.32
14	43.31	0.229	51.11	1.81	0.13
15	87.50	2.955	6.62	2.52	1.17
16	43.49	0.78	63.8	2.11	0.37
17	30.28	0.145	92.41	1.47	0.10
18	84.27	2.453	11.88	2.51	0.98
19	85.68	2.488	11.32	2.7	0.92
20	63.24	1.184	30.38	2.18	0.54
21	67.33	0.57	25.93	2.27	0.25
22	80.91	3.13	10.38	2.67	1.17
23	85.86	3.14	6.71	2.55	1.23
24	81.23	2.793	12.16	2.61	1.07
25	84.23	1.582	11.95	2.41	0.66
26	63.10	1.403	30.15	2.05	0.68
27	76.21	1.79	21.54	2.58	0.69
28	60.20	0.526	33.31	2.03	0.26
29	76.06	0.549	21	2.5	0.22
30	76.15	1.068	20.42	1.88	0.57
31	73.11	1.584	20.39	2.195	0.72
32	60.02	1.122	32.64	2.043	0.55
33	65.18	1.059	25.38	2.11	0.50
34	75.22	1.798	18.41	2.263	0.79
35	65.15	0.97	22.72	1.85	0.52
36	73.12	1.88	15.25	1.57	1.20

Table C-1 Continued

Sample	Particles <45 microns (%)	Calculated surface (m2/cm3)	Mean particle size (microns)	Specific gravity	Specific surface area (m2/g)
37	49.93	0.217	45.06	2.4759	0.09
38	70.57	1.519	23.18	2.0953	0.72
39	73.48	1.37	21.99	1.9107	0.72
40	80.54	1.633	20.04	2.1825	0.75
41	72.11	1.963	19.01	2.41	0.81
42	83.8	2.888	12.09	2.21	1.31
43	82.89	0.97	18.83	1.9698	0.49
44	69.77	1.466	24.07	2.0423	0.72
45	76.74	1.458	19.69	2.1123	0.69
46	85.71	1.56	13.77	2.1882	0.71
47	72.15	1.364	21.81	2.1743	0.63
48	75.31	1.812	16.09	2.023	0.90
49	90.79	2.882	11.33	2.3561	1.22
50	77.54	1.572	20.52	2.3055	0.68
51	73.06	1.374	21.40	2.36	0.58
52	92.00	0.608	14.08	2.207	0.28
53	84.05	1.272	17.49	2.361	0.54
54	91.21	1.763	13.67	2.432	0.72
55	74.20	0.428	24.88	2.204	0.19
56	86.30	3.23	9.50	2.641	1.22
57	70.52	0.3	30.29	1.97	0.15
58	86.57	3.01	11.37	2.51	1.20
59	78.25	1.29	17.69	2.32	0.56
60	72.24	1.45	20.68	2.195	0.66

Table C-2 Chemical properties of FA samples

FA class	FA sample	SiO_2	Al_2O_3	SiO_2/Al_2O_3	$SiO_2+Al_2O_3$	CaO	Fe_2O_3	LOI
C	1	37.77	19.13	1.97	56.9	22.45	7.33	0.17
C	2	32.41	18.4	1.76	57.9	28.07	7.17	0.38
C	3	55.61	19.87	2.80	75.48	12.93	4.52	0.23
F	4	58.52	20.61	2.84	79.13	5	9.43	0.05
F	5	61.01	20.06	3.04	81.07	5.48	7	0.08
F	6	61.23	19.2	3.19	80.43	5.64	7.27	0.06
F	7	62.12	19.59	3.17	81.71	5.01	6.88	0.1
F	8	59.32	19.72	3.01	79.04	6.9	7.22	0.15
C	9	48.7	16.6	2.93	65.3	18.72	6.93	0.49
F	10	55.07	28.61	1.92	83.68	1.97	6.22	1.82
F	11	56.22	27.15	2.07	83.37	5.43	3.73	2.69
F	12	56.39	27.36	2.06	83.75	4.69	3.34	3.41
F	13	57.11	28.18	2.03	85.29	5.18	4	0.44
F	14	57.35	27.78	2.06	85.13	5.57	3.65	0.83
F	15	40.75	22.79	1.79	63.54	4.64	17.76	5.72
F	16	66.5	18.8	3.54	85.3	4.91	1.95	0.26
C	17	39.25	21.09	1.86	60.34	23.53	4.99	0.11
C	18	33.02	19.82	1.67	52.84	26.19	6.75	0.16
F	19	59.25	18.43	3.21	77.68	9.23	5.61	0.04
C	20	56.42	17.63	3.20	74.05	11.66	5.74	0
C	21	27.15	17.57	1.55	44.72	33.39	6.08	0
C	22	31.26	19.76	1.58	51.02	28.53	6.47	0
C	23	30.85	17.07	1.81	47.92	28.47	6.79	0
C	24	49.9	19.32	2.58	69.22	15.22	7.63	0.09
C	25	55.15	23.55	2.34	78.7	10.6	4.63	0.31
F	26	52.81	20.83	2.54	73.64	0.98	13.05	0.19
F	27	45.65	20.37	2.24	66.02	6.23	19.43	0.2
F	28	58.04	28.15	2.06	86.19	4.24	3.29	0.07
F	29	51.46	28.04	1.84	79.5	2.96	10.34	2.78
F	30	51.69	21.37	2.42	73.06	3.1	8.28	8.88
C	32	57.55	19.84	2.90	77.39	10.25	5.08	1.38
F	33	52.57	25.22	2.08	77.79	5.1	7.76	2.14
F	34	49.3	24.71	2.00	74.01	2.93	14.66	2.42
F	35	42.06	21.76	1.93	63.82	5.26	14.16	8.49
C	36	27.98	23.3	1.20	51.28	28.53	7.2	7.08
F	37	52.48	25.63	2.05	78.11	3.3	9.36	2.1
F	38	55.05	24.58	2.24	79.63	3.46	8.52	2.36
F	39	54.63	21.09	2.59	75.72	7.6	5.8	0.8
F	40	55.65	20.93	2.66	76.58	7.25	5.55	0.45
F	41	51.4	33.75	1.52	85.15	4.44	4.31	0.49
F	42	50.76	31.87	1.59	82.63	6.81	3.62	0.32

Table C-2 Continued

FA class	FA sample	SiO₂	Al₂O₃	SiO₂/ Al₂O₃	SiO₂+ Al₂O₃	CaO	Fe₂O₃	LOI
F	43	63.42	21.09	3.01	84.51	2.84	6.75	0.00
F	44	66.79	17.41	3.84	84.2	3.65	6.89	1.1
F	45	58.04	24.04	2.41	82.08	4.94	6.76	0.78
F	46	59.7	22.53	2.65	82.23	4.02	7.45	0.61
F	47	38.8	43.34	0.90	82.14	6.15	5.53	1.31
F	48	47.48	36.53	1.30	84.01	4.83	4.14	0.14
F	49	48.14	27.12	1.78	75.26	8.51	9.14	0.54
F	50	62.35	18.53	3.36	80.88	5.5	6.08	0.34
F	51	45.96	37	1.24	82.96	2.74	8.49	0.82
C	52	54.61	21.47	2.54	76.08	11.2	7.3	0.24
C	53	54.51	21.44	2.54	75.95	11.15	7.29	0.41
F	54	47.98	31.17	1.54	79.15	8.14	6.5	1.11
C	55	29.52	15.8	1.87	45.32	31.51	6.01	0.4
F	56	42.88	25.06	1.71	67.94	6.867	10.4	7.11
C	57	34.5	19.18	1.80	53.68	25.01	6.17	0.17
C	58	57.2	19.18	2.98	76.38	11.76	4.44	0.5
F	59	55.7	23.51	2.37	79.21	9.385	6.35	0.31
F	60	48.4	27	1.79	75.4	1.724	14.2	0.72
F	Min.	38.80	17.41	0.9	63.54	0.98	1.95	0.00
	Max.	66.79	43.34	3.84	86.19	9.38	19.43	8.88
	Avg.	53.94	25.01	2.28	78.96	5.03	7.89	1.53
C	Min.	27.15	15.80	1.20	44.72	10.25	4.44	0.00
	Max.	57.55	23.55	3.20	78.70	33.39	7.63	7.08
	Avg.	42.81	19.48	2.20	62.65	20.48	6.23	0.63

REFERENCES

[1] Swayze, M. A., "Early concrete volume changes and their control," *ACI Journal, Proc.* Vol. 38, (1942)

[2] Ryan, H.; Peter, B.; Dale, B.; Tommy, N.; and Jason, W., "Plastic shrinkage cracking in internally cured mixtures made with pre-wetted light weight aggregate," *Concrete International*, vol. 32(2), 2010, (49-54)

[3] Jun, Z.; Dongwei, H.; and Haoyu, C., "Experimental and theoretical studies on autogenous shrinkage of concrete at early ages," *Journal of Materials in Civil Engineering*, vol. 23(3), 2011, (312-320)

[4] Guneyisi, E.; Gesoglu, M.; and Ozbay, E., "Strength and drying shrinkage properties of self-compacting concretes incorporating multi-system blended mineral admixtures," *Construction and Building Materials*, vol. 24(10), 2010, (1878-1887)

[5] Feldman, R. F.; and Sereda, P. J., "A model of hydrated Portland cement paste as deducted from sorption length change and mechanical properties," *Materials and Structures*, vol. 11, 1938, (509-519)

[6] Bernal, J. D.; Dasgupta, D. R.; and Mackay, A. L., "The oxides and hydroxides of iron and their structural inter-relationships" *Clay Materials Bulletin*, vol. 4(21),1959, (15-30)

[7] Bentz, D. P.; Quenard, D. A; Bouny, V. B.; and Jennings, H. M., "Modeling drying shrinkage of cement paste and mortar part1. Structural models from nanometers to millimeters," *Materials and Science*, vol. 28, 1995, (450-458)

[8] Aitcin, P. C., "High performance concrete," 36th Conference on Our World in Concrete and Structures, 2011, (14-16)

[9] Heath, A. C.; and Roesler, J. R., "Shrinkage and thermal cracking of fast setting hydraulic cement concrete pavement in Palmadale, California," University of California-Barkley Pavement Research Center, California.

[10] Jensen, O. M.; and Hansen, P. F., "Water-entrained cement based materials I, principle and theoretical background," *Cement and Concrete Research*, vol. 31(5), 2001, (647-654)

[11] Gardner, N. J.; and Lockman, M. J., "Design provisions for drying shrinkage and creep of normal-strength concrete," *ACI Materials Journal*, vol.98 (2), 2001, (159-167)

[12] Qiao, Z.; Linhua, J.; and Xu, J., "Models for autogenous shrinkage in low water-binder ratios concrete," *Advanced Materials Research*, vol. 487, 2012, (435-439)

[13] Zuanfeng, P.; Chung, C. F.; and Jiang, Y., "Uncertainty analysis of creep and shrinkage effects in long-span continuous rigid frame of Sutong Bridge," *Journal of Bridge Engineering*, vol. 16, 2011, (248-258)

[14] Miyazawa, S.; Tazawa, E.; and Sato, K., "Autogenous shrinkage stress of ultra-high-strength concrete caused by restraint of reinforcement," *Transaction of the Japan Concrete Institute*, vol. 15, 1993, (115-122)

[15] Monkman, S.; and Shao, Y., "Carbonation curing of slag cement-concrete for binding CO_2 and improving performance" *Journal of Materials in Civil Engineering*, vol. 22(4),2010, (296-304)

[16] Parrott, L. J., "A review of carbonation in reinforced concrete," A review carried out by C&CA under a building research establishment contract, July 1987.

[17] Brooks, J. J.; and Neville, A. M., "Creep and shrinkage as affected by admixtures and cement replacement materials, creep and shrinkage of concrete: effect of materials and environment," *ACI Special Publication*, SP-135, 1992, (19-36)

[18] Pickett, G., "Effect of aggregate on shrinkage of concrete and hypothesis concerning shrinkage," *Journal of ACI*, vol. 52, 1956, (581-590)

[19] Weber, S.; and Reinhardt, H. W., "A new generation of high performance concrete: concrete with autogenous curing," *Advanced Cement Based Materials*, vol. 6, 1997, (59-68)

[20] Deshpande, S.; Darwin, D.; and Browning, J., "Evaluating free shrinkage of concrete for control of cracking in bridge deck," Structural Engineering and Engineering Materials, SM report No.89. The University of Kansas Center for Research, January 2007.

[21] Johnston, C. D.; Gamble, B. R.; and Malhotra, V. M., "Effects of superplasticizers on properties of fresh and hardened concrete," 58th Annual Meeting of the Transportation Research Board, Washington District of Columbia, United States.

[22] Shideler, J. J.; and Amer, J., "Chloride in concrete," *Journal of American Concrete Institute*, March 1952 p. 537.

[23] Loser, R.; and Leemann, A., "Shrinkage and restrained shrinkage cracking of self-compacting concrete compared to conventionally vibrated concrete," *Materials and Structures*, vol. 42, 2009, (71-82)

[24] Bentur, A.; and Kolver, K., "Evaluation of early age cracking characteristics in cementitious system," *Materials and Structures*, vol. 36, 2003, (183-190)

[25] Chen, T. C.; Yin, W. Q.; and Ifju, P. G., "Shrinkage measurement in concrete materials using cure reference method," *Experimental Mechanics*, 50, 2010, (999-1012)

[26] Neville, A. M.; and Aitcin, P. C.; "High performance concrete-An overview," *Materials and structures*, vol.33, 1998, (111-117)

[27] Rodriguez, J. A.; and Aristizabal, J. D., "Short and long-term deflections in reinforced prestressed and composite concrete beams," *Journal of Structural Engineering*, vol. 133, 2007, (495-506)

[28] Glanville, W. H., "Studies in reinforced concrete III- creep or flow of concrete under load," *Building Research Technology*, vol. 12, 1933, (51-54)

[29] Troxel, G. E.; Raphael, J. M.; and Davis, R. W., "Long term creep and shrinkage test of plain and reinforced concrete," *ASTM Proceeding*, 58, 1958, (1101-1120)

[30] Lorman, W. R., "The theory of concrete creep," *ASTM Proceedings*, vol. 40, 1940, (1082-1102)

[30] Zeinab, A. T., "Reinforced concrete corrosion and protection," *Concrete Research*, vol. 3(1), 2012, (359-372)

[31] Jerga, J., "Physico-mechanical properties of carbonated concrete," *Construction and Building Materials*, vol. 18(9), 2004, (645-652)

[32] Rashid, M. A.; Mansur, M. A.; and Paramasivam, P., "Correlation between mechanical properties of high-strength concrete," *Materials Journal*, vol. 14(3), 2002, (230-238)

[33] Fernandez Bertos, M.; and Simons, S. J. R., "A review of accelerated carbonation technology in the treatment of cement-based materials and sequestration of CO_2," *Journal of Hazardous Materials*, vol. 112, 2004, (193-205)

[34] Mc Polin, D. O.; Basheer, P. A .M.; and Long, A. E., "New test method to obtain pH profiles due to carbonation of concretes containing supplementary cementitious materials," *Journal of Materials in Civil Engineering*, vol. 19(11), 2007, (936-946)

[35] Swamy, R. N.; and Stavrides, H., "Influence of fiber reinforcement on restrained shrinkage and cracking," *Journal of American Concrete Institute*, vol. 76(3), 1979, (443-460)

[36] Moon, J. H.; Rajabipour, F.; Pease, B.; and Weiss, J., "Quantifying the influence of specimen geometry on the results of the restrained ring test," *Journal of ASTM International*, vol. 3(8), 2006, (14-29)

[37] Hossain, A. B.; and Weiss, J., "The role of specimen geometry and boundary conditions on stress development and cracking in the restrained ring test," *Cement and Concrete Research*, vol. 36(1), 2006, (189-199)

[38] Hossain, A. B.; and Weiss, J., "Assessing residual stress development and stress relaxation in restrained concrete ring specimens," *Cement and Concrete Composite*, vol.26(5), 2004, (531-540)

[39] Jonasson, J. E., "Analysis of creep & shrinkage in concrete and its application to concrete top layers," *Cement and Concrete Research*, vol. 8, 1978, (441-454)

[40] Madsen, H. O.; and Bazant, Z. P., "Uncertainty analysis of creep and shrinkage effects in concrete structures," *ACI Journal*, vol.80 (2), 1983, (116-127)

[41] Hwang, S. D.; and Khayat, K. H., "Effect of mixture composition on restrained shrinkage cracking of self-consolidating concrete used in repair," *ACI Material Journal*, vol. 105(5), 2008,(499-509)

[42] Yang, I. H., "Uncertainty and sensitivity analysis of time-dependent effects in concrete structures," *Engineering Structure*, vol. 29 (7), 2007, (1366-1374)

[43] Dilger, W. H,; and Wang, C., "Time dependent properties of high performance concrete," *Proceedings of the 8th FIP congress*, Amsterdam, Netherlands, May 1998 (205-213)

[44] Neville, A. M.; Dilger, W. H.; and Brooks, J. J., "Creep of plain and structural concrete," Construction Press, London and New York, (1983)

[45] Sakata, K., "A study of moisture diffusion in drying and drying shrinkage of concrete," *Cement and Concrete Research*, vol. 13(2), 1993, (216-224)

[46] Bazant, Z. P.; and Baweza, S., "Justification and refinements of model b3 for concrete creep and shrinkage1statics and sensitivity," *Materials and Structure*, vol. 28(180), 1995, (415-430)

[47] Bazant, Z., "Viscoelasticity of solidifying material-concrete," *Journal of Engineering Mechanics*, vol. 103(EM6)1977, (1049-1067)

[48] FIB Structural concrete: Textbook of Behaviour, Design and Performance, Updated Knowledge of the CEB/FIP Model Code 1990. Bulletin No. 2, Federation international de beton (FIB), Lausanne, Vol. 1 (1999) (35-52)

[49] Gardner, N. J.; and Lockman, M. J., "Design provisions for drying shrinkage and creep of normal-strength concrete," *ACI Materials Journal*, vol.98 (2), 2001, (159-167)

[50] Kwesi, S. C.; Trevor, B.; and Alan, T., "Drying shrinkage and creep performance of geopolymer concrete," *Journal of Sustainable Cement Based Materials*, vol. 2(1), 2014, (35-42)

[51] Shah, H. R.; and Weiss, J., "Quantifying shrinkage cracking in fiber reinforced concrete using the ring test," *Materials and Structure*, vol. 39, 2006, (887-899)

[52] See, H. T.; Attiogbe, E. K.; and Miltenberger, M. A., "Shrinkage cracking characteristics of concrete using ring specimens," *ACI Materials Journal*, vol. 100(3), 2003, (239-245)

[53] Grzbowski, M.; and Shah, S. P., "Model to predict cracking in fiber reinforced concrete due to restrained shrinkage," *Magazine of Concrete Research*, vol. 41(148), 1989, (125-135)

[54] Carlson, R. W.; and Reading, T. J., "Model study of shrinkage cracking in concrete building walls," *ACI Structure Journal*, vol. 85(4), 1988, (395-404)

[55] Whiting, D. A.; Detwiler, R. J.; and Lagergren, E. S., "Cracking tendency and drying shrinkage of silica fume concrete for bridge deck applications," *ACI Materials Journal*, vol.97(1), 2000, (71-77)

[56] Robertson, I. N.; and Li, X., "Shrinkage and creep predictions evaluated using 10-years monitoring of the north halawa valley viaduct," *Shrinkage and Creep of Concete*, vol. 1, 2005, (143-162)

[57] Rahman, M. K.; Baluch, M. H.; and Al-Gadhib, A. H., "Simulation of shrinkage distress and creep relief in concrete repair," *Composites Part B Engineering*, vol. 31, 2000, (541-553)

[58] Provis, J. L.; Duxon, P.; and Van Deventer, J. S. J., "The role of mathematical modeling and gel chemistry in advancing geopolymer technology," *Chemical Engineering Research and Design*, vol. 83(7), 2005, (853-860)

[59] Hardjito, D.; Wallah, S. E.; Sumajouw, D. M.; and Rangan, B. V., "On the development of fly ash-based geopolymer concrete," *ACI Materials Journal*, vol. 101(6), 2004, (467-472)

[60] Montgomery, D. C.; Peck, E. A.; and Vining, G. G., "Introduction to linear regression analysis," 4th Edition, Wiley-Interscience, New- Jersey, 2006, (122-153)

[61] Breiman, L., "Heuristics of instability and stabilization in model selection", *Annals of Statistics*, Vol. 24, 1996, (2350-2383)

[62] George, H. J.; Ron, K.; and Karl, P., "Irrelevant features and the subset selection porblem," Proceedings of the Eleventh International Conference, San Francisco, CA (121-129)

[63] Horel, A. E.; and Kennard, R. W., "Ridge regression: Application to nonorthogonal problemes," *Technometrics*, Vol. 12(1), 1970, (69-82)

[64] Tibshirani, R., "Regression shrinkage and selection via LASSO," *Journal of Regression Statistic Society*, vol. 58(1), 1996, (267-288)

[65] Diaz, E. I.; Allouche, E. N.; and Eklund, S., "Factors affecting the suitability of fly ash as source material for geopolymer," *Fuel*, vol. 89, 2010, (992-996)

[66] Fernandez, J. A.; and Palomo, A., "Characterization of fly ashes: Potential reactivity as alkaline cements," *Fuel*, vol. 82, 2003, (2259-2265)

[67] Islam, R.; Montes, C.; and Allouche, E. N., "Correlation between chemical and phase composition of fly ash and mechanical properties of geopolymer concrete," *International Journal of Environmental Engineering and Natural Resources*, vol. 1(5), 2014, (235-239)

[68] Diaz, E. I.; and Allouche, E. N., "Recycling of fly ash into geopolymer concrete: Creation of a database," *Green Technologies Conference*, 2010 IEEE. (1-7)

[69] Davidovits, J., "Geopolymers: inorganic polymeric new materials," *Journal of Thermal Analysis*, vol. 37, 1991, (1633-1656)

[70] De Silva, P.; Sagoe-Crenstil, K.; and Sirivivatnanon, V., "Kinetics of geopolymerization: Role of Al_2O_3 and SiO_2," *Cement and Concrete Research*, vol. 37, 2007, (512-518)

[71] Davidovits, J., "Chemistry of geopolymeric systems, terminology," *Geopolymer International Conference*, France, 1999.

[72] Diamond, S., "On the glass present in low-calcium and in high-calcium fly ashes," *Cement and Concrete Research*, vol. 13, 1983, (459-464)

[73] Kovler, K., "Testing system for determining the mechanical behavior of early age concrete under restrained & free uniaxial shrinkage," *Materials and Structures*, vol. 27, 1994, (324-330)

[74] Hossain, A. B.; Pease, B.; and Weiss, J., "Quantifying early-age stress development and cracking in low water to cement concrete: restrained ring-test with acoustic emission," *Transportation Research*.vol. 1834, 2003, (24-32)

[75] Moon, J. H.; and Weiss, J., "Estimating residual stress in the restrained ring under circumferential drying," *Cement and Concrete Composites*, vol. 28(5), 2006, (486-496)

[76] Manzi, S.; Mazzotti, C.; and Bignozzi, M. C., "Short and long-term behavior of structural concrete with recycled concrete aggregate," *Cement and Concrete Composites*, vol. 37, 2013, (312-318)

[77] Guneyisi, E.; Gesoglu, M.; and Ozbay, E., "Strength and drying shrinkage properties of self-compacting concretes incorporating multi-system blended mineral admixtures," *Construction and Building Materials*, vol. 24(10), 2010, (1878-1887)

[78] Grasley, Z. C.; and Ambrosia, M. D., "Viscoelastic properties and drying stress extracted from concrete ring tests," *Cement & Concrete Composites*, vol. 33, 2011, (171-178)

[79] Bentz, D. P.; Quenard, D. A.; Baroghel-Bouny, V.;Garboczi, E. J.; and Jennings, H. M., "Modeling drying shrinkage of cement paste and mortar part1. Structural models from nanometers to millimeters," *Materials and Science*, vol.28, 1995, (450-458)

[80] Nasser, K. W.; and Al-Manseer, A. A., "Shrinkage and creep of concrete containing 50% Lignite Fly Ash at high temperature," *Cement Concrete and Aggregates*, vol. 9, 1987, (95-100)

[81] Zhu, Q.; Jiang, L.; and Xu, J., "Models for autogenous shrinkage in low water-binder ratios concrete," *Advanced Materials Research*, vol. 487, 2012, (435-439)

[82] Palomo, A.; and Grutzeck, M. W., "Alkali-activated fly ashes a cement for the future," *Cement and Concrete Research*, vol. 29, 1999, (1323-1329)

[83] Schiessel, P.; Beckhaus, K.; Schachinger, I.; and Rucker, P., "New results on early-age cracking risk of special concrete," *Cement Concrete Aggregate*, vol. 26(2), 2004, (139-147)

[84] Carol, I.; and Bazant, Z. P., "Viscoelasticity with aging caused by solidification of nonaging constituent," *Journal of Engineering Mechanics*, vol. 119(11), 1993, (2252-2259)

[85] Krenchel, H.; and Shah, S. P., "Restrained shrinkage tests with pp-fiber reinforced concrete," ACI SP105; 1987,(141-158)

[86] Read, W. T., "Stress analysis for compressible viscoelastic materials," *Journal of Applied Physics*, vol. 21, 1950, (671-674)

[87] Grasley, Z. C.; and Lange, D. A., "Constitutive modeling of the aging viscoelastic properties of Portland cement paste," *Mechanics of Time Dependent Materials*, vol.11, 2007,(175-198)

[88] Padevet, P; and Bittnar, P., "Influence of fly ash concrete in cement paste on size of creep," *Procedia Engineering*, vol. 48, 2012, (520-524)